

Asymmetric particles for pulmonary drug delivery

Dissertation
zur Erlangung des Grades
des Doktors der Naturwissenschaften
der Naturwissenschaftlich-Technischen Fakultät III
Chemie, Pharmazie, Bio- und Werkstoffwissenschaften
der Universität des Saarlandes

von
Dorothee Anna Luise Kohler
Saarbrücken
2010

Tag des Kolloquiums:	21.01.2011
Dekan:	Prof. Stefan Diebels
Vorsitzender:	Prof. Dr. Rolf Hartmann
1. Gutachter:	Prof. Dr. Claus-Michael Lehr
2. Gutachter:	Prof. Dr. Helmuth Möhwald
Akad. Mitarbeiter:	Dr. Ana Melero Zaera

In Memoriam
Dr. Michael Krüger

Table of Contents

Summary	7
Zusammenfassung	8
1. General Introduction	9
1.1. Lung Anatomy	9
1.1.1. General Considerations	9
1.1.2. Conducting Zone	10
1.1.3. Gas Exchange Zone	10
1.2. Particle Engineering for Pulmonary Drug Delivery	10
1.2.1. General Considerations	10
1.2.2. Particle Aerodynamic Diameter	11
1.2.3. Aerosolization	13
1.2.4. Lung Deposition	14
1.2.5. Particle Clearance	17
1.2.6. Multifunctional Drug Delivery	19
1.3. Asymmetric Particles in Vivo	20
1.3.1. General Considerations	20
1.3.2. Carbon-Nanotubes	21
1.3.3. Health Effects	22
1.3.4. In Vivo Circulation	22
1.3.5. Macrophage Clearance	23
1.4. Asymmetric Particle Preparation	24
1.4.1. State of the Art	24
1.4.2. Electrospinning	25
1.4.3. Tubes by Fiber Template (TUFT)	26
1.4.4. Template Technique	27
2. Aim of this Work	40
3. Template assisted Polyelectrolyte Encapsulation of Nanoparticles into Dispersible, Hierarchically Nanostructured Microfibers	41
3.1. Introduction	42
3.2. Materials and Methods	43
3.2.1. Particle Infiltration	43
3.2.2. Microfiber Formation	44

3.2.3.	Microfiber Imaging.....	45
3.3.	Results and Discussion.....	46
3.3.1.	Microfiber Morphology.....	46
3.3.2.	Multifunctional Microfibers.....	48
3.3.3.	Polyelectrolyte Capsule Containing Microfibers.....	49
3.4.	Conclusion.....	51
3.5.	Experimental Details.....	52
4.	Spatial Aspect Ratio Dependent Macrophage Uptake of Biocompatible Nanostructured Microfibers.....	53
4.1.	Introduction.....	54
4.2.	Materials and Methods.....	55
4.2.1.	Agarose Infiltration.....	55
4.2.2.	Nanoparticle Infiltration.....	56
4.3.	Results and Discussion.....	60
4.3.1.	Cytotoxicity Test.....	60
4.3.2.	Macrophage Uptake.....	61
4.4.	Conclusion.....	64
4.5.	Experimental Details.....	64
5.	Aspect Ratio Dependent Aerosolization behaviour of Drug loaded Microfibers.....	67
5.1.	Abstract.....	68
5.2.	Introduction.....	68
5.3.	Template Technique.....	69
5.4.	Generating Drug Loaded Microfibers and Introducing Porosity.....	70
5.5.	Aerosolization of Microfibers.....	71
5.6.	Results and Discussion.....	72
5.7.	Conclusion.....	74
5.8.	Experimental Details.....	75
6.	Overall Conclusion and Outlook.....	76
7.	Annex.....	77
7.1.	Particle Aggregation.....	77
7.1.1.	General Consideration.....	77
7.1.2.	Plasma Cleaning.....	78
7.1.3.	Gold Layer.....	79
7.1.4.	Gold Layer and Hydrophobisation.....	81

7.1.5. Sacrificial Layer	83
7.2. Cytotoxicity Test.....	85
7.2.1. MTT Assay	85
7.2.2. LDH Assay	86
7.3. Chemical Structures	86
Curriculum Vitae	105
Publication List	107
Acknowledgements	108

Summary

Targeted drug delivery and controlled release are current challenges in pulmonary drug delivery. The deposition pattern and clearance from deposition site are two key parameters for drug delivery carrier design. Asymmetric particles allow an increase in peripheral drug delivery compared to spherical particles and furthermore, affect particle clearance mechanisms from the lung. Therefore, the main aim of this thesis was to develop new synthesis strategies to produce well-dispersible, biocompatible, biodegradable microfibers with a variety of aspect ratios and porosities. The macrophage response to the resulting microfibers was investigated. The aerosolization properties of the resulting microfibers were examined. From the obtained results it can be concluded that:

1. A new template-assisted synthesis strategy to produce monodisperse microfibers with defined dimensions has been developed.
2. The technique has been extended to various materials and process parameters for cell testing, drug loading and aerosolization tests.
3. Microfibers were successfully taken up by macrophages, only when they were approached from the pointy end.
4. Aerosolization studies showed good dispersion properties of microfibers with relatively high fine particle fractions.

In summary, this new technique may allow to produce microfibers for pulmonary drug delivery, which will lead to a better understanding of their in vivo behaviour such as mucoadhesion, macrophage interaction and deposition behaviour.

Zusammenfassung

Die aktuellen Herausforderungen der inhalativen Therapie sind die gezielte Wirkstoffdeposition und die kontrollierte Wirkstofffreisetzung in der Lunge. Asymmetrische Partikel haben dabei durch ihre erhöhte tiefe Lungendeposition und ihren Einfluss auf die Clearance-Mechanismen erhöhtes Interesse gefunden. Ziel dieser Arbeit war daher die Entwicklung einer neuen Herstellungsmethode, um gut vereinzelte, biokompatible, bioabbaubare Mikrofasern mit variablen Aspektverhältnissen und Porositäten zu generieren. Weiteres Ziel war die Testung der Makrophagen-Mikrofaser-Interaktion und des Aerosolisierungsverhaltens. Die gewonnenen Ergebnisse führen zu folgenden Aussagen:

1. Es wurde eine neue Methode zur Herstellung monodisperser Mikrofasern mit definierten Maßen entwickelt.
2. Mikrofasern aus diversen Materialien wurden in späteren Versuchen für Zelltests, Wirkstoffbeladung und Aerosolisierungsstudien verwendet.
3. Die Aufnahme von Mikrofasern durch Makrophagen zeigte eine Korrelation zum Faserdurchmesser, wobei diese nur vom spitzen Ende her aufgenommen wurden.
4. Aerosolisierungsstudien zeigten eine gute Dispergierung der Mikrofasern mit hohen Fine-Particle-Fractions.

Die entwickelte Methode kann zu einer Optimierung der pulmonalen Wirkstoffapplikation und einem besseren Verständnis des Verhaltens asymmetrischer Partikel im Körper beitragen. Die Mukoadhäsion, die Makrophagen-Interaktion und das Depositionsverhalten in der Lunge können mittels dieser Fasern weiter untersucht werden.

1. General Introduction

1.1. Lung Anatomy

1.1.1. General Considerations

Large surface area, extensive vascularisation and the ability to avoid the first pass effect are the main advantages for drug administration via the lung. Furthermore the presence of a thin epithelial barrier in the lung allows the fastest uptake of any route of delivery other than intravenous [1].

Anatomically the lung can be divided into two main parts according to their function during breathing. The first 16 airway generations – conducting or proximal airways -, including mouth, nose, trachea and bronchiolus terminalis, mainly warm, wet and clean air. The airway generations 17-23 form the peripheral airways, i.e. gas exchanges zone, including bronchiolus respiratorius and saccus alveolaris [2].

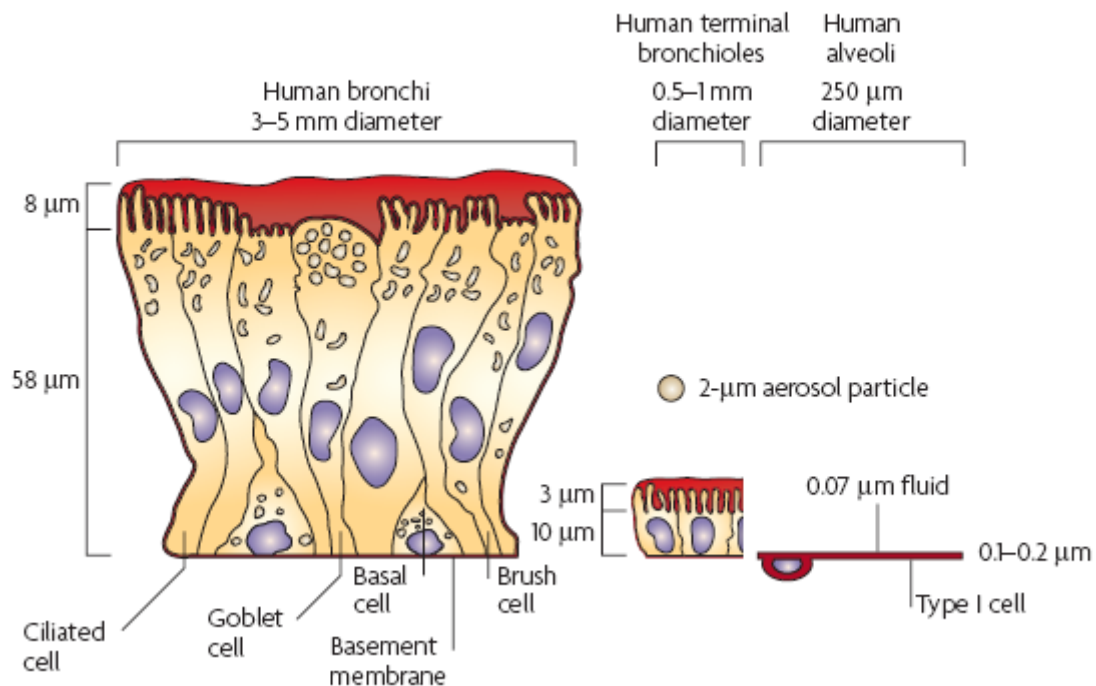


Figure 1: Comparison of the lung epithelium at different sites within the lungs taken from ref. [3].

1.1.2. Conducting Zone

The proximal airways (tracheobronchial compartment) are covered by a layer of epithelial cells comprising ciliated cells, goblet cells, and a variety of other secretory cells, with varied cell compositions in different airway generations [4] (Figure 1). The basal cells are progenitor cells for the epithelium. The goblet cells produce mucus, which is moved by the ciliated cells, and thus gives rise to the mucociliar clearance [3].

1.1.3. Gas Exchange Zone

The epithelium of the peripheral compartment is covered by a monolayer composed of broad and very thin (0.1 μ m) type 1 cells (95%), and lung surfactant producing type 2 cells (5%) interconnected by tight junctions. This ensures a thin barrier for gas exchange [5]. The clearance in the alveoli differs from the mucociliar clearance described above. No cilia are present in the alveoli, leaving macrophages and dendritic cells responsible for clearance of deposited materials [6].

1.2. Particle Engineering for Pulmonary Drug Delivery

1.2.1. General Considerations

Pulmonary drug delivery has gained significant attention during the past decade. The large lung surface area (\sim 140m²) and thin epithelial barrier (0.1 μ m in the alveoli) make the lung an interesting drug delivery route due to the high drug absorption and the ability to circumvent the first pass effect [7, 8]. Pulmonary drug delivery can therefore be used to treat local diseases as cystic fibrosis, asthma and chronic obstructive pulmonary disease (COPD) as well as systemic diseases i.e. diabetes (Exubera®, Pfizer).

The effectiveness of drug formulation is closely related to efficient delivery to the lung [9]. Till now, delivery carriers have been optimized in terms of size, morphology and structure. The aim of particle engineering is to obtain particles with narrow particle size distribution (PSD), improved dispersibility, optimum deposition pattern, sustained release profiles and/or specific targeting.

1.2.2. Particle Aerodynamic Diameter

The aerodynamic diameter (d_{aer}) has a major impact on particle deposition in the lung, thus determining the site of drug release. The d_{aer} is defined as the diameter of a unit density sphere having the same terminal settling velocity as the particle sampled [6]. The d_{aer} depends on the particle properties such as geometric size, shape and density, and can be estimated by

Equ. 1:
$$d_{aer} = d_{geo} \sqrt{\rho}$$

where d_{geo} is the geometric diameter and ρ is the particle density. To achieve the desired deposition pattern, the d_{aer} can be modified by the geometric diameter and the particle density ρ i.e. by modifying the porosity [10, 11].

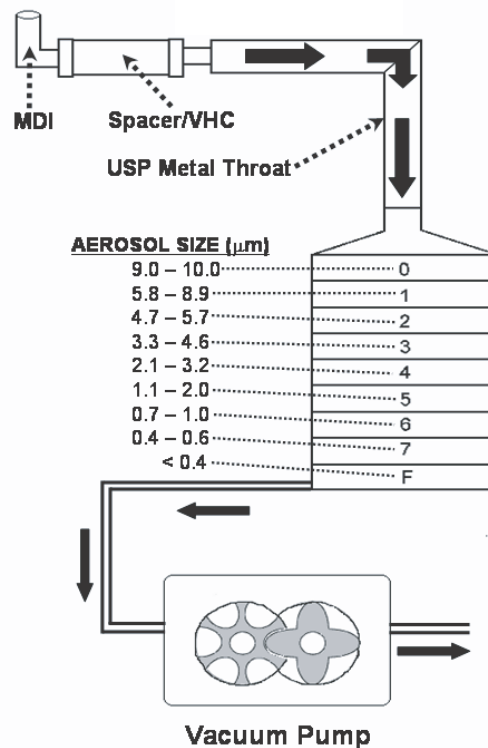


Figure 2: Schematic diagram of an Andersen Cascade Impactor taken from ref. [12].

The aerodynamic diameter can be assessed by cascade impactor testing, described in both European and US pharmacopeias [13, 14] (Figure 2). Particles moving in air at constant flow rate are subjected to a change in flow direction allowing for size separation of particles [15, 16]. A port of entry (preseparator) mimicking the oropharynx, located immediately behind the inhalation device, collects particles with

aerodynamic diameters $\geq 10 \mu\text{m}$. Particles of progressively smaller diameters are collected on arranged stages with decreasing cut off diameters, as the aerosol flows through the instrument [16]. Particles pass through plates containing jets of defined size. Particles are collected on a surface located underneath the plate by deflecting the flow. The particle inertia causes deposition if their size exceeds a critical value, while smaller particles remain airborne [15, 16].

1.2.2.1. Particle Size

Particle size and morphology mainly influence the aerosol deposition and clearance during pulmonary drug delivery. Reducing the amount of deposited particles in the oropharyngeal region to achieve increased lung deposition requires optimum particle size formulation. The desired particle size to target the peripheral lung compartments is reported to be $d_{\text{aer}} = 1\text{-}5 \mu\text{m}$. Particles having diameters between $0.2\text{-}1 \mu\text{m}$ suffer the fate of being exhaled, while ultrafine particles of $0.005\text{-}0.2 \mu\text{m}$ again show high deposition efficiencies in the deep lung area [17]. Due to limitation of the administered amount of drug by ultrafine particles and the absence of formulation technologies to process these particles, ultrafine particles are not used in pulmonary drug delivery nowadays. Particles with d_{aer} exceeding $10 \mu\text{m}$ will deposit in the extrathoracic region.

Another aerosol parameter is the particles size distribution (PSD), which is described by the median particle diameter and its geometric standard deviation. To target best aerosol performance, small PSD is required [6].

1.2.2.2. Porosity

Edwards et al. discovered that porous particles are advantageous for pulmonary drug delivery, as they show small d_{aer} while having a bigger d_{geo} . This results in reduced particle-particle contact and thus fewer tendencies to aggregate. By this increased efficiency for deep lung deposition can be achieved [10, 11, 18]. Furthermore, large porous particles can escape macrophage clearance leading to increased bioavailability and the opportunity for sustained drug delivery [11, 19].

1.2.2.3. Particle Shape

Shape engineering is still at its infancy, but during the past decade research gained more interest in shape as new design parameter to directly influence the particle fate in vivo [20]. By particle shape the pulmonary deposition pattern after inhalation can be optimized. Sturm and Hofmann [21] concluded that fibers show higher probability to deposit in the peripheral lung compared to spherical particles of the same volume. This can be explained, as the aerodynamic behaviour of elongated particles is mainly influenced by the fiber diameter. By these higher doses to treat lung diseases, for example tuberculosis could be administered, targeting macrophages, reducing systemic side effects and optimizing therapy [22-24].

Pulmonary clearance mechanisms will be greatly influenced by elongated particles, as macrophage uptake depends on the particle shape at the point of first contact [25]. Particle size additionally impacts on the success of phagocytosis or whether frustrated phagocytosis will occur [26]. Particle aggregation and dispersibility also show shape dependency [27], thus modifying the deposition pattern during inhalation. Particle geometry has an additional impact on the degradation behaviour and thereby on the release kinetics of administered drugs [28]. Therefore, new synthesis strategies to produce particles with well defined dimension and geometry are highly attractive.

1.2.3. Aerosolization

1.2.3.1. Fine Particle Fraction / Delivered Dose

The efficiency of drug delivery to the lung is mainly influenced by the delivered dose (DD). This depends on the emitted dose (ED) from the inhaler and the fine particle fraction (FPF). High fractions of both, ED and FPF are desired. The FPF is considered to describe the amount of particles with a d_{aer} smaller than $4.7\mu m$ [16, 29]. To optimize formulation performance, particle adhesion and cohesion both affecting FPF and ED due to insufficient disaggregation during inhalation, need to be controlled [30]. The aggregation can be minimized by increasing the d_{geo} , lowering powder bulk density, or using particles with irregular surfaces to reduce the contact area and forces between particles.

1.2.3.2. Crystallinity

Powder dispersibility and disaggregation properties can be changed during storage, i.e. recrystallization, thus modifying the aerosol performance. Particle formulations for dry powder inhalers (DPI) therefore need to be in their most stable form, i.e. crystalline to avoid potential changes during storage. Amorphous forms on the other hand provide fast dissolution kinetics, and are sometimes the only available form of active ingredients, i.e. many therapeutic proteins [9]. To obtain optimum particle performance, crystallinity and stability during shelf-life need to be investigated.

1.2.3.3. Outlook for Particle Formulation

Particle engineering for pulmonary drug delivery is greatly restricted by the number of excipients approved for lung administration by regulatory agencies such as the European Medicines Agency (EMA) and Food and Drug Administration (FDA), including Lactose, Lecithin, Mannitol and Polysorbate [31]. Furthermore, particle engineering needs high stability and good dispersibility for long shelf life. Narrow particle size distribution, low surface energy, high chemical and physical stability as well as non-spherical morphology and low density or high porosity is needed for optimal aerosol performance. Additionally, the new particle design paradigm asks for cell targeting and modified release kinetics, making particle design more complicated and challenging.

1.2.4. Lung Deposition

The pulmonary particle deposition pattern greatly influences the site of action of delivered drugs. The patient's breathing pattern and the administered aerodynamic particle size are the main parameters. Optimal aerosol performance requires reduction of the amount of powder deposited in the oropharyngeal region and increase of the amount reaching the targeted lung area.

Particles avoiding deposition in the extrathoracic region enter the lung, where inertial impaction is the main deposition mechanism in the first airway generations. With ongoing airway generation and reducing airway diameter, the flow viscosity rapidly

decreases, making gravitational deposition dominate the deposition in small bronchial airways [6] (Figure 3)

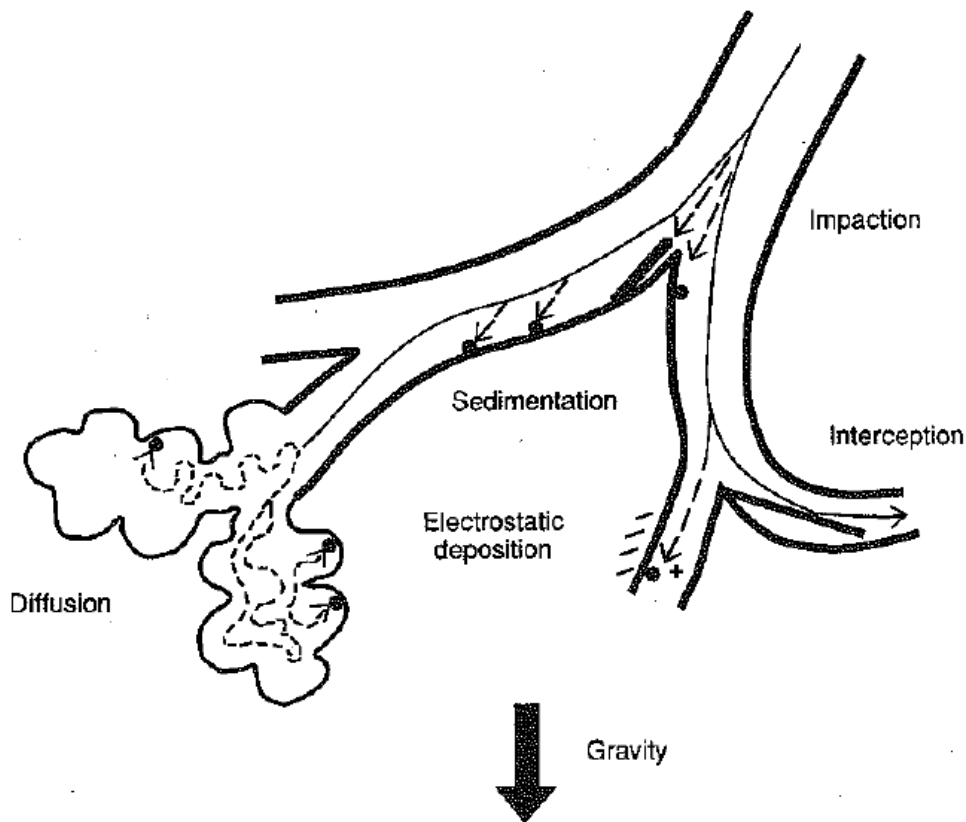


Figure 3: Primary mechanisms of deposition of inhaled particles in the respiratory tract taken from ref. [6].

1.2.4.1. Particle Deposition

Particles deposit inside the lung upon striking the mucus layer covering the conducting airways or interacting with surfactant in the alveolar region. Five main mechanisms determine the aerosol deposition pattern:

1. *Impaction* is the main deposition mechanism for particles $>1 \mu\text{m}$. The probability increases with increasing d_{aer} and airflow velocity. It is the main mechanism for extrathoracic deposition (nasal and oral cavities) as well as deposition in the large bronchi.
2. *Sedimentation* is important for particles with $d_{\text{aer}} >0.5 \mu\text{m}$ to deposit in the small bronchi, bronchioles and alveoli. Deposition by sedimentation increases

with prolonged residence time in the airways, i.e. breath hold at the end of inhalation.

3. *Brownian motion* greatly influences the deposition pattern of particles with $d_{aer} < 0.5 \mu\text{m}$. Decrease of the geometric diameter and increase of the residence time result in increased deposition by Brownian motion.
4. *Electrostatic interactions* play the dominant role for deposition of $0.1\text{-}10 \mu\text{m}$ charged particles and are most important for their deposition in small airways.
5. *Interception* is most important for fiber morphology, as it requires that the particle diameter is a significant fraction of the airway diameter. The center of gravity of an elongated particle is in the gas phase while one of its ends touches an airway wall.

The effect of particle size on the deposition pattern in the lung is shown in Figure 4. It is worth noting that particles with d_{aer} $0.2\text{-}1 \mu\text{m}$ can be exhaled and thereby have reduced deep-lung deposition [32].

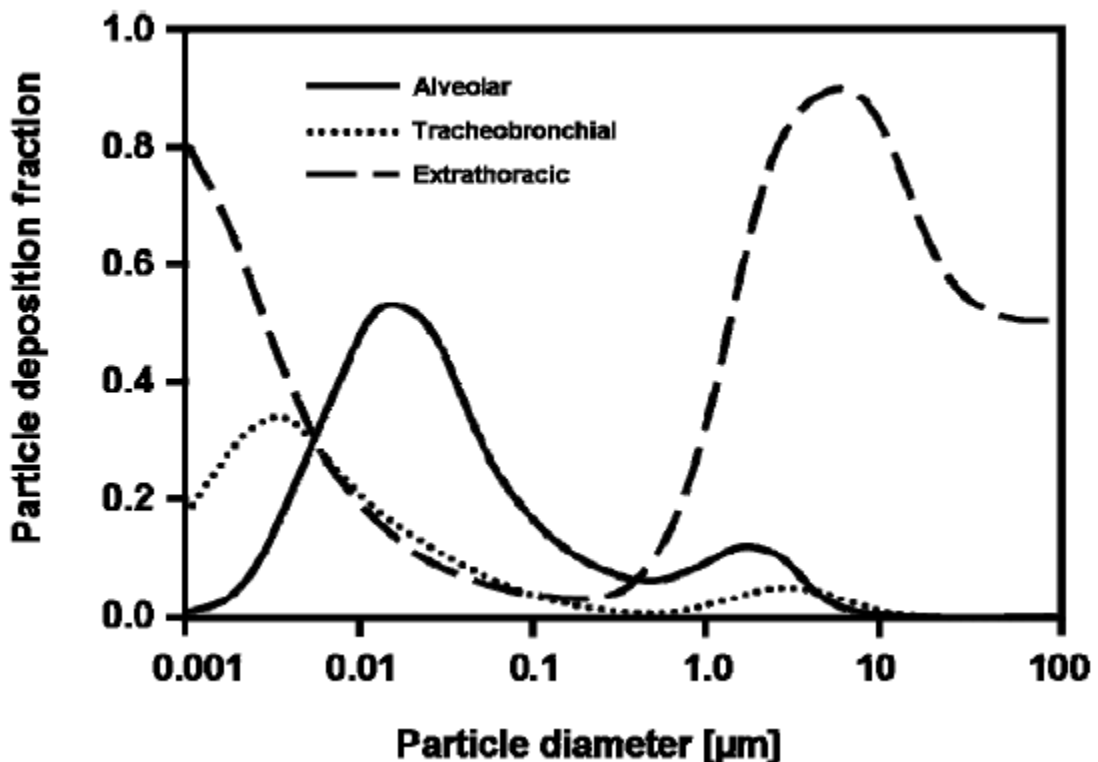


Figure 4: The effect of particle size and overall inhalation maneuver on the deposition of aerosol particles in the human respiratory tract taken from ref. [33].

1.2.4.2. Fiber Deposition

Fibers are a special class of particles, defined by the WHO in 1985 as elongated objects for which the aspect ratio – the ratio of length-to-diameter - is greater than 3 [34, 35]. The aerodynamic diameter of a fiber as main parameter for lung deposition is mainly determined by its geometric diameter, while the length is of minor impact [21, 25]. Su and Cheng [36] showed that fibers have a higher probability to reach the peripheral lung due to reduced deposition in the oral and nasal airways compared to spherical particles of the same aerodynamic diameter (Figure 5). Due to their larger volume, higher payloads can be administered.

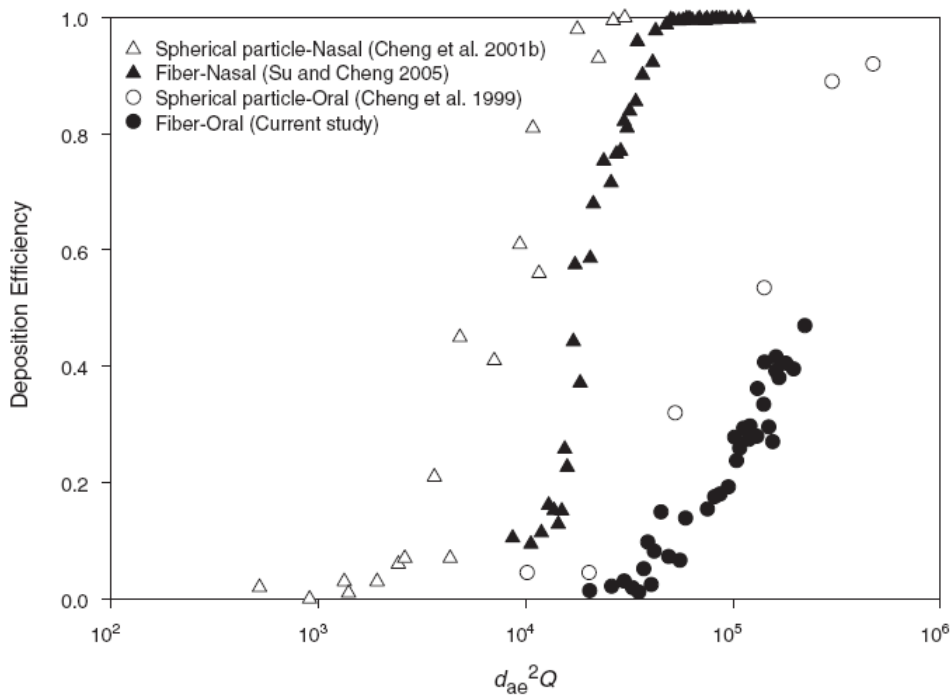


Figure 5: Comparison of the deposition efficiencies between fibers and spherical particles in human oral airway and nasal airway hold taken from ref. [36].

1.2.5. Particle Clearance

1.2.5.1. General Considerations

Particle clearance is defined as the movement away from the initial deposition location of each individual particle. During normal breathing, air, particles and microorganisms are inhaled. While bigger particles deposit in the upper airways (nose and throat), smaller particles can sediment into the lung. The mucus covered

cilia of the conducting airways and alveolar macrophages clear deposited particles to maintain in the lung a sterile environment and to protect its primary function, gas exchange [37].

1.2.5.2. Mucociliar Clearance

The conducting airways are lined by cilia containing epithelial cells and mucus producing goblet cells. Particles deposited in the tracheobronchial airways interact with the mucus layer and are cleared by two major pathways. The major pathway thereby is mucociliar clearance, where the mucus is transported towards the throat by metachronal coordinated movement of the cilia followed by swallowing [33]. The second pathway is the absorption of material across the epithelium. Most particles deposited on mucus are cleared within 24 – 48 h after deposition [6].

1.2.5.3. Alveolar Clearance

There are no cilia and no mucus in the alveoli. Alveolar macrophages (AM) are therefore responsible for phagocytosis of foreign material deposited inside the lung. Particles in the size range 0.5-2 μ m, with a maximum at 1 μ m, manifest the highest deposition probability in the alveolar region [38]. After phagocytosis, the macrophages are either removed by mucociliar clearance or penetrate into the peripheral lung. Long residence times in the peripheral lung might cause diseases (silicosis, asbestosis). A smaller fraction of particles can be cleared by AM derived transport across the alveolar epithelium membrane [6].

1.2.5.4. Outlook for Particle Formulation

Sustained drug release in pulmonary drug delivery requires prolonged residence times of particles within the lung. Thus strategies to slow down mucociliar clearance as well as to circumvent or prolong particle uptake by alveolar macrophages are required. These strategies allow release kinetics determined by the dissolution kinetics of the carrier system. Long acting formulations with reduced clearance will improve patient compliance due to increased dosing interval.

1.2.6. Multifunctional Drug Delivery

The recent times have seen an increase in research effort to design of multifunctional particles to create, improved and more complex drug delivery systems. Increased stability, prolonged in vivo circulation, desired biodistribution as well as targeting and responsive release triggered by physiological stimuli are important characteristics for drug delivery vehicles [39]. Four main components are most often desired to be incorporated (Figure 6):

1. Matrix component as basis to incorporate additional components
2. Active pharmaceutical ingredient (API)
3. Imaging domains including organic dyes and/or semiconductor quantum dots (QD) [40], as well as magnetic sub-domains (Fe_3O_4) for magnetic resonance imaging [41]
4. Targeting agent such as antibodies or magnetic sub-domains (Fe_3O_4) [42-45]

These complex particles will be the next generation of drug carriers, which can be used as therapeutic and/or diagnostic agents, named theranostics, and offer the possibility of simultaneous targeted drug delivery of various agents combined with triggered release kinetics [46].

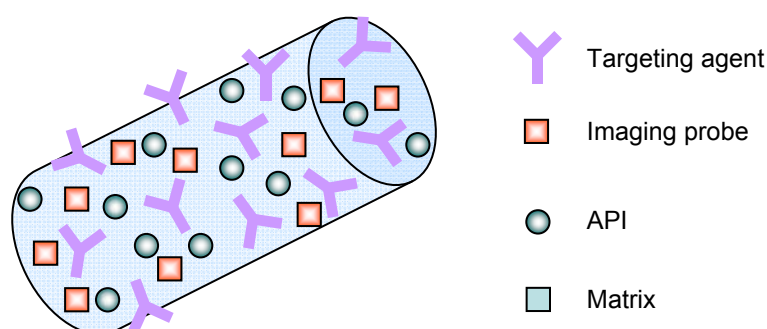


Figure 6: Multifunctional particle containing multiple sub-components such as API, Fe_3O_4 particles, imaging probes and targeting agents (i.e. antibodies).

1.3. *Asymmetric Particles in Vivo*

Recently, elongated particles have been rapidly emerging in biomedical and biotechnological applications. Aspects about distribution and interaction pathways of asymmetric particles are still not clearly understood due to limited availability of model particles for intensive studies under controlled conditions. Increased blood circulation of filomicelles were reported lately [47, 48], as well as shape induced inhibition of phagocytosis [25]. New synthesis strategies are therefore urgently asked for.

1.3.1. General Considerations

Asbestos and carbon nanotubes (CNT) represent a group of microfibers widely used in material science due to their good isolation and electrical properties. Asbestos was extensively used in the 20th century during house construction and many other application fields. After the confirmation in 1970 that long term inhalation of Asbestos can cause malignant lung cancer (mesothelioma), the European Union banned all use of asbestos. CNT show dimensions comparable to Asbestos, and are therefore under suspicion to possess comparable health related effects. Due to the fiber structure and biopersistence Asbestos and CNT exhibit high lung deposition, thereby causing inflammation and lesions in membrane cells.

Asbestos describes a group of hydrated silicate fibers and can be divided into six types based on their different chemical and physical properties, namely chrysotile, crocidolite, amosite, anthophyllite, tremolite and actinolite [49]. Asbestos as natural occurring silicate shows high heat resistance and has been therefore widely used for isolation [50]. Due to its fibrous structure it can be easily incorporated into cement materials, brakes, pipes and boiler insulation, making it an ideal material for large scale use [51]. Upon ongoing exposure a pandemic of lung diseases in the middle of twentieth century developed [52], resulting in a deep mistrust in fibrous particles that are small enough to be inhaled. During the last decade, carbon nanotubes, rolled up graphene sheets, gained increased attention for their use in medicine, electronics and aerospace industries due to its shape, electrical, mechanical and thermal properties [53]. CNT comprise various types of cylindrical carbon forms, differing in

shape and/or chemical composition, thereby showing different in vivo response. Again the toxicology and health effects of such nano-sized fibers are widely discussed in literature, trying to avoid another upcoming pandemic caused by fibrous material.

1.3.2. Carbon-Nanotubes

CNT are composed of a single sheet of graphite rolled up to form a cylinder, and are classified into two categories, multi-walled carbon nanotubes (MWCNT) and single-walled carbon nanotubes (SWCNT). The length of CNT is determined by the synthesis time, while the diameters of the SWCNT are controlled by the starting metal nanoparticles, varying between 0.8 – 3nm for SWCNT and 10-200nm for MWCNT [54].

The pathogenicity of fibers is influenced by various parameters, where the three Ds: dose, dimension and durability of fibers have the highest impact. The fiber dimensions show a major impact on the deposition pattern inside the lung as well as on the clearance kinetics. Thereby CNT bundle held together due to attractive Van der Waals forces will have a modified deposition pattern compared to well dispersed single nanotubes [55]. The higher the administered dose, the higher the fibrosis incidence is. Durability of fibers inside the lung is mainly influenced by the fiber dissolution kinetics. The higher the dissolution kinetics, the lower the toxicology profiles will be [56] as well as the clearance by mucociliar action or phagocytosis. Furthermore chemical and surface properties will influence the toxicity profile of fibers inside the lung.

Two factors mainly contribute to the airborne fiber toxicity, namely the surface area and surface reactivity [57]. CNT contain impurities on the fiber surface caused by their synthesis strategy, metals like Co, Fe or Ni, of which some are also present in asbestos, contribute to their toxic effect. Due to the increased surface area per unit mass for nanoparticles, any intrinsic toxicity of present impurities will be emphasized [58].

1.3.3. Health Effects

Shortness of breath and dry cough are most common symptoms of asbestosis due to the restrictive defects and the decrease in diffusion capacity [59]. Fibers such as asbestos cause fibrosis and cancer either due to the direct effects of fibers on cells or as a result of oxidative stress from fibers on the inflammatory response. Asbestosis and silicosis are both characterized by a persistent inflammatory response. The development of asbestosis requires a prolonged exposure to fibrous material; further factors governing the appearance of the disease are the fiber dose, fiber type and smoking. Only above a threshold concentration asbestosis will occur [60].

Inflammation and fibrogenesis caused by fibers can be linked to their surface chemistry as an important driving force for oxidant production and additional harmful reactions in the lung. Due to the length of fibrous materials, frustrated phagocytosis by alveolar macrophages can occur, resulting in release of proinflammatory markers [60]. Inflammation can result in numerous pathological processes such as fibrosis, airway diseases or cancer [61].

Fiber accumulation in the lung is caused by inefficient phagocytosis by alveolar macrophage and insufficient degradation under physiological conditions of fibers and thereby their clearance from the lung [54]. Further Davis and Jones [62] showed that longer fibers were more fibrogenic than short fibers, which can be explained by the slower clearance kinetics by macrophages above a threshold of $\sim 16 \mu\text{m}$ [63], by the increased surface area and high aspect ratios [64].

Due to the inflammatory effect and resulting severe lung diseases (i.e. fibrosis and cancer), fibers of inhalable size should undergo extensive toxicological testing before large scale use.

1.3.4. In Vivo Circulation

Increased in vivo residence time is desired for prolonged drug delivery, in order to provide sufficient time for complete drug release. Filomicells show ten times longer blood circulation times compared to spherical particles [47], by this demonstrating the importance of the drug carrier shape. Increased mucoadhesion in the gastro

intestinal tract (GI) of glass beads, where the long nanowires provided the greatest adhesion was demonstrated by Fischer et al. [65]. This effect could be explained by increased Van der Waals forces in combination with increased surface area, which can also be found in gecko feet [66]. Mucoadhesion in the lung would result in decreased mucociliar clearance, by this enabling prolonged drug release in pulmonary delivery.

1.3.5. Macrophage Clearance

Target geometry plays an important role during macrophage recognition, being the first step in target elimination [67]. During phagocytosis, Fc receptors are responsible for initial recognition by binding to antibody coated targets [68]. The binding of ligands to the Fc receptors causes activation of intracellular signalling cascades, resulting in formation of an actin cup, which is essential for phagocytosis. Polymerization of actin into coordinated structures promotes the membrane to push around the particle to start and finalize phagocytosis [69]. Particle shape can affect the ingestion process, while particle size can influence the efficiency of uptake and the extent of actin organization [70, 71]. Champion et al. compared macrophage uptake of spherical particles with worm shaped particles, where the internalization of worms was up to ~20 times slower than that of spheres of the same volume [20, 25].

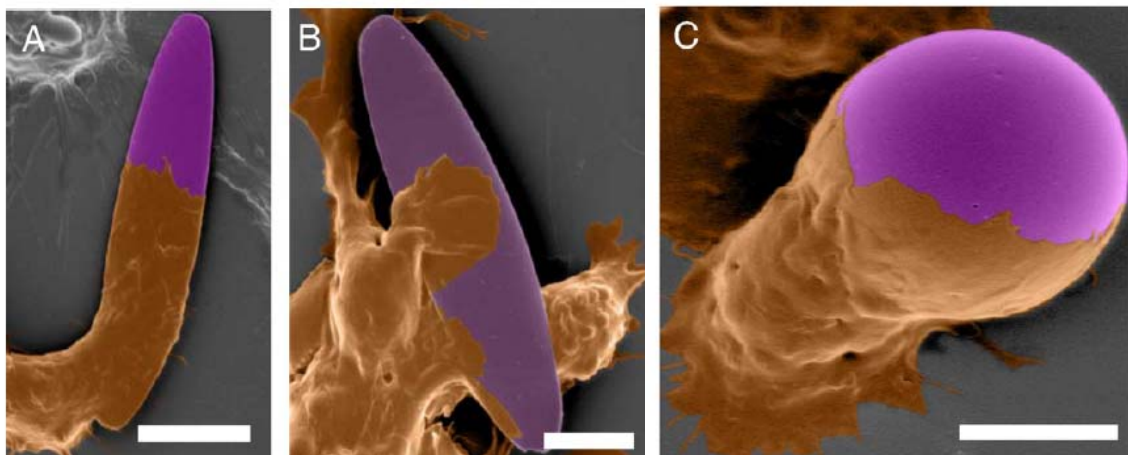


Figure 7: Coloured scanning electron micrograph of alveolar macrophages (brown) interacting with PS particles (purple). Scale bar = 10 μ m (a) and 5 μ m (b,c) respectively hold taken from ref. [69].

Investigation of the target shape at the point of first contact with macrophages and by this the incidence angle between macrophage and particle determines whether

macrophages will only spread on the particle surface or if an actin cup for phagocytosis will be formed. Elongated particles were only taken up from the pointy edge (Figure 7). Furthermore, the particle size was found to be the predominant parameter to influence successful phagocytosis when the target volume is smaller than the macrophage volume [72] (Figure 8).

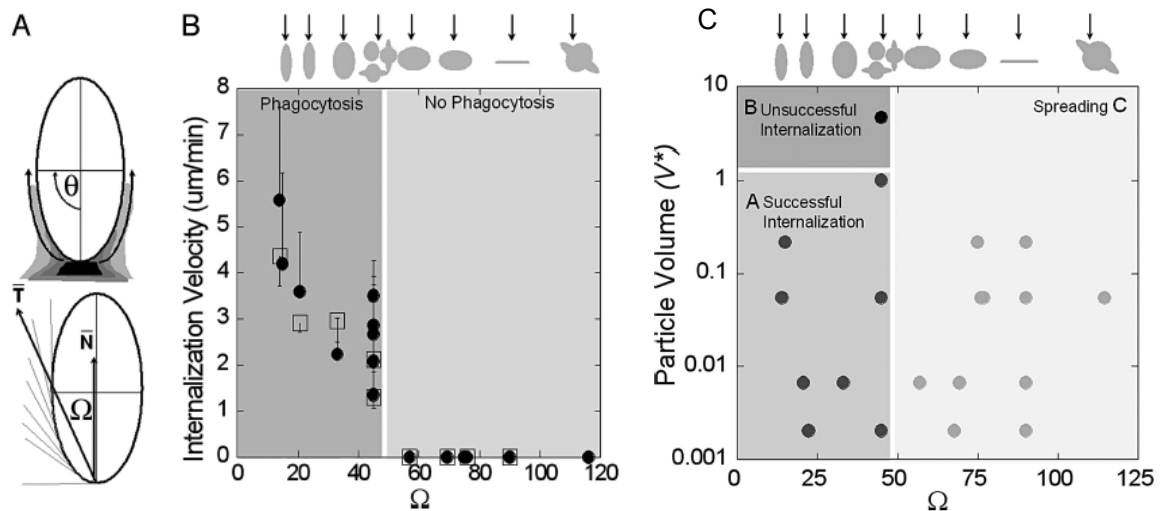


Figure 8: Role of target geometry in phagocytosis hold taken from ref. [72].

1.4. Asymmetric Particle Preparation

1.4.1. State of the Art

To date, polymeric nano-fibers and nano-tubes for therapeutic lung targeting have had limited importance. Polymeric nano-fibers and nano-tubes can be manufactured both by methods of self organization and by means of template procedures. The preparation of polymeric nano-fibers and nano-tubes by template procedures permits, contrary to the methods of self organization the custom-made tuning of physical, chemical and biological characteristics of the aimed structures and thus renders a larger range of variation.

Up to date, four methods are mainly used to synthesise nanofibers or nanotubes, as described below: electrospinning, co-electrospinning, TUFT process and the template technique.

1.4.2. Electrospinning

Electrospinning is an efficient technique for polymer fiber fabrication, as it allows the production of continuous fibers from various polymers [73]. During the electrospinning process, a high voltage of several kV is applied onto the spinning solution, where the positively charged electrode is submerged in the solution and the negatively charged electrode is located at the collector plate. The spinning solution forms a droplet at the outlet capillary due to surface tension. By applying the electric field, charging of the droplet occurs. Increasing the electric field leads to the elongation of the droplet the moment the electrostatic repulsion overcomes the surface tension [73], by this forming a charged jet which is ejected from the tip. During spinning the jet is exposed to circular bending motions causing strong elongation and jet thinning [74]. The solvent evaporates during the spinning process, and dried fibers can be collected on the collector plate (Figure 9).

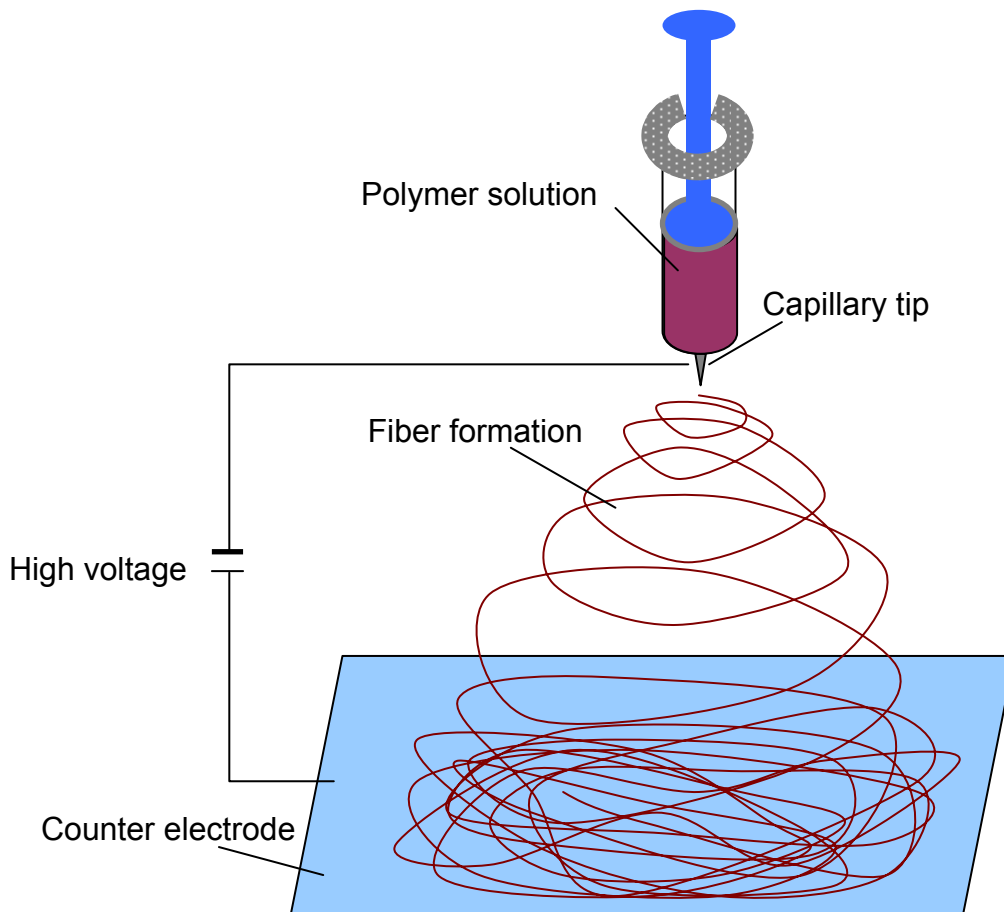


Figure 9: Schematic diagram for electrospinning (modified from www.dfg-nanohale.de).

The main process parameters influencing the product quality are the solution properties, mainly viscosity, surface tension, elasticity and conductivity. For example

higher viscosity will result in larger resulting fiber diameter [75]. Additionally, the electric potential at the capillary tip has a major impact on the fiber diameter, as with higher voltage more fluid will eject from the tip. Furthermore the tip-collector distance determines the diameter and fiber morphology [73]. A precise parameter control is necessary in order to avoid bead and defect incorporation during spinning.

Continuous fibers with dimensions within the range of several micrometers down to a few nanometers can be obtained. Drugs can be incorporated directly into fibers by electrospinning [76]. The infinitely long fibers have to be cut prior to drug delivery to a given length by mechanical methods or by UV cutting, respectively.

Co-electrospinning allows for the incorporation of nanoparticles (NPs) and functional polymer segments [73], by blending the spinning solution with NPs [77].

A major drawback of electrospinning is the burst release of incorporated drugs. Furthermore no precise control over the fiber length is possible during the spinning process.

1.4.3. Tubes by Fiber Template (TUFT)

The TUFT process uses fibers as templates to create fibers with diameters between ten nanometres and a few micrometers. The crucial step is the formation of the template fibers, which are mainly formed by electrospinning [78]. The template fibers are coated by means of vapour deposition, dipping processes, spraying procedures or by processes involving plasma treatment [74]. Hollow fibers can be produced using this technique by removing the template fiber by solvent or annealing after desired material deposition, yielding hollow fibers (Figure 10).

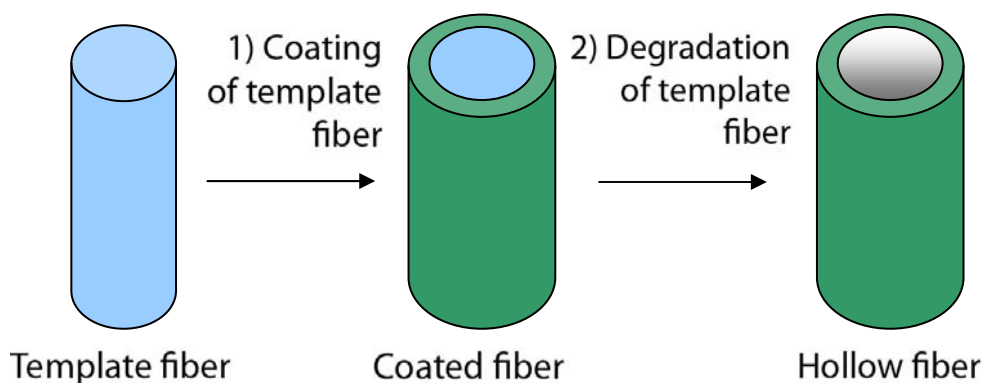


Figure 10: Schematic diagram of the TUFT process.

1.4.4. Template Technique

The template technique is a well established method to produce nanorods and nanofibers of defined dimensions [79-85]. A hard membrane with straight pores is used as template, where the pore diameter and membrane thickness define the resulting microfiber dimension (Figure 11). Infiltration of the desired material with subsequent template decomposition yields tubes and rods with defined aspect ratios. Martin established the method by infiltration of monomers and subsequent oxidative polymerisation, before Steinhart et al. extended the infiltration procedure to polymer melts and solutions [79, 82-85]. Nowadays various approaches for material deposition onto the membrane pore are reported in literature. Wetting [83-86], chemical vapour deposition [87], electrodeposition [80], layer-by-layer (LbL) [88-94] and in situ polymerization are only few to mention. Tubes have been synthesized for various applications [95], such as drug delivery [96, 97], bioseparation [98], DNA delivery [99-101] and MRI imaging [40, 102]. Template degradation yields liberated nanostructures.

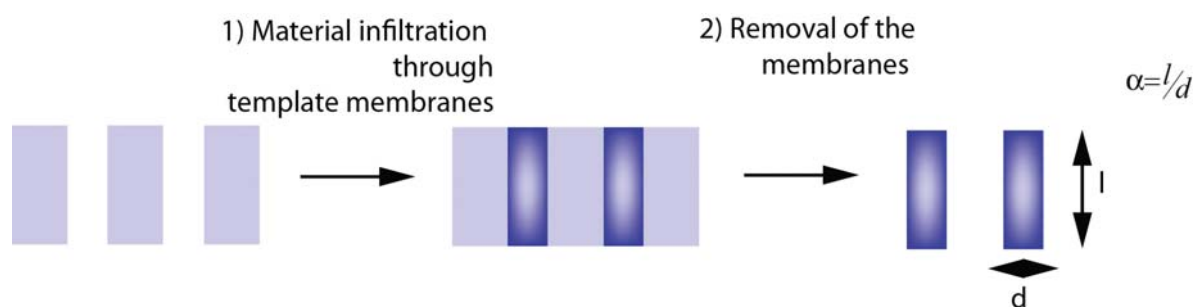


Figure 11: Schematic diagram of the template technique.

To circumvent the template decomposition and thus overcoming a bottleneck of the template technique, Grimm et al. [103, 104] invented a non-destructive mechanical release procedure allowing for later scaling-up of the template technique.

1.4.4.1. Template Fabrication

Template fabrication is a crucial step during fiber fabrication using the template technique, as the resulting fibers are negatives of the pore structure. Commonly two types of membrane are used, containing straight pores of cylindrical shape, namely track-etched polymer membranes and nanoporous anodic aluminium oxide (AAO) [105]. The more uniform and higher the pore density, the greater the number of well

structured fibers produced per template membrane [80]. Both membrane types are commercially available, having advantages and disadvantages for the fiber preparation as discussed below.

1.4.4.1.1. Anodization

Masuda and Fukada [106] first described the two step electrochemical etching of Al_2O_3 -structures with ordered pore orientation containing straight pores with monodisperse diameter ranging from 20 nm-4 μm (Figure 12).

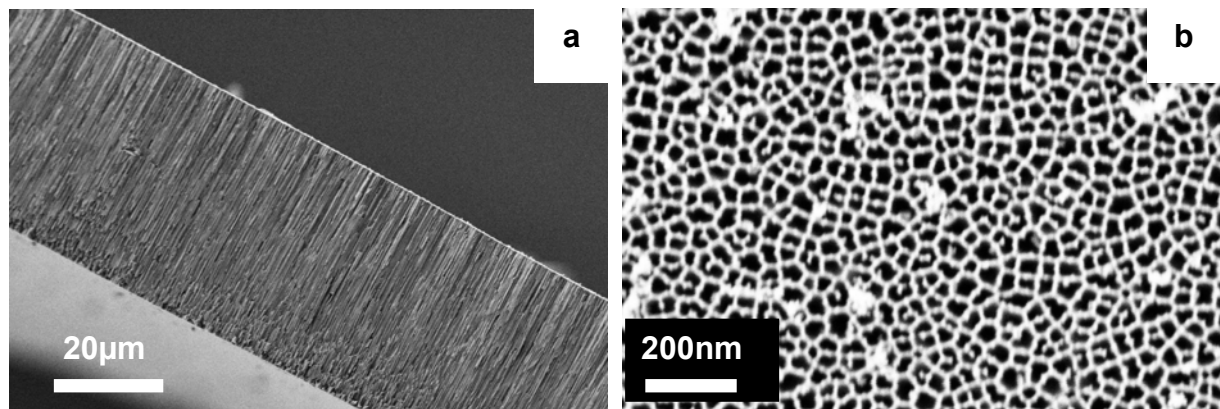


Figure 12: Scanning electron micrographs of a) cross-section and b) top of a commercially available anodically etched alumina membrane.

The electrochemical growth of aluminium oxide from aluminium metal in acidic media [107, 108] is a four step process as depicted in Figure 13. First a uniform barrier of oxide is formed on the aluminium substrate. Due to fluctuations at the Al_2O_3 surface, field-enhanced dissolution of oxides occurs in the oxide layer [109]. Pore growth originates from these fluctuations and the field strength focus. Thickening of the film at the protuberances concentrates the current. The film growth attempts to reach uniform film thickness in order to maintain constant field strength [110]. O^{2-} and OH^- ions produced by splitting of H_2O at the oxide-electrolyte-interface migrate across the metal and react at the metal-oxide-interface with generated Al^{3+} ions. An equilibrium state of oxide formation and field-enhanced dissolution of alumina at the pore bottom leads to homogeneous pore growth at the pore openings, limited by the chemical dissolution kinetics.

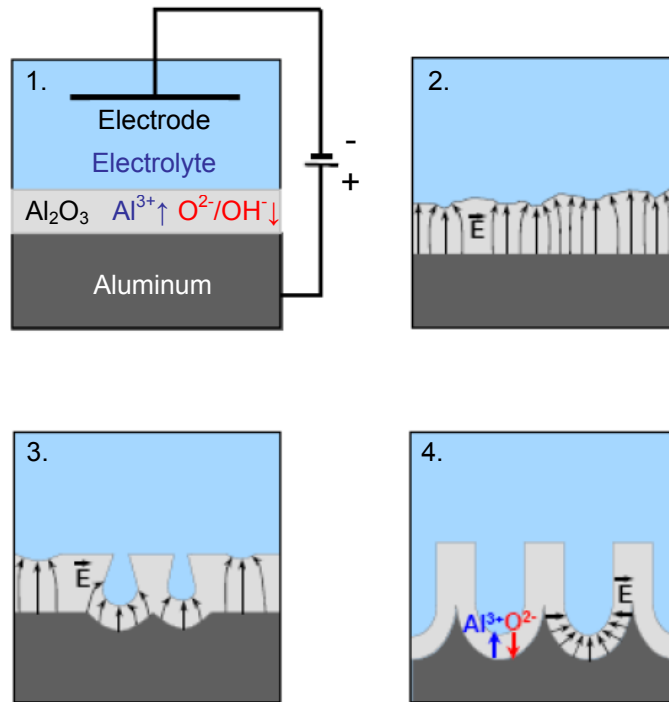


Figure 13: Schematic configuration of pore growth: 1.) growth of barrier-oxide; 2.) formation of fluctuations; 3.) beginning of pore growth; 4.) stable pore growth taken from ref. [111].

For templating AAO membranes have the advantage to be heat stable and resistant to organic solvents allowing for material infiltration at elevated temperatures and pore filling of organic materials using organic solvents [105]. Commercially available AAO suffer from the non-uniformity of their pore-structure. Many pores are interconnected and do not show homogenous hexagonal orientation (Figure 12). These membranes are sufficient for proof of concept studies, but for more detailed structure analysis of prepared tubes, tailor-made membranes should be used [111]. AAO membranes form tubular structures during etching, comparable to microfibers produced by the template technique [89, 112]. The chemical identity of microfibers prepared by the template technique in AAO membranes should therefore be confirmed by different types of measurements, such as XRD, additional to SEM investigations.

1.4.4.1.2. Track Etching

The track etch method was first described by Fleisher et al. [113]. Nonporous sheets of desired material are bombarded (“tracked”) with ion beams, producing latent tracts within the material [105]. During bombarding new polymer chain ends and other chemically reactive sites are formed, as fast charged particles eject electrons from

atoms close to their path. Pore formation occurs during wet chemical etching of the produced latent cracks (Figure 14) [80]. Pore diameters down to 10nm can be obtained by track etching, and pore densities of up to 10^{10} pores per square centimetre, where the pore diameter and density can be varied independently. As the incident ion beams form an angle of up to 34° with respect to the surface normal, pores may intersect inside the membrane [114].

Polycarbonate is mainly used as track etched membrane for template synthesis [80, 97, 99, 115-117]. Due to interconnected pores, cross-linked particles during template synthesis may occur. Furthermore the use of track etched membranes is restricted by their limited heat resistance and instabilities in organic solvents.

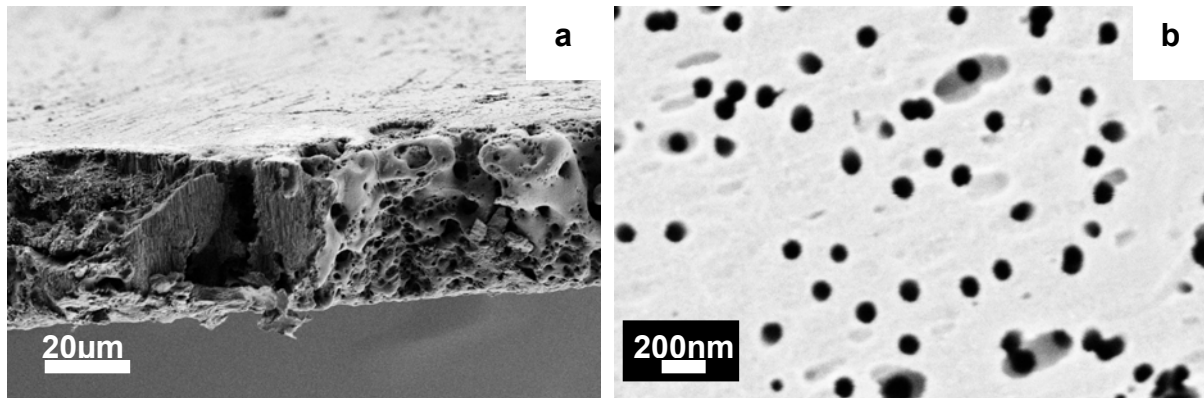


Figure 14: SEM images, a) cross-section and b) top of a commercially available track etched polycarbonate membrane.

1.4.4.2. Infiltration

A variety of strategies have been developed to deposit material inside template membranes in order to synthesise fibers and tubes of defined dimension. Wetting [83-86], electrodeposition [79, 80, 118, 119], layer by layer (LbL) [88, 89, 91-94, 120] and in situ polymerization are only few to mention [114].

Martin et al. [80] first described the use of AAO membrane pores as template for electrodeposition. By coating one side of the membrane with a metal film, a cathode for electroplating of metal nanowires (i.e. Au, Ni) is formed. The length of the resulting metal nanowires can be precisely controlled by the deposited amount, where the deposition time mainly influences the resulting wall thickness [80, 114].

The material growth on the pore walls can thereby be explained by formation of polycations, resulting in solvophobic interactions between the polymer and the pore walls. Nowadays also conductive polymers (i.e. polyanilin and polypyrrol) can be used to form tubes by electrodeposition [121, 122].

Besides electrodeposition, polymerization can be used for material infiltration into membrane pores, by immersing the membrane into a monomer solution containing the polymerization agent. As the polymers preferentially nucleate and grow in the membrane pores, short deposition times result in tube formation, while increased deposition times yield solid fibers [121, 123].

Template wetting as infiltration technique allows the infiltration of a broad range of materials. Up to now, it is poorly understood as many parameters influence the rod- or tube formation during the infiltration process. The wetting process can be represented by capillary wetting and precursor wetting, both being two different kinetic routes to the equilibrium of pore wetting, which is characterized by complete filling of the pores with polymer [124]. Due to wetting of a substrate with liquid, the surface energy of the substrate will be lowered, resulting in free energy as driving force of the wetting procedure [111]. Therefore the parameter determining the wetting mechanism is the energetic and entropic energy required to remove the polymer chains from the bulk reservoir and draw them into the pores.

Interfacial interactions dominate the infiltration process. According to Young's law

Equ. 2:
$$\cos \theta = \frac{\gamma_{SV} - \gamma_{SL}}{\gamma_{LV}}$$

with γ_{SL} = interfacial tension of solid-liquid
 γ_{SV} = surface tension of the substrate
 γ_{LV} = surface tension of the liquid
 θ = contact angle

the surface energy of the substrate, the surface tension of the liquid and the liquid-solid-interfacial energy determine the contact angle at the liquid-vapour-solid

interface [105]. A zero contact angle is equivalent to the spreading of the liquid, resulting in maximization of the liquid-solid contact area [125]. Therefore wetting occurs when adhesion forces acting between liquid and surface are larger than cohesion forces inside the liquid.

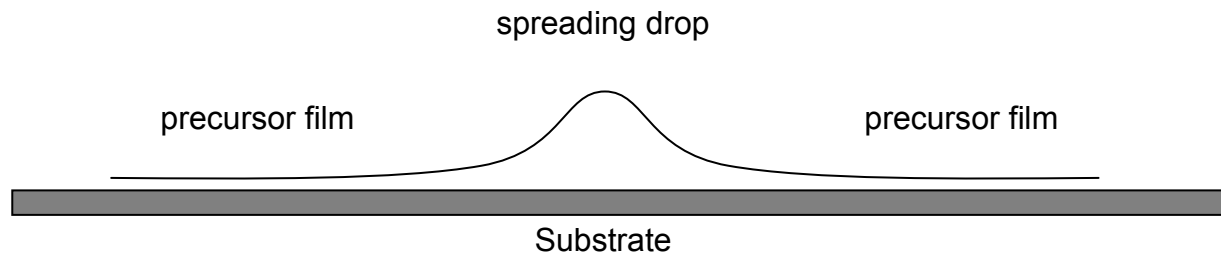


Figure 15: Schematic diagram of a liquid drop spreading on a smooth substrate taken from ref. [105].

Low surface energy melts spread on high surface energy substrates by the formation of a precursor film of nanometer thickness [84, 85, 125] (Figure 15). With ongoing spreading more and more liquid is transferred into the precursor film, where Van der Waals forces are the underlying driving force for wetting of the complete pore within tens of seconds [83]. The wetted state is kinetically stable, but thermodynamically instable. The cohesive forces needed for complete pore filling are weak and need to overcome the considerably strong viscous forces of the wetting fluid.

If the infiltration conditions do not allow for precursor film formation, filling via classical capillarity proceeds [105]. As the strong adhesive forces are too weak to drive single molecules from the bulk reservoir to form the spreading precursor film, a meniscus is formed and slowly moves into the pores. A solid cylinder of the liquid but viscous polymer moves until the pore is entirely filled [126]. During solvent evaporation the polymers adsorb onto the pore walls, where the polymer concentration is the crucial parameter determining whether solid or hollow tubes are obtained [127]. Precursor wetting occurs for low molecular weight polymers, while capillary wetting takes place for higher molecular weight polymers [86, 105]. Solid polymers melt by heating well above their glass transition temperature and wet high surface energy pore walls via precursor wetting [124]. Besides the molecular weights of infiltrated polymers and infiltration temperature, the pore diameters of template membranes influence the structure of the resulting particle. The pores with diameters

twice smaller than the gyration radii of the infiltrated polymers result in complete filling of the hollow space of the pores, thus yielding solid rods [128, 129].

Tubes and rods are obtained either by cooling polymer melts below their solidification temperature, or via solvent evaporation, allowing processing of high performance polymers like PTFE [85].

The layer by layer technique offers an additional method for material infiltration into template pores. By this technique, a nanoscopic multilayer system with precisely controlled layer composition can be obtained [105]. LbL offers the advantages of being a well established, simple, versatile and low-cost strategy technique on flat surfaces [117]. The assembly process details will be discussed below.

1.4.4.3. Layer by Layer Technique

The layer by layer (LbL) technique has been developed for fabrication of multilayers of tailored architecture by alternate adsorption of polyanions and polycations [130]. By dipping a charged substrate alternating into aqueous solutions of oppositely charged polyelectrolytes, the polyelectrolytes are deposited LbL onto the substrate [131, 132] (Figure 16). The electrostatic assembly process is driven by the gain in entropy due to the release of counterions [133], where electrostatic repulsion restricts polyelectrolyte adsorption to a single layer [111, 134]. This opens the possibility for oppositely charged molecules to adsorb during the next deposition step, allowing controlled build up of multilayers. Due to charge reversal during each adsorption step, the number of deposited layers can be unlimited. Film thickness can therefore be tuned by the number of adsorbed layers [91], each having a thickness determined by the deposition conditions, ranging between several angstroms and few nanometers [135]. As the process is solution based, the choice of the substrate is not limited by the surface size and/or morphology [99]. The LbL technique has been extended for coating spherical particles as substrates [136-138]. Nowadays spherical particles are widely used in preparation of hollow polyelectrolyte capsules by core dissolution after polyelectrolyte assembly.

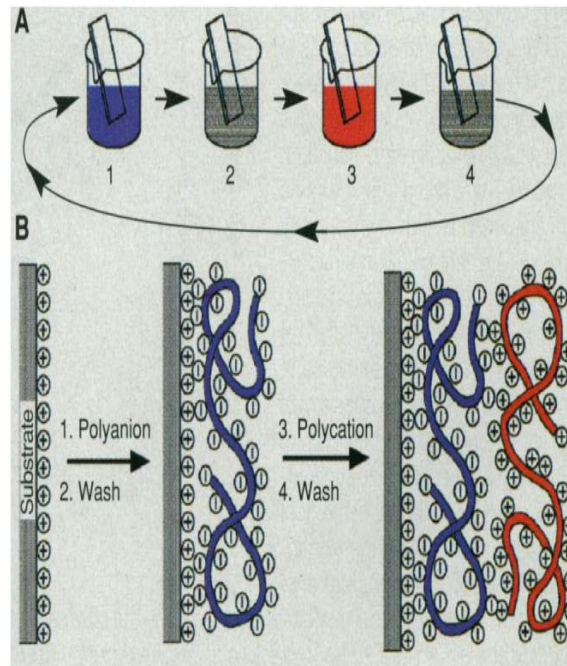


Figure 16: Schematic diagram of the layer by layer technique taken from ref. [130].

The interactions to apply the LbL technique have been extended from electrostatic interactions to various kinds of interactions, including H-bonding [93], hydrophobic interactions and amide bonds. By this a broad range of materials including biological macromolecules [139], dyes [140] and nanoparticles [141] can be incorporated. The easily prepared multilayered films of various compositions allow control of the permeability and physicochemical properties of the multilayers [142, 143]. Besides dipping, multilayer build-up can be prepared using spraying [144] or spin coating [79], opening for more time-efficient assembly processes. The versatile, fast, and simple preparation with a broad variety of materials being used allows the application of LbL in various fields, such as drug delivery, implant coating and many others [117].

1.4.4.3.1. Polyelectrolytes

Polyelectrolytes are charged polymers. They can be divided into polycations bearing positive charges and polyanions with negative charges. Polymers containing both positively and negatively charged segments are polyampholites. Most prominent natural occurring polyelectrolytes are proteins and DNA.

Polyelectrolytes, although having a hydrophobic backbone, are soluble in water due to the gain in entropy by the release of counter ions into solution [145]. The

polyelectrolyte properties depend on the fraction of dissociated groups, solvent quality for the polymer backbone and the salt concentration. Polyelectrolytes, with ionization degree independent of the environmental pH are regarded as strong polyelectrolytes. In contrast, weak polyelectrolytes show pH dependent ionisation, and the ionization degree can be described by the Henderson-Hasselbalch-equation

Equ. 3:

$$pK_a = pH + \lg\left(\frac{c(HA)}{c(A^-)}\right)$$

On account for the non cooperative interactions between neighbouring groups, an apparent pK_a is defined, as unprotonated groups with charged neighbours have higher effective pK_a compared to groups with non charged neighbours, resulting in broadened titration curves [146].

Due to the electrostatic interactions, polymer conformation in solution is largely determined by the ionic strength of the solution. Free ions assemble onto charged groups, thus screening charges along the polyelectrolyte chain. The electrostatic repulsion along the chain decreases at high salt concentrations allowing polyelectrolytes to behave as uncharged polymers, leading to coil formation. At low ionic strength the repulsion between the charges of polycation or polyanion is large, thus stretching the polymer.

1.4.4.3.2. Layer by Layer Self Assembly

Ladam et al. [147] introduced the zone model to describe multilayer formation during LbL formation. Multilayered films can be divided into three zones, where the borders between the zones are not sharp but gradual [131] (Figure 17).

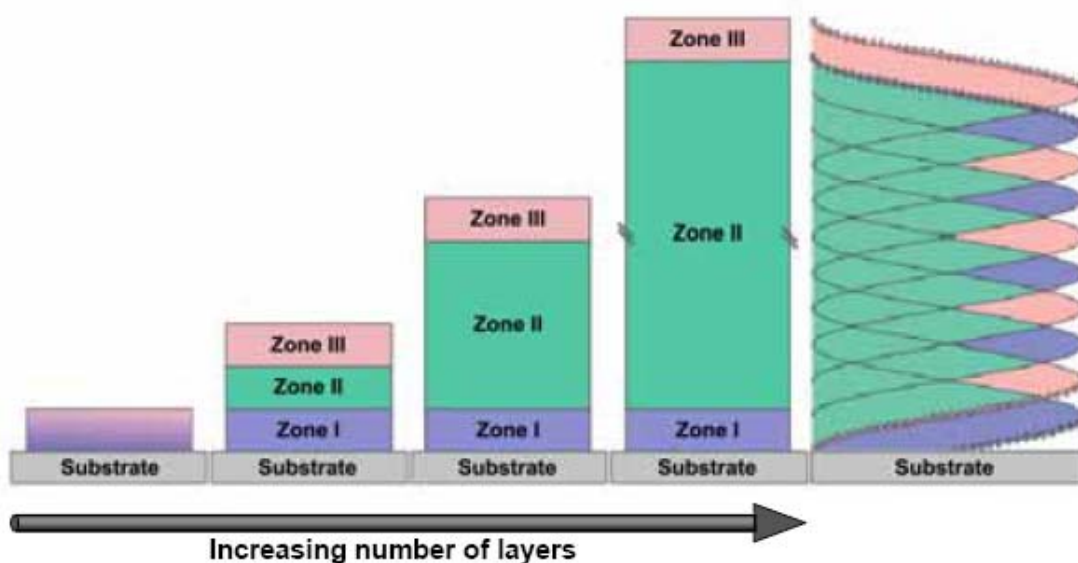


Figure 17: Schematic diagram of the zone model of polyelectrolyte multilayer assembly. The concentration profile on the right depicts the strong overlap between adjacent layers taken from ref. [131].

Zone I describes the precursor zone located closest to the substrate. The layer structure is thereby influenced by the solid substrate, resulting in slightly decreased layer thickness in zone I compared to the bulk film.

Zone III is the outer zone being in contact with the solution. Polymer chains dangle into solution and excess charges determine the local zone properties [145].

Zone II is referred to as the bulk phase. During polyelectrolyte adsorption only this layer grows after zone I and III reached their final composition. The newly deposited layer will be adsorbed onto the outermost layer comprising zone III, and thus the transition zone between II and III will move up layer by layer [147].

Multilayer thickness depends on various parameters such as the substrate composition, polyelectrolyte properties, and the deposition conditions. The choice of polyelectrolytes mainly impacts upon the growth regime, due to the impact on penetration depth for diffusing polyions. Exponential growth of multilayers can be observed during the development of zone III, where the amount of deposited polyelectrolytes increases with ongoing assembly. After a critical thickness is reached, determined by the choice of assembled polymers, the penetration depth of

polyions is limited, resulting in linear growth of zone II. The diffusion depth thereby influences the extent of layer interpenetration [131, 145].

By variation of the ionic strength [148], precise control over the layer thickness can be achieved. High ionic strength mainly influences the polymer coil conformation in solution. Due to shielding of charges, polymers arrange in low gyration radii. During adsorption of coiled polymers onto the substrate surface, increased layer thicknesses are obtained, accompanied by increase in surface roughness [149]. The rearrangement of chains after multilayer assembly is hindered by the kinetic stability of the multiple ionic bonds formed between highly interconnected polymers.

The film structure can be modified by high ionic strength [150]. Rearrangement of polyions can be promoted by high ionic strength. Due to the screening of charges by small ions, smoothening and additional interdiffusion of polymer chains can be observed [151]. Very high ionic strength films that are not stabilized by additional interactions, such as hydrophobic or H-bonding, are decomposed due to loosening of electrostatic interactions [152].

Weak polyelectrolytes can be assembled into multilayers. These films show pH sensitivity, since upon pH changes the ionization degree of weak polyelectrolytes is affected [133, 153]. The generation of electrostatic repulsions between the layers leads to restructuring of the film network, and thus to swelling, roughness changes or decomposition, making weak polyelectrolytes suitable building blocks for sacrificial layers [145, 154-156].

Temperature also influences the internal structure of multilayer assemblies. Köhler et al. [157] showed that polyelectrolyte capsules shrink in aqueous environment upon heating. Shrinkage is accompanied by an increase of wall thickness.

The responses of multilayered films to external stimuli [158] render the LbL technique a versatile method for drug delivery application.

1.4.4.3.3. Layer by Layer Infiltration

Ai et al. [88] first reported the infiltration of PAH/PSS into pores by means of the LbL procedure, obtaining nanotubes whose mechanical stability mainly depend on the number of deposited bilayers. Proteins incorporated into tube walls show increase in activity after nanotube release [105]. Nanotubes prepared by LbL infiltration into template pores found their first application as reversible pH-induced hysteretic gating [159] as well as in protein analysis [160].

Ai et al. [88] discovered that PAH/PSS tubes assembled in $0.2\ \mu\text{m}$ AAO membranes yielded wall thicknesses of a magnitude larger compared to film thicknesses obtained on flat surfaces. The same effect was reported by Lee et al. [161]. Due to these findings, Alem et al. [162] investigated the growth mechanism for polyelectrolytes inside confined space, proposing an enrichment of polyelectrolytes inside pores, resulting in a dense and swollen polyelectrolyte gel filling the pores. Roy et al. [117] further investigated the impact of pore size, molecular weight and the ionic strength on the adsorbed layer thickness, the polyelectrolyte-pore wall-interaction and the chain diffusion rate inside the pores. Two growth regimes were observed, where the first comprises linear growth with a bilayer thickness comparable to flat surfaces including the influence of ionic strength. The second regime is slower in terms of kinetics resulting from interconnections between polyelectrolyte chains across the pores leading to a dense gel (Figure 18).

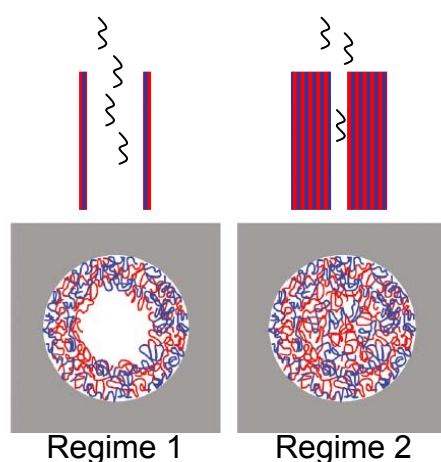


Figure 18: Schematic diagram of polyelectrolyte infiltration regimes, with free polymer diffusion in regime 1 and decreased diffusion rate in regime 2 due to gel formation.

In the first growth regime free diffusion of the infiltrated polymer is possible, as the pore diameter is large enough compared to the hydrodynamical radius of the polymer chain. If 70% of the pore diameter is filled by assembled polyelectrolyte multilayers, infiltrating polymer chains establish interconnections across the pore. This entanglement increases with ongoing deposition cycles resulting in dense gel formation. The formed gel slows down the diffusion rate and therefore polyelectrolyte multilayer growth. Even though the influence of ionic strength and the molecular weight in the second growth regime could not be confirmed in the study by Roy et al. [117], both parameters influence the polyelectrolyte conformation and may therefore have an impact on the gel formation.

2. Aim of this Work

Aerosolization and the deposition site are mainly influenced by the particle size and morphology. Additionally, pulmonary clearance mechanisms affecting the particle retention inside the lung and their release properties can also be modified by particle dimensions. Thus by optimizing the deposition pattern and circumventing the clearance from targeted lung areas, particle engineering aims for targeted drug delivery systems [9]. As particle shape may allow for drug delivery to specific cell types leading to targeted drug delivery, side effects due to untargeted delivery can be reduced.

The aim of this work was to develop a new and versatile method to produce biodegradable, biocompatible fibers for controlled drug delivery. These fibers shall allow for optimized particle deposition in the peripheral lung and furthermore shall minimize macrophage clearance to allow for systemic and/or retarded aerosol therapy.

The major aims of this thesis were:

- 1.) To develop a new and feasible method to produce biocompatible, biodegradable fibers via the template technique.
- 2.) To test the macrophage response on fiber shape and size.
- 3.) To investigate the aerosolization behaviour of the obtained fibers.

3. Template assisted Polyelectrolyte Encapsulation of Nanoparticles into Dispersible, Hierarchically Nanostructured Microfibers

This chapter is the pre-peer reviewed version of the following article that will be published in *Advanced Materials*:

Kohler D., Schneider M., Krüger M., Lehr C.-M., Möhwald H., Wang D. (2011):
Template-Assisted Polyelectrolyte Encapsulation of Nanoparticles into Dispersible, Hierarchically Nanostructured Microfibers.

3.1. Introduction

Replication of the forms of biological organisms such as viruses can lead to unprecedented advanced materials and particularly transform the original, adverse, biological functions into the tailor-designed, favorable, material properties to revolutionize existing biotechnologies. The recent progress has evidenced that colloidal microtubules or microfibers can mimic in vivo transportation properties of such as viruses and flagella [47], avoid phagocytosis [20, 25], prolong in vivo circulation time [47], improve targeting efficiency [43, 44, 69], etc. Accordingly, there is much speculation about using elongated particles as innovative delivery carriers. The study of the biological response to the shapes of colloidal particles and the impact of anisotropic particles on drug delivery, however, are largely limited by the experimental challenge to synthesize colloiddally dispersible, biocompatible, elongated particles with long, defined, but varied aspect ratios.

Various methods have been developed to produce anisotropic particles, such as self-assembly [47], mechanical stretching [163], electrospinning [74], and microfluidics [164]. Among them, using membranes with cylindrical nanopores as sacrificial templates for material deposition is still the most versatile and flexible to produce elongated particles with any diameter, length, and aspect ratio, depending on the geometry of the pores, from various materials [84, 165]. Template-assisted electrochemical deposition allows selective material deposition within the membrane nanopores to produce individual elongated particles after the membrane decomposition, which, however, is specific to conducting materials such as metals and conjugated polymers and thus limits its applicability in pharmaceutical formulation [166]. The simple and general deposition way is infiltration of materials of interest into template membranes, which, however, cannot avoid deposition of materials outside the nanopores and thus results in continuous thin films on the membranes. Consequently, elongated particles embedded in the nanopores, are connected by these thin films on template membranes and severely aggregated after being liberated from the template membranes. This greatly limits the success of template-assisted deposition strategy in technical application for instance in drug delivery, in which individual particles with good colloidal dispersibility are necessitated. In order to circumvent this technical issue we infiltrated materials of

interest in the form of nanoparticles (NPs) rather than single molecules into nanoporous membranes and then encapsulate these NPs located in the nanopores by polyelectrolytes [61] based on electrostatic attraction (Figure 19). The present protocol referred to as template-assisted PE encapsulation of NPs, leads to colloiddally dispersible, hierarchical, nanostructured microfibers. It can directly be generalized for pharmaceutical formulations and the microfibers obtained can be used as sophisticated carriers for drug loading and delivery.

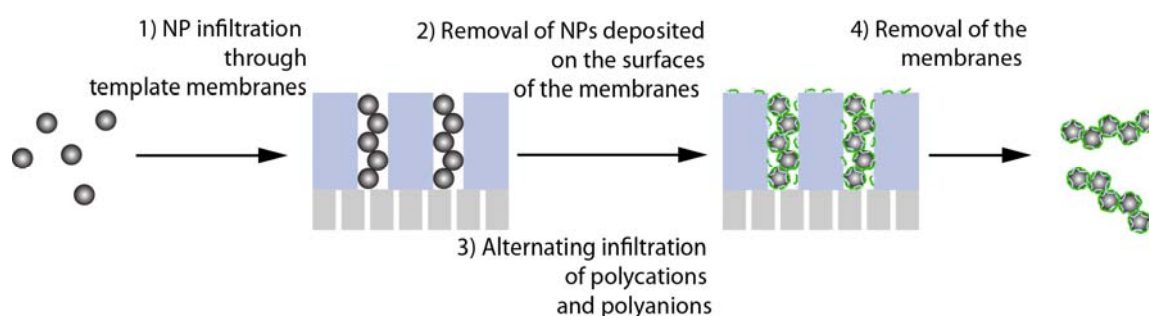


Figure 19: Schematic depiction of template-assisted polyelectrolyte encapsulation of NPs without polyelectrolyte coating to produce colloiddally dispersible, hierarchical, nanostructured microfibers.

3.2. *Materials and Methods*

3.2.1. Particle Infiltration

Despite being of theoretical interest for decades [167], packing of spheres in cylindrical cavities has recently been experimental implemented [168-170]. However, few experimental protocols developed thus far can be adapted for pharmaceutical formulations. Commercially available, monodisperse, spherical SiO₂ nanoparticles with the sizes in the range of 400 – 1000 nm were used as models of drug aggregates in the present proof-of-concept study for the benefit of characterization. The major technical advantage of using NPs instead of single molecules for infiltration is threefold: 1) to exclusively block the NPs in the pores of the template membranes by placing additional membranes with pore sizes much smaller than the NP sizes underneath the template membranes, as shown in Scheme 1; 2) to easily fill the template nanopores with a maximum volume fraction of NPs by one or two times infiltration of dilute NP dispersions (0.1 wt%); 3) to easily wipe away NPs

deposited on the membranes by tissue papers, thus obviating the risk of interconnecting of the NP aggregates confined in the template nanopores.

3.2.2. Microfiber Formation

Negatively charged SiO₂ NPs, loaded within the nanopores, were subsequently encapsulated by alternating infiltration of positively charged polyallylamine hydrochloride (PAH) and negatively charged poly(sodium 4-styrenesulfonate) (PSS) through template membranes (Figure 19). Aqueous solution of each PE (3 mg/mL in the presence of 0.5M NaCl) was infiltrated 3 or 4 times to efficiently encapsulate the SiO₂ NPs in the pores but to minimize the risk of forming continuous PAH/PSS multilayer films on the membranes. Dye-labeled PAH was used for infiltration (at least once) to visualize the PE coating and its encapsulated NPs by confocal laser scanning microscopy (CLSM). Note that the encapsulation protocol was based on well-established layer-by-layer assembly and a wide spectrum of synthetic and naturally occurring PEs are available to improve the biocompatibility [130, 171]. 10 μm thick polycarbonate [172] membranes with cylindrical pores of sizes in the range of 1 – 5 μm were used to template the infiltration of SiO₂ NPs and PEs. The subsequent dissolution of the PC membranes in dichloromethane (DCM) yielded PE-encapsulated SiO₂ NP aggregates microfibers, denoted as SiO₂NP@(PAH/PSS)_n microfibers (*n* is 3 or 4, the infiltration number of each PE).

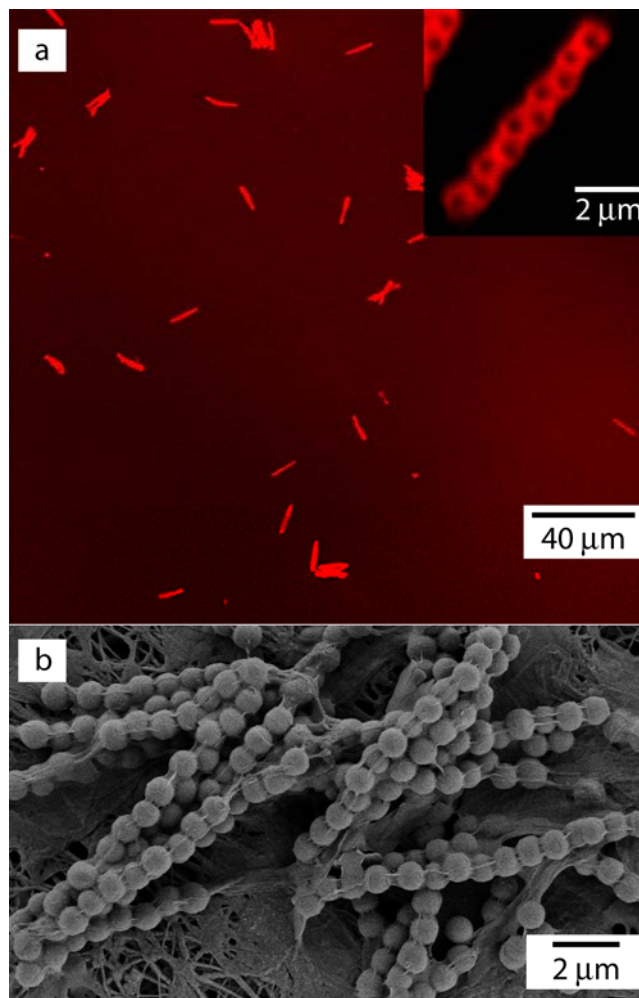


Figure 20: Fluorescence (a) and SEM images (b) of $\text{SiO}_2\text{NP}@\text{(PAH/PSS)}_3$ microfibers obtained by infiltration of 841 nm SiO_2 NPs through PC membranes with 1 μm cylindrical pores. The microfibers are dispersed in DCM. Rhodamine-labeled PAH was infiltrated once to impart the microfibers with red fluorescence. The high magnification fluorescence micrograph is shown in the inset in Figure 20a. In Figure 20b the microfibers are supported on PTFE membranes.

3.2.3. Microfiber Imaging

The resulting microfibers were collected on a polytetrafluoroethylene (PTFE) membrane with the pore sizes smaller than the diameters of SiO_2 NPs via filtration, washed three times by DCM to remove free PC chains derived from the membrane dissolution, and redispersed in DCM.

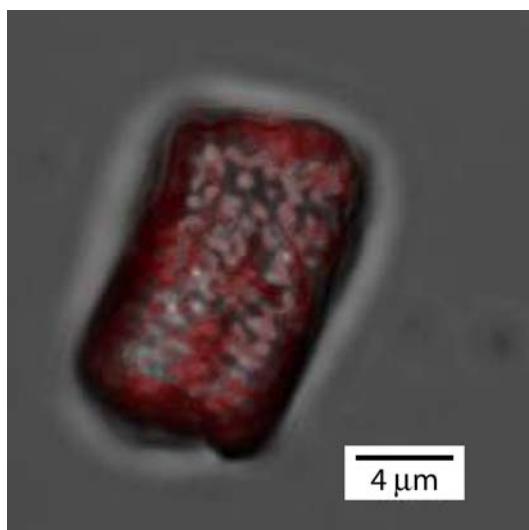


Figure 21: Overlay of fluorescence and transmission CLSM images of $\text{SiO}_2\text{NP}@\text{(PAH/PSS)}_3$ microfibers obtained by infiltration of 841 nm SiO_2 NPs through PC membranes with 5 μm cylindrical pores. The microfibers are dispersed in DCM. Rhodamine-labeled PAH was infiltrated for once to impart the microfibers with red fluorescence.

3.3. Results and Discussion

3.3.1. Microfiber Morphology

As shown in Figure 20 and Figure 21, $\text{SiO}_2\text{NP}@\text{(PAH/PSS)}_n$ microfibers are well-dispersed in DCM and composed of non-fluorescent SiO_2 NP chains encapsulated by fluorescent PE shells. The aspect ratios of the microfibers are comparable to those of the template pores. The packing structures of SiO_2 NPs in the resulting microfibers were characterized by scanning electron microscopy (SEM), showing a clear dependence on the size ratio of NPs to the membrane pores (Figure 22).

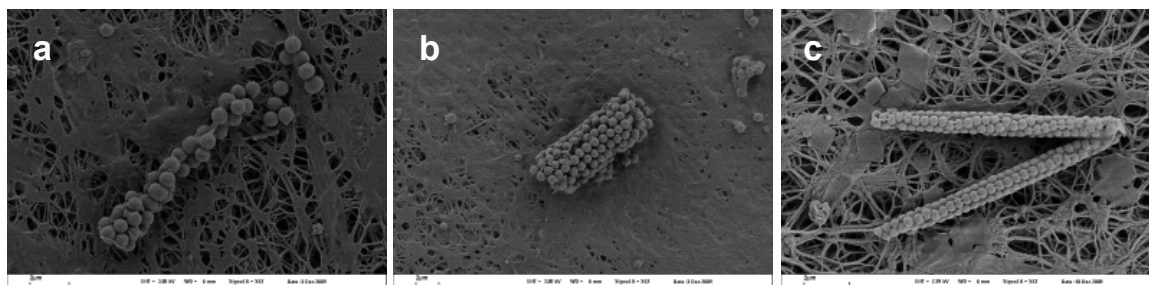


Figure 22: SEM images of $\text{SiO}_2\text{NP}@\text{(PAH/PSS)}_3$ microfibers obtained by infiltration of 841 nm SiO_2 NPs through PC membranes with cylindrical pores of diameters of 2 (a) and 5 μm (b), and by infiltration of 403 nm SiO_2 NPs through PC membranes with 1 μm cylindrical pores (c). The scale bar is 2 μm . The non-uniformity of the resulting $\text{SiO}_2\text{NP}@\text{(PAH/PSS)}_3$ microfibers is due to the fact that the nanopores of PC templates are not perfectly cylindrical.

$\text{SiO}_2\text{NP}@(\text{PAH}/\text{PSS})_n$ microfibers with the morphologies precisely defined by the pores of template membranes were counted with the aid of CLSM, suggesting a production yield of $\sim 60\%$. The well-dispersibility of $\text{SiO}_2\text{NP}@(\text{PAH}/\text{PSS})_n$ microfibers in DCM should arise from the non-negligible contribution of the hydrophobic, hydrocarbon backbones of PEs to the solubility, as suggested in literature [173, 174].

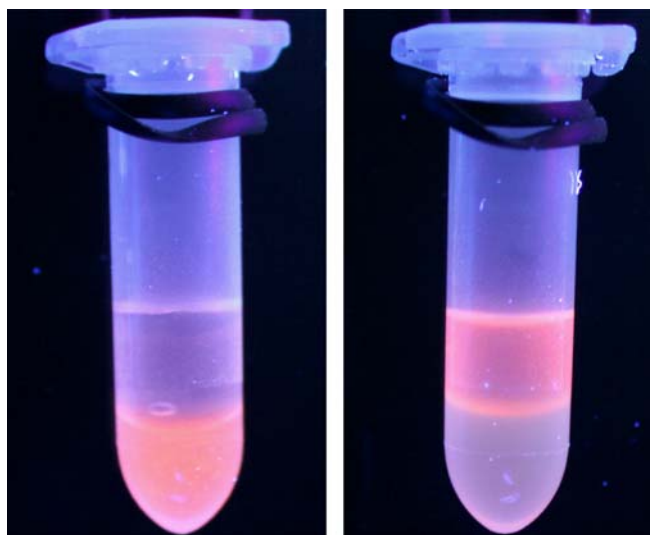


Figure 23: Fluorescence photographs of a plastic eppendorf tube containing water (upper phase) and DCM (lower phase). $\text{SiO}_2\text{NP}@(\text{PAH}/\text{PSS})_3$ microfibers, obtained by infiltration of 841nm SiO_2 NPs through PC membranes with $1\mu\text{m}$ cylindrical pores, were initially dispersed in the DCM phase (left panel), but they were readily to transfer to the water phase after vigorous shaking (right panel). Rhodamine-labeled PAH was infiltrated once to impart the microfibers with red fluorescence. The photographs were shot under irradiation with a UV lamp.

Intriguingly, $\text{SiO}_2\text{NP}@(\text{PAH}/\text{PSS})_n$ microfibers were readily transferred from DCM to water when their DCM dispersions were brought in contact with water, followed by vigorous shaking, which should be a result of excellent hydrophilicity of their PE coating (Figure 23). $\text{SiO}_2\text{NP}@(\text{PAH}/\text{PSS})_n$ microfibers remained little changed before and after phase transfer (Figure 24). It is worth noting that this simple process allows selective phase transfer of $\text{SiO}_2\text{NP}@(\text{PAH}/\text{PSS})_n$ microfibers to water from DCM without removal of free PC chains via filtration through PTFE membranes, allowing for simple sample preparation for future in vivo application.

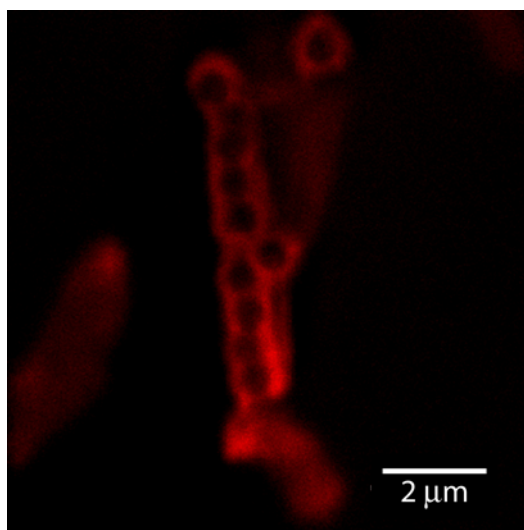


Figure 24: Fluorescence CLSM image of $\text{SiO}_2\text{NP}@\text{(PAH/PSS)}_3$ microfibers obtained by infiltration of 841 nm SiO_2 NPs through PC membranes with 5 μm cylindrical pores. The microfibers are dispersed in water. Rhodamine-labeled PAH was infiltrated for once to impart the microfibers with red fluorescence.

3.3.2. Multifunctional Microfibers

In the current work, SiO_2 NPs were also coated with defined numbers of PAH/PSS multilayer shells via layer by layer assembly [136, 175], $\text{SiO}_2@\text{(PAH/PSS)}_m$ NPs (m is the (PAH/PSS) bilayer number). Using nanoporous PC membranes to template subsequent infiltration of $\text{SiO}_2@\text{(PAH/PSS)}_m$ NPs and PEs, followed by the membrane dissolution by DCM, $\text{SiO}_2@\text{(PAH/PSS)}_m \text{ NP}@\text{(PAH/PSS)}_n$ microfibers were obtained (Figure 25).

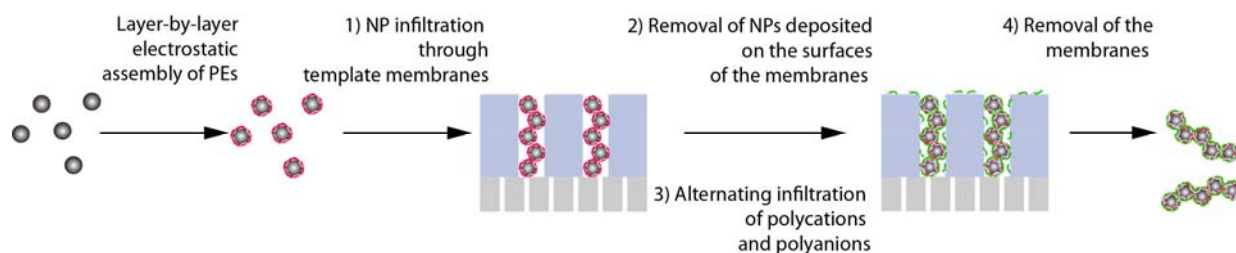


Figure 25: Schematic depiction of template-assisted polyelectrolyte encapsulation of NPs coated with polyelectrolytes to produce colloiddally dispersible, hierarchical, nanostructured microfibers.

The (PAH/PSS)_m shells coated on the SiO_2 NPs and the (PAH/PSS)_n on the microfibers were easily distinguished by CLSM microscopy by labeling one PAH layer

of them with different fluorescent dyes; the former was labeled by Rhodamine the latter by Fluorescein (Figure 26). This demonstrates that the present strategy is not only general for different types of NPs but also flexible to add multiple functions to microfibers by deliberately adding functional PEs or charged species on NPs before or after infiltration into template membranes.

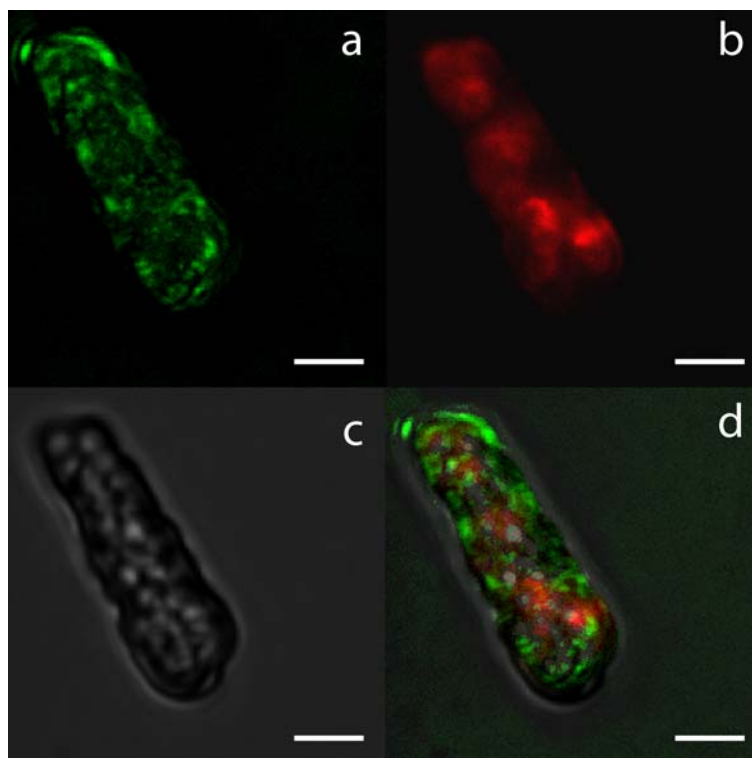


Figure 26: Fluorescence (a and b) and transmission (c) CLSM images of $\text{SiO}_2\text{@(PAH/PSS)}_3\text{NP@(PAH/PSS)}_3$ microfibers, obtained by using PC membranes with $2\ \mu\text{m}$ cylindrical pores to template infiltration of $841\ \text{nm}$ SiO_2 NPs coated with $(\text{PAH/PSS})_3$ shells, and (d) Overlay of these fluorescence and transmission images. Fluorescein-labeled PAH was infiltrated for once and thus the PE layers encapsulated on the NP microfibers are green fluorescent (a). The $(\text{PAH/PSS})_3$ shells on the NPs contain a layer of Rhodamine-labeled PAH and thus they are red fluorescent (b). The microfibers are dispersed in DCM. The scale bar is $2\ \mu\text{m}$.

3.3.3. Polyelectrolyte Capsule Containing Microfibers

The present protocol was also extended to encapsulate polystyrene (PS) NPs coated with $(\text{PAH/PSS})_m$ shells (Figure 27).

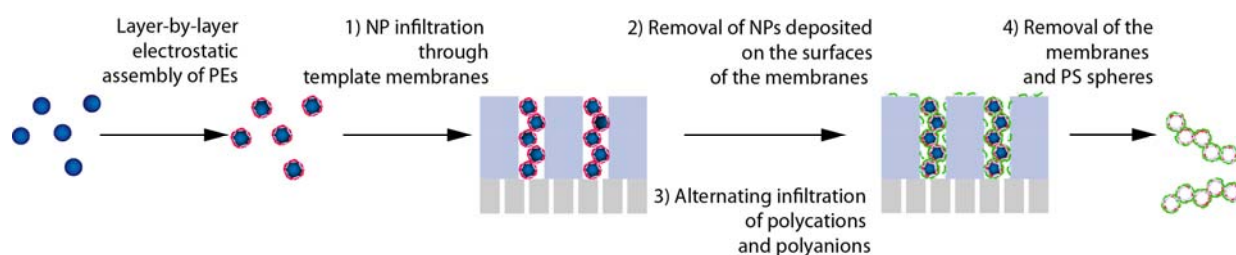


Figure 27: Schematic depiction of template-assisted polyelectrolyte encapsulation of PS NPs coated with polyelectrolytes to produce colloiddally dispersible, hierarchical, nanostructured microfibers.

Because DCM dissolved both PC template membranes and PS NPs, we obtained dispersible microfibers with closed porous structures, invited to the packing structure of the original PS NPs (Figure 28 and Figure 29).

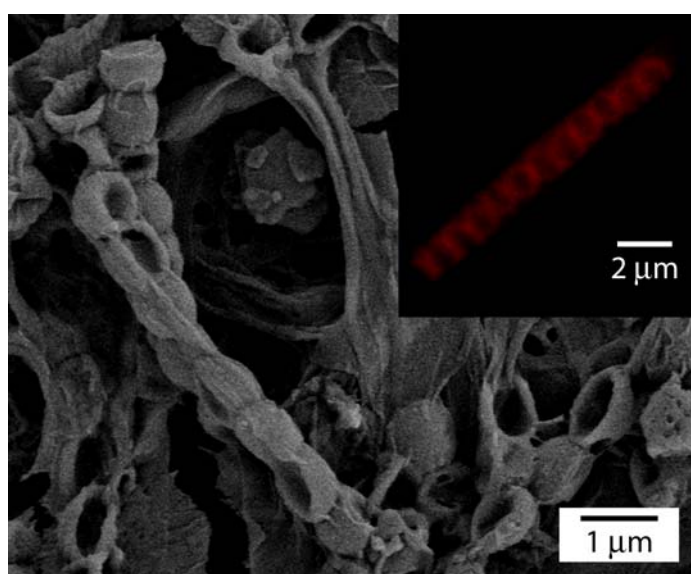


Figure 28: SEM image of $(\text{PAH/PSS})_5@(\text{PAH/PSS})_3$ microfibers obtained by using PC membranes with 1 μm cylindrical pores to template infiltration of 836 nm PS NPs coated with $(\text{PAH/PSS})_5$ shells. The PS NPs were removed via dissolution in DCM. The inset is the fluorescence micrograph of hollow microfibers dispersed in DCM.

Thanks to extensive studies of using PE microcapsules for drug loading and controlled release [136, 175], porous $(\text{PAH/PSS})_m@(\text{PAH/PSS})_n$ microfibers may provide sophisticated multi-compartment drug delivery carriers.

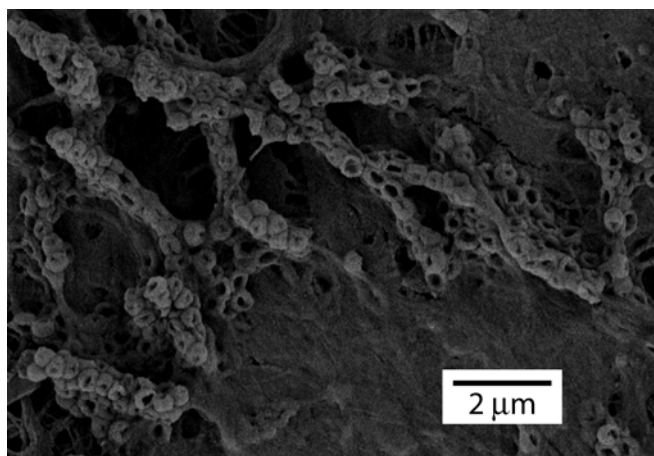


Figure 29: SEM image of $(\text{PAH/PSS})_5@(\text{PAH/PSS})_3$ microfibers obtained by using PC membranes with $1\ \mu\text{m}$ cylindrical pores to template infiltration of $428\ \text{nm}$ PS NPs coated with $(\text{PAH/PSS})_5$ shells. The PS NPs were removed via dissolution in DCM.

3.4. Conclusion

In summary, we have successfully prepared colloiddally dispersible, multifunctional, and multi-compartment microfibers by using nanoporous membranes as templates of PE encapsulation of colloidal NPs. The present protocol involves two key techniques: 1) membrane-template infiltration of materials in the form of NPs rather than single molecules to avoid the severe interconnecting problem of elongated particles liberated after template removal; 2) alternating infiltration of differently charged PEs based on electrostatic attraction, which embraces all the advantages associated with electrostatic self-assembly of PEs, developed thus far, to diversify the structures and functions of the resulting microfibers. The present protocol is simple and independent of the chemical nature of NPs and PEs. Thanks to its good dispersibility in a wide range of solvents of different polarity such as water and DCM, the surface PE coating allows free transfer of the resulting microfibers into various aqueous and organic media, thus enabling the present protocol to easily adapt to different formulation conditions. Our ensuing project is to extend the present protocol to drug NPs of pharmaceutical interest. In vitro study of the macrophage response to the resulting microfibers and their cytotoxicity is underway. The recent theoretical study has suggested that as compared with isotropic ones, anisotropic particles, such as microfibers, show a higher chance to deposit in the deep lung [21, 36]. As such, the study of the aerodynamic behavior of the resulting microfibers in human oral and nasal airways is under exploitation.

3.5. Experimental Details

PAH (Aldrich, Mw 56,000) and PSS (Aldrich, Mw 70,000) were dissolved in water at the concentration of 3 mg/mL in the presence of 0.5M NaCl. PAH was labelled by rhodamine or fluoresceine isothiocyanate (FITC) as described elsewhere [175]. SiO₂ and PS NPs were purchased from Microparticles GmbH, Berlin, Germany. They were coated by PAH/PSS multilayer shells according to a well-established layer-by-layer procedure [136, 175]. PC membranes were purchased from Whatman. 0.1 wt% aqueous suspensions of SiO₂ or PS NPs, coated with and without PAH/PSS multilayer shells, were infiltrated into template PC membranes. In order to efficiently block the NPs in the pores of the template membranes, additional PC membranes with the pores much smaller than the NPs were placed underneath the template membranes. The NP infiltration was repeated 2 times with an ultrasound treatment for 5min after each step to ensure a dense loading of the NPs in the template pores. After drying over night at room temperature, NPs deposited on the membrane surfaces were wiped away with Kimtech Science® tissue. Subsequently, the NP-loaded membranes were immersed in aqueous solutions of PAH (3mg/ml, containing 0.5M NaCl) for 30 min, followed by 3 times washing with water. The membranes were consecutively immersed in aqueous solutions of PSS (3 mg/ml, containing 0.5M NaCl) for 30min, followed by 3 times washing with water. After 3 or 4 repetition of this cycle, the membranes were dissolved by DCM to liberate the NP microfibers. The resulting microfibers were collected on PTFE membranes with the pores smaller than the NPs via filtration, washed three times by DCM to remove free PC chains derived from the membrane dissolution, and redispersed in DCM. Upon being in contact with water, the microfibers were transferred from DCM to water by vigorous shaking. The resulting NP microfibers were visualized by SEM (Gemini LEO 1550, operated at 3kV) and CLSM (Leica DM IRBE with a 30 W UV lamp ($\lambda = 350$ nm) as the light source).

4. Spatial Aspect Ratio Dependent Macrophage Uptake of Biocompatible Nanostructured Microfibers

Parts of this chapter will be submitted to Langmuir:

Kohler D., Bai S., Schneider M., Wolkenhauer M., Lehr C.-M., Möhwald H., Wang D.
in prep.:

Versatile loaded biocompatible microfibers studying macrophage response.

4.1. Introduction

Recently asymmetric particles have gained increasing attention, as anisotropic particles have shown to prolong in vivo circulation times in blood [47], and increase mucoadhesion in the intestine [65]. Combining the prolonged mucoadhesion and the reduced macrophage uptake reported by Mitragotri will result in prolonged lung residence time [25, 72]. New interesting drug carrier systems for pulmonary drug delivery with retarded release kinetics can therefore be achieved. Nowadays investigations of the macrophage response to asymmetric particles with well defined geometry and aspect ratio is largely limited by the challenge to synthesize colloidal dispersible, biocompatible, elongated particles with long, defined, but varied aspect ratios. Here we fabricate biocompatible asymmetric particles with well defined aspect ratio by the template technique which can be loaded with hydrophilic or hydrophobic drugs.

Hydrophobic drugs have recently provoked many challenges in formulation. As most new high potential drugs suffer from poor water solubility, new formulation strategies are asked for. Here we rely on a solvent exchange method for loading of hydrophobic drugs into hydrogels to meet this challenge [176]. The solvent exchange method allows for direct incorporation of hydrophobic nanoparticles into hydrophilic hydrogels. Hydrogels can be dispersed in a broad range of solvents, thereby transferring incorporated hydrophobic nanoparticles from water immiscible organic solvents to aqueous media.

The present protocol combines the template assisted formation of asymmetric particles with the solvent exchange method to produce colloidal dispersible microfibers with well defined dimensions and the ability to be loaded with hydrophilic or hydrophobic drugs. Despite being of practical interest for drug delivery, biocompatible microfibers are needed to get a deeper understanding of asymmetric particle uptake by macrophages, being an important process in particle clearance from the body [177]. However, few experimental protocols developed thus far can produce biocompatible microfibers with defined shape and aspect ratio. The first results from macrophage uptake studies will be presented here.

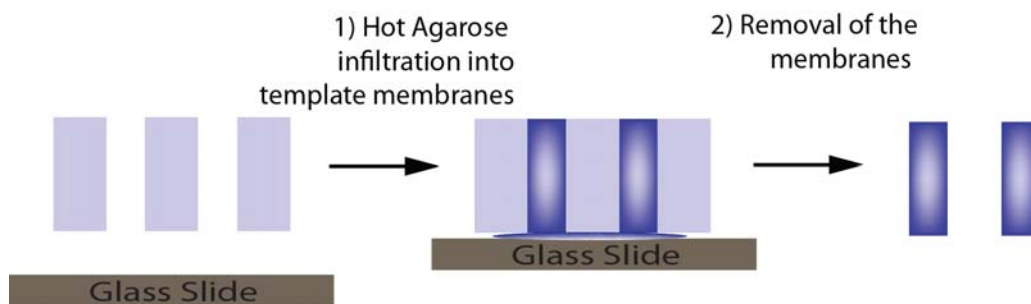


Figure 30: Schematic depiction of template-assisted Agarose infiltration to produce colloidal dispersible microfibers. 1) Hot (100°C) aqueous Agarose solution (1.5 wt%) is placed on a glass slide and drawn into template pores by capillary force. 2) Microfiber liberation by template decomposition in DCM.

4.2. Materials and Methods

4.2.1. Agarose Infiltration

Agarose, as natural sugar with good biocompatibility, is an ideal candidate for drug delivery application. The hot (100°C) aqueous solution of Agarose (1.5 wt%) was loaded into nanopores of commercially available membranes (Figure 30). After cooling of the system, Agarose deposited on the membranes was wiped away by tissue paper, thus obviating the risk of interconnecting microfibers confined in the template nanopores. 10 µm thick polycarbonate membranes with cylindrical pores of sizes in the range of 1 – 5 µm were used to template the infiltration of Agarose. The subsequent dissolution of the PC membranes in dichloromethane (DCM) yielded well dispersed Agarose microfibers (Figure 31). The aspect ratios of the microfibers are comparable to those of the template pores. The resulting microfibers were washed three times by DCM to remove free PC chains derived from the membrane dissolution and visualized by confocal laser scanning microscopy (CLSM).

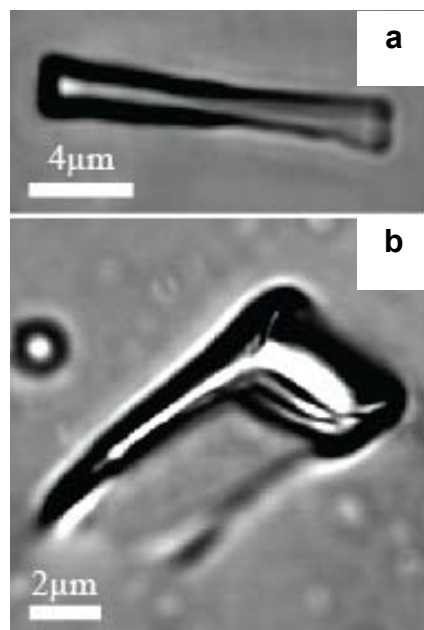


Figure 31: Transmission image of Agarose microfibers with (a) 1 μm and (b) 5 μm diameter obtained by infiltration of Agarose into PC membranes with 1 or 5 μm cylindrical pores respectively. The microfibers are dispersed in H_2O .

4.2.2. Nanoparticle Infiltration

4.2.2.1. Silica Particle Infiltration

Macrophage interaction studies need fluorescent labelling for in-situ detection under the CLSM after macrophage uptake. Commercially available, monodisperse, spherical 841 nm SiO_2 nanoparticles (SiO_2NPs) coated with one layer Rhodamin labeled positively charged polyallylamine hydrochloride (PAH_{Rh}) denoted as $\text{SiO}_2\text{NP}@ \text{PAH}_{\text{Rh}}$ were used as labels and at the same time as models of drug particles in the present proof-of-concept study for the benefit of characterization. The particle coating was done as described elsewhere [136, 178].

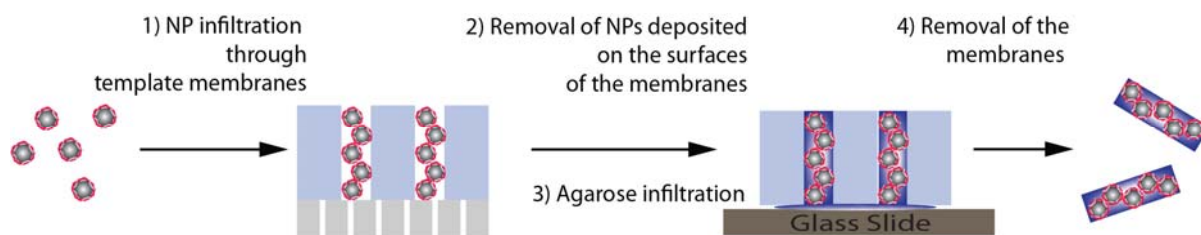


Figure 32: Schematic depiction of template-assisted formation of $\text{SiO}_2\text{NPs}@ \text{PAH}_{\text{Rh}}$ containing Agarose microfibers.

The $\text{SiO}_2\text{NP}@PAH_{\text{Rh}}$ particles were infiltrated into the template membranes by exclusively locking the NPs in the pores by placing additional membranes with the pore sizes much smaller than the NP sizes underneath the template membranes, and by one or two times infiltration of dilute NP dispersions (0.1 wt%) a maximum volume fraction of NP inside template pores can be obtained (Figure 32). The NPs deposited on the membranes can be easily wiped away by tissue paper. Agarose was subsequently infiltrated into the $\text{SiO}_2\text{NP}@PAH_{\text{Rh}}$ filled nanopores, resulting in $\text{SiO}_2\text{NP}@PAH_{\text{Rh}}$ containing Agarose microfibers. Well dispersible microfibers with defined inner packing structure of infiltrated $\text{SiO}_2\text{NP}@PAH_{\text{Rh}}$ are obtained, where the aspect ratio is determined by the template pore dimension (Figure 33).

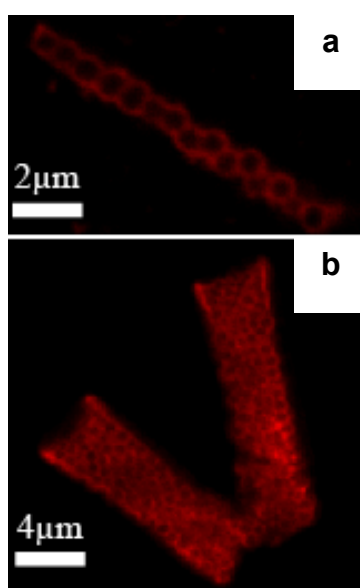


Figure 33: Fluorescence image of $\text{SiO}_2\text{NP}@PAH_{\text{Rh}}$ containing Agarose microfibers with (a) 1 μm and (b) 5 μm diameter obtained by infiltration of 841 nm SiO_2 NPs through PC membranes with 1 or 5 μm cylindrical pores respectively. The microfibers are dispersed in DCM.

4.2.2.2. Quantum Dot Infiltration

Thanks to good solubility in different solvents with largely varied polarity Agarose allows exchange of the local environment of microfibers from organic media to aqueous ones. This exchange may overcome the bottleneck from pharmaceutical industry to formulate high potent hydrophobic drugs, and as well to be suitable for hydrophilic components.

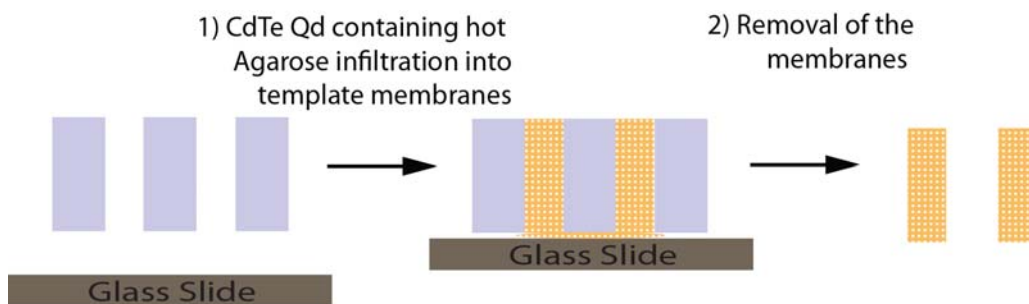


Figure 34: Schematic depiction of template-assisted formation of CdTe QD's containing Agarose microfibers.

Hydrophilic model drugs (CdTe Quantum Dots (QDs)) were incorporated into Agarose microfibers by mixing QDs and tempered Agarose prior to the loading into nanopores (Figure 34). After liberation of the microfibers from the template membrane, well dispersed fluorescent microfibers are obtained (Figure 35)

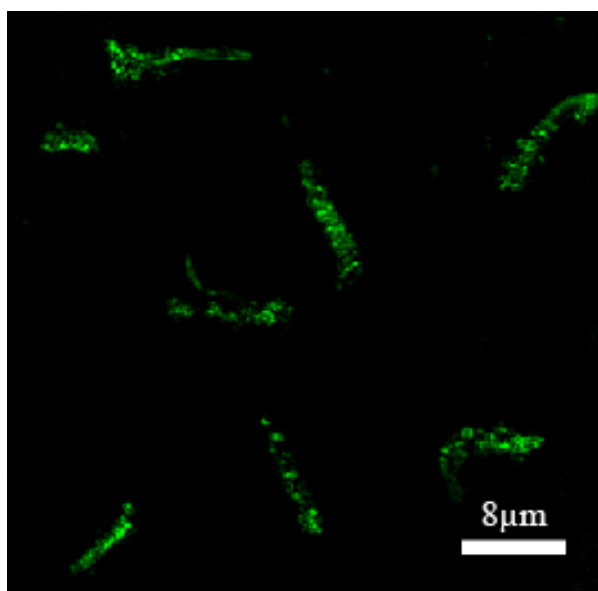


Figure 35: Fluorescence image of 1 μm diameter QD containing Agarose microfibers dispersed in H₂O.

4.2.2.3. Fe₃O₄ Nanoparticle Infiltration

Oleic acid and oleylamine coated iron oxide nanoparticles (Fe₃O₄ NPs) (8-9 nm) in DCM were used as model of hydrophobic drugs in the present proof-of-concept study for the benefit of characterization, while hydrophilic CdTe QDs with sizes in the range of 2-4 nm were used as models of hydrophilic drugs. Hydrophobic drugs were loaded into microfibers during the decomposition of the PC template by Fe₃O₄ NP containing DCM, where the Fe₃O₄ NP partition into the Agarose network (Figure 36).

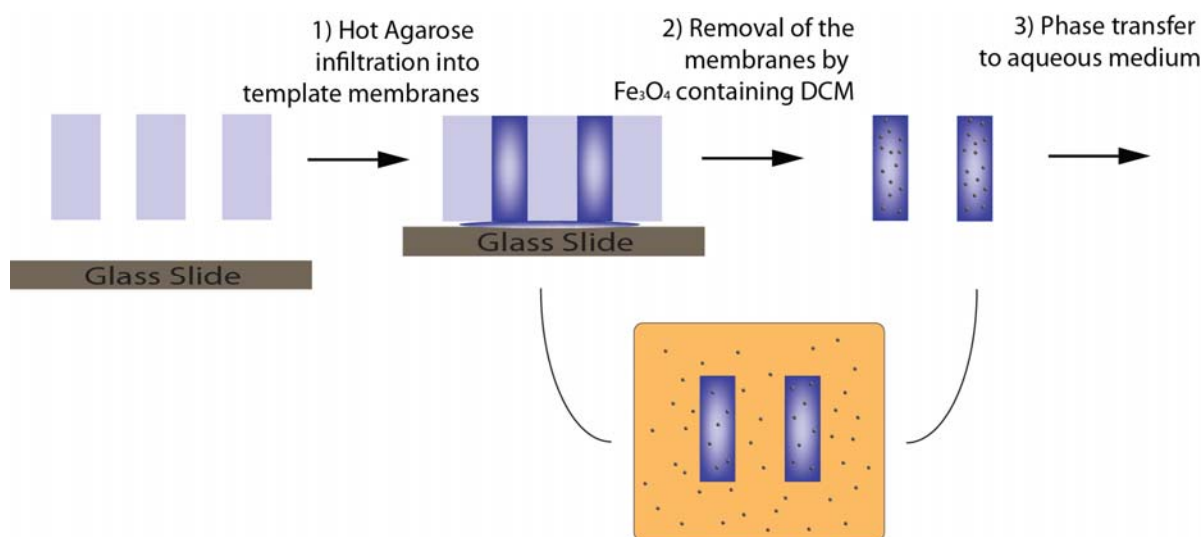


Figure 36: Schematic depiction of template-assisted formation of Fe_3O_4 containing Agarose microfibers.

By transfer of the microfibers into aqueous medium, the Fe_3O_4 NPs are trapped inside the hydrophobic surrounding of the hydrogel. By this the solvent exchange technique yields biocompatible microfibers loaded with hydrophobic drugs. Using Fe_3O_4 NP additionally allows introducing superparamagnetic properties, and by this enabling for targeted drug delivery as was reported by Dames [42] (Figure 37).



Figure 37: Superparamagnetic Fe_3O_4 NP containing Agarose microfibers ($\varnothing = 5 \mu\text{m}$) in H_2O after template decomposition and phase transfer in presence of a magnet.

4.3. Results and Discussion

4.3.1. Cytotoxicity Test

Cytotoxicity tests were conducted for all microfibers used for macrophage uptake studies. MTT test for viability testing and LDH test for cytotoxicity studies were performed [179]. Little toxicity was observed for all microfibers (Figure 38). Viability of only ~65% was found for SiO₂NP@PAH_{Rh} containing Agarose microfibers. This finding can be explained by insufficient SiO₂NP@PAH_{Rh} coating by Agarose. PAH being highly cytotoxic [180] can therefore interact with A549-cells, causing cell death. The viability of nearly 97% found for Fe₃O₄ NP containing 1 μm diameter Agarose microfibers confirms this finding. It additionally proved that incorporated Fe₃O₄ NPs are not toxic. Furthermore these data showed that microfiber purification and the removal of free polymer chains after template decomposition was successful. Due to limited microfiber amounts, and due to lack of quantification of actual microfiber concentration in solution, no concentration dependent cytotoxicity data were obtained, but only solutions used for macrophage uptake studies were investigated for their cytotoxicity. Further cytotoxicity studies are urgently needed, to get a deeper understanding on the particle shape effect on cytotoxicity.

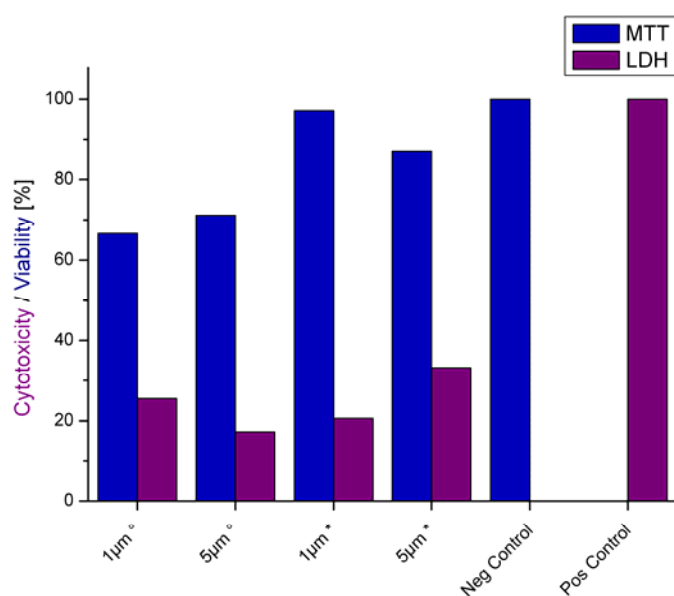


Figure 38: Cytotoxicity (LDH) and viability (MTT) data after 3h incubation for 1 and 5 μm diameter Agarose microfibers containing (°) SiO₂NP@PAH_{Rh} or (*) Fe₃O₄ NP. Triton-X being the pos. control, whereas pure buffer describes neg. control.

4.3.2. Macrophage Uptake

Mouse macrophages, MHS cells, were used as model macrophages. Microfibers with an aspect ratio of $\alpha = 2$ and 10 were tested, where the microfiber length was fixed to 10 μm . The direction of microfiber uptake was determined as well as the uptake kinetics.

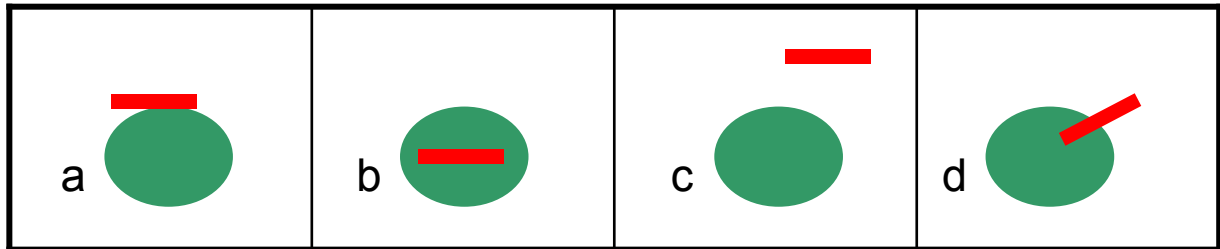


Figure 39: Schematic depiction of microfiber orientation with respect to cell orientation, with a) parallel alignment of the microfiber with its longitudinal side along the cell wall, b) complete microfiber uptake by the macrophage, c) microfiber being far apart from cells and d) partial uptake of the microfibers by MHS cells.

Four orientations were distinguished (Figure 39):

- a) Parallel alignment of the microfiber with its longitudinal side along the cell wall
- b) Complete microfiber uptake by the macrophage
- c) Microfiber being far apart from cells
- d) Partial uptake of the microfibers by MHS cells.

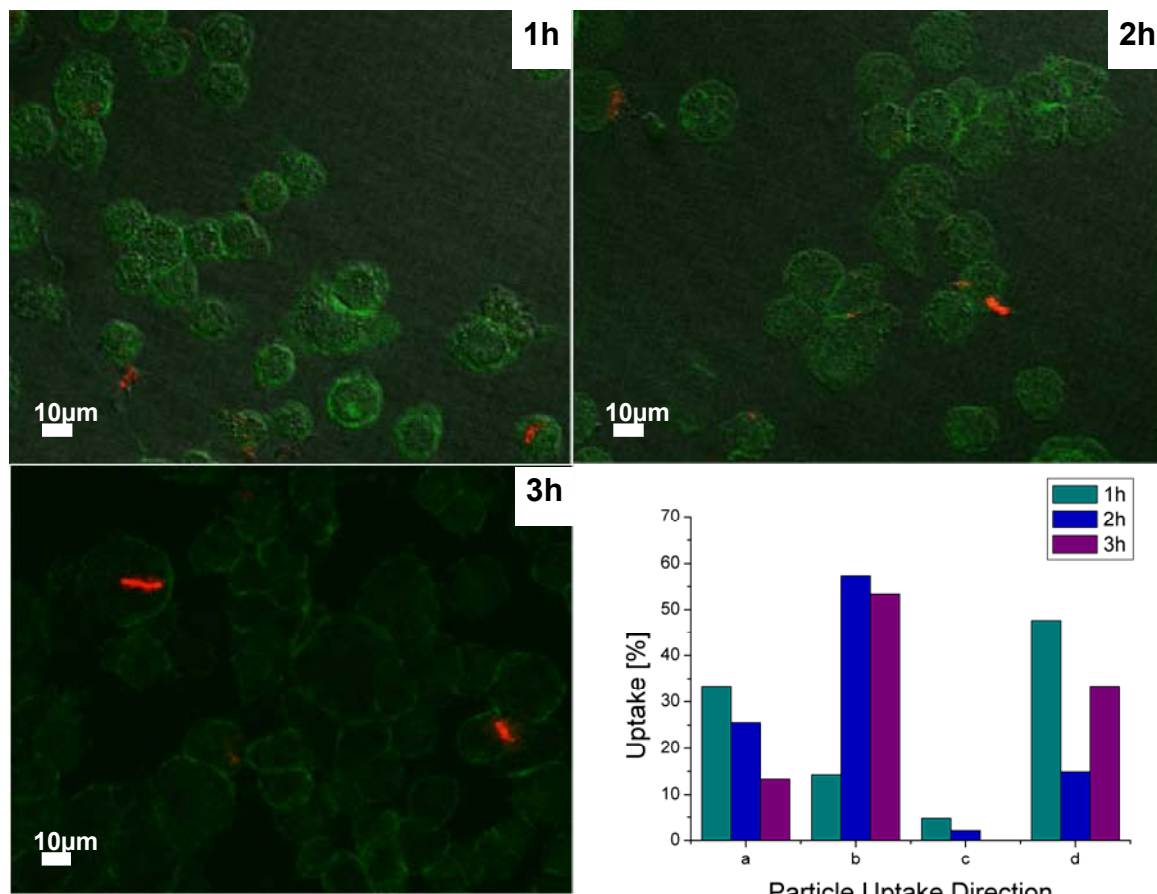


Figure 40: Fluorescence images of MHS cells after 1 h, 2 h and 3 h incubation with 1 μm diameter SiO₂NP@PAH_r containing Agarose microfibers in MHS medium at 37 °C and 5%CO₂. The amount of particle uptake is plotted vs. the particle-cell-orientation.

4.3.2.1. Silica Nanoparticle Containing Microfiber Uptake

1 μm diameter microfibers ($\alpha = 10$) were incubated for 3 h and each 60 min microfiber orientation in respect to the cells was examined (Figure 40). 80% of the microfibers are aligned parallel or not in contact with the cells after 1h incubation, while only 20% are about to be phagocytosed. After 3 h incubation, all microfibers are in contact with cells, where 85% are at least partially phagocytosed and only 15% are aligned parallel to the cell surface, unable to be taken up.

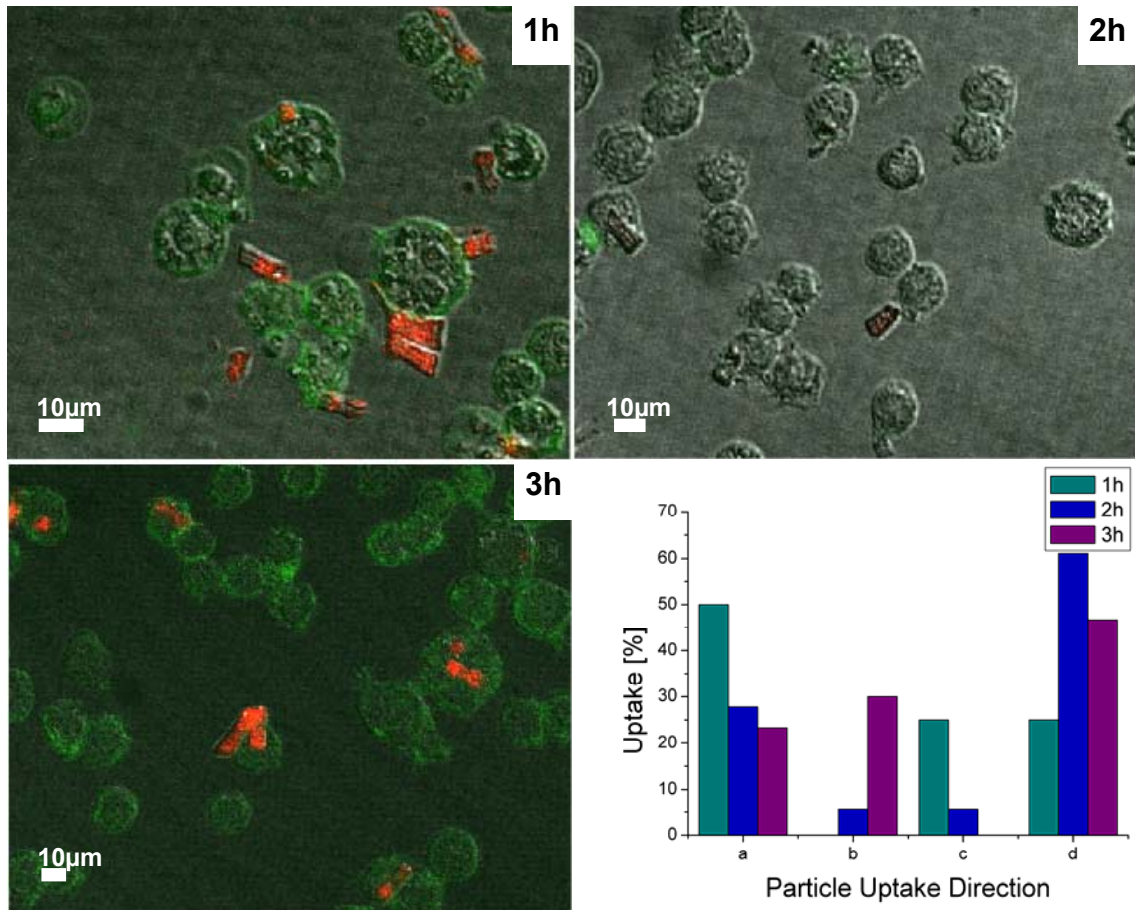


Figure 41: Fluorescence images of MHS cells after 1 h, 2 h and 3 h incubation with 5 μm diameter $\text{SiO}_2\text{NP@PAH}_{rh}$ containing Agarose microfibers in MHS medium at 37 $^\circ\text{C}$ and 5% CO_2 . The amount of particle uptake is plotted vs. the particle-cell-orientation.

5 μm diameter microfibers ($\alpha = 2$) show a slower phagocytosis of elongated particles compared to $\alpha = 10$ microfibers (Figure 41). Only 30% of the microfibers are completely phagocytosed after 3 h incubation time for $\alpha = 2$ compared to 55% for $\alpha = 10$ microfibers, while more microfibers are partially phagocytosed for 5 μm diameter particles (45%) than for 1 μm diameter particles (30%). Again no free particle without cell contact could be found after a 3 h incubation period. No comparison to spherical Agarose particles could be performed, as no synthesis strategy is known to produce monodisperse spherical Agarose particles.

For none of the particles aligned parallel to the cell membrane phagocytosis was observed, confirming the theory by Mitragotri [72] that elongated particles are only taken up from the pointy end. Hence the first contact angle theory could not be confirmed by our observations. Furthermore it was observed, that the smaller the pointy end is the faster is the rate of phagocytosis. This correlates to the finding for

spherical particles, where phagocytosis seems to be optimal for particles in the size range of 0.5 – 2 μm with a maximum at 1 μm [38].

4.3.2.2. Fe_3O_4 Nanoparticle Containing Microfiber Uptake

Macrophage uptake studies were prepared with Fe_3O_4 NP containing microfibers. Due to little substance amount and difficulties in imaging, only the cell-microfiber orientation was investigated. Again it was seen that particles aligned parallel with the longitudinal side to the cell wall were not taken up, while phagocytosis could be observed from the pointy side only.

4.4. Conclusion

In summary, we have successfully prepared the first biocompatible microfibers loaded with hydrophilic model drugs during preparation or hydrophobic model drugs by the solvent exchange method after synthesis of microfibers by using the template technique in combination with solvent exchange. The present protocol is simple and independent of the chemical nature of NPs and drugs to be used. By introducing Fe_3O_4 NPs superparamagnetic microfibers can be synthesized. Macrophage interaction studies with the prepared microfibers showed that microfiber orientation plays a dominant role in particle uptake, as well as a time dependence of microfiber uptake in dependence on the particle diameter.

Our ensuing project is to extend the present protocol to drug NPs of pharmaceutical interest. In vitro study of their cytotoxicity is underway. A recent theoretical study has suggested that as compared with isotropic particles, microfibers, show a higher probability to deposit in the deep lung [36]. As such, the study of the aerodynamic behaviour of the resulting microfibers in human oral and nasal airways is under exploitation.

4.5. Experimental Details

SiO₂ NP labelling: PAH (Aldrich, Mw 56,000) was dissolved in water at the concentration of 3 mg/mL in the presence of 0.5 M NaCl. PAH was labelled by

rhodamine as described elsewhere [175]. 841 nm SiO₂ NPs were purchased from Microparticles GmbH, Berlin, Germany. They were coated by one layer PAH_{Rh} according to a well-established procedure [136, 175].

SiO₂NP@PAH_{Rh} infiltration: PC membranes were purchased from Whatman. 0.1 wt% aqueous suspensions of coated SiO₂ NPs were infiltrated into template PC membranes. In order to efficiently block the NPs in the pores of the template membranes, additional PC membranes with the pores much smaller than the NPs were placed underneath the template membranes. The NP infiltration was repeated 2 times with an ultrasound treatment for 5min after each step to ensure a dense loading of the NPs in the template pores. After drying over night at room temperature, NPs deposited on the membrane surfaces were wiped away with Kimtech Science® tissue.

Microfiber synthesis: Capillary infiltration of 120 °C tempered 1.5% Agarose solution into bare or SiO₂NP@PAH_{Rh}-loaded membranes was performed. After cooling down to room temperature, membranes were peeled off from the glass slide. Agarose deposited on the membrane surface was wiped away with Kimtech Science® tissue. SiO₂NP@PAH_{Rh}-loaded membranes were dissolved by DCM to liberate the SiO₂NP@PAH_{Rh}-loaded microfibers. Threefold washing by DCM, followed by threefold washing in THF and EtOH allowed for redispersion of SiO₂NP@PAH_{Rh}-loaded microfibers in water. 1/3 dilution with MHS medium is performed prior to cell testing.

Fe₃O₄ NP loading: Fe₃O₄ NP stabilized by oleic acid and oleylamine provided by S. Bai were loaded into PC templates containing bare Agarose microfibers, by dissolving the template in Fe₃O₄ NP containing DCM. After 4 h incubation Fe₃O₄ NP containing microfibers are collected by magnet application, washed three times by DCM to remove free PC chains derived from the membrane decomposition, and redispersed in water. 1/3 dilution with MHS medium (500 ml RPMI 1640 containing 2 mM L-Glu, 5 ml Hepes 1 M, 1 mM Sodiumpyruvat, 2,25 g Glucose, 0,75 g Bicarbonate, 1,95 mg 2-Mercaptoethanol, 50 ml FCS) is performed prior to cell testing.

Macrophage Uptake: 20.000 MHS cells are grown on a 24 well-plate. 500 µl NP containing microfibers are incubated with MHS cells for 1 h, 2 h and 3 h respectively. For visualization cell membranes are labelled after particle incubation by 10min incubation at 37 °C with 0.5 ml WGA-FITC in PBS (1/40). Cells are fixed by 4% formalin incubation for 10 min prior to visualization by CLSM (Zeiss LSM510 META with a 30 W UV lamp ($\lambda = 350$ nm) as light source).

MTT test: A549 cells are incubated with 200 µl NP containing microfibers (sample), HBSS buffer (negative control) and 1% Triton-X (positive control) in triplicates for 4 h at 37 °C, 5% CO₂ and 90% humidity. After incubation 10 µl MTT solution (5 mg/ml HBSS) is added, and incubated at 37 °C, 5% CO₂ and 90% humidity for 4 h. After supernatant is removed, 50 µl DMSO is added to solubilise the formazan crystals, followed by 20 min incubation under light exclusion. After 1 min shaking, UV absorbance is measured at 550nm.

LDH test: LDH test is prepared using the Cytotoxicity Detection Kit (LDH) by Roche Applied Science, Mannheim, Germany. A549 cells are incubated with 200µl NP containing microfibers (sample), HBSS buffer (negative control) and 1% Triton-X (positive control) in triplicates for 4 h at 37 °C, 5% CO₂ and 90% humidity. 100 µl supernatant of each well is transferred to a probe sampling plate. 100 µl reaction mixture is added to each well, followed by 5 min incubation at room temperature in the dark. Absorption is measured at 492 nm.

5. Aspect Ratio Dependent Aerosolization behaviour of Drug loaded Microfibers

Parts of this chapter will be submitted to the Journal of Aerosol Science:

Kohler D., Wolkenhauer M., Möhwald H., Wang D., Lehr C.-M. and Schneider M.,
Generation of Biocompatible Drug Loaded Microfibers by Template Technique.

5.1. Abstract

A method of producing monodisperse aerosol fibers with defined aspect ratio is described. This method involves the infiltration of desired material into membrane pores, and the subsequent decomposition of the template. Diameter and length of the fibers could simply be varied by choosing desired pore dimensions for fiber preparation. Fibers of varying diameter ranging from 1 to 5 μm were produced. It was found that well dispersed fibers with defined porosity can be formed. Drug loading was achieved during fiber formation. Further modification of the process is expected to allow for large scale production of fibers with uniform aspect ratio.

5.2. Introduction

Fibers are a special class of particles, defined by the WHO in 1985 as elongated objects for which the aspect ratio – the ratio of length of the object to its diameter- is greater than 3 [34, 35]. The aerodynamic diameter of a fiber as main parameter for lung deposition is mainly determined by its geometric diameter, where the length is of minor impact [21, 54]. Su et al. [36] showed that fibers have higher probability to reach the peripheral lung compared to spherical particles of same aerodynamic diameter. Furthermore Edwards et al. [11] proved, that introducing porous architecture and thereby reducing particle density, allows for large particle deposition in the peripheral lung. Therefore fibers with and without porous structure open a new way of accessing pulmonary drug delivery systems with high delivered doses.

Particle design for optimized drug delivery gained increasing attention lately [9]. It was shown that asymmetric particle geometry greatly influences particle phagocytosis [20, 25, 163], allows for prolonged in vivo circulation time [47, 65] and improves targeting efficiency [43, 44, 69]. By decreasing macrophage uptake in the alveoli and increased mucoadhesion in the proximal lung, reduced clearance from lung and by thus long acting formulations aiming for improved patient compliance due to decreased dosing interval can be achieved.

Systematic studies on the pathways of asymmetric particles are limited by the existence of suitable model particles. New synthesis strategies allowing for large

scale production of elongated particles with well defined dimensions are urgently asked for. We present a method, which allows for the production of biocompatible, biodegradable, highly monodisperse fibers with variable aspect ratio using the template technique.

5.3. Template Technique

We used the template technique based on the approach of Martin [80] to produce biocompatible, biodegradable microfibers. Commercially available track etched polycarbonate membranes (Nucleopore, Whatman Inc., Florham Park, New Jersey, USA) containing straight pore structures are used as template for fiber generation. Fiber dimensions are defined by the pore dimensions, where the membrane thickness and pore diameter determine fiber length and diameter, respectively. Material deposition is accomplished by capillary infiltration of aqueous solution of desired material into pores and subsequent drying (Figure 42).

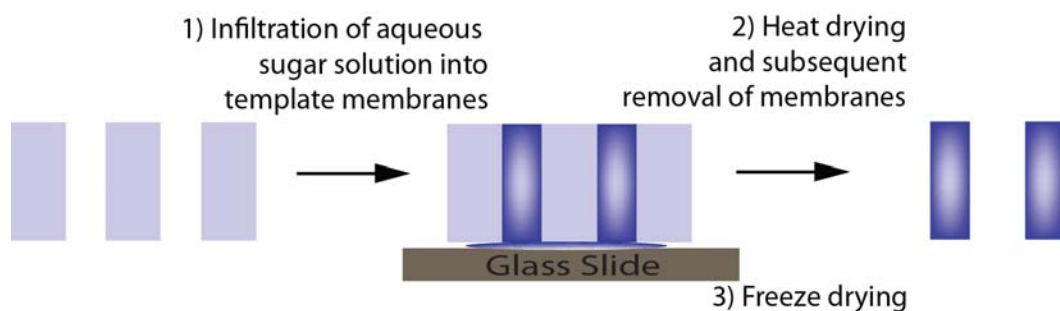


Figure 42: Schematic depiction of template-assisted formation of sugar microfibers.

After template decomposition in Dichloromethane (DCM) followed by three fold washing to remove free polymer chains, freeze drying is performed. Well dispersible microfiber powders are obtained.

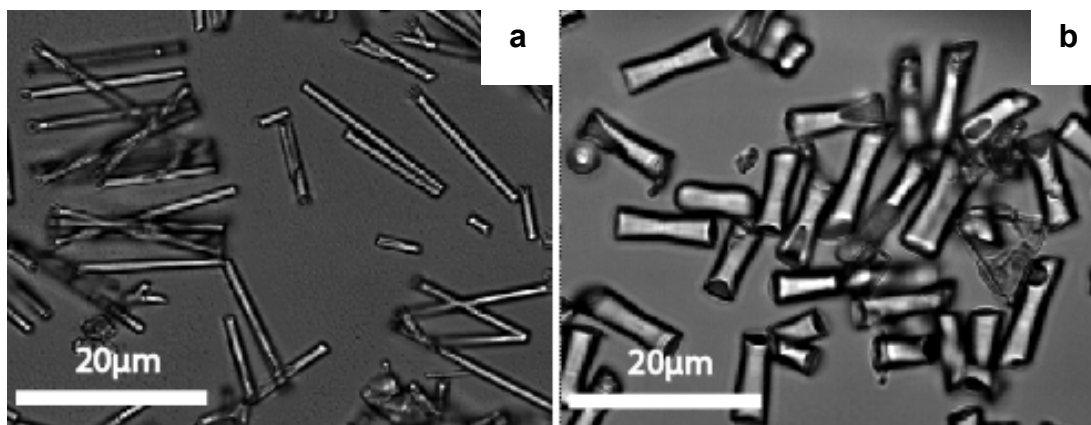


Figure 43: Microscopic images in transmission mode of lactose microfibers, obtained by using PC membranes with (a) 1 μm and (b) 5 μm cylindrical pores. The microfibers are freeze dried after template decomposition and subsequent washing.

The fibers of Figure 43 are composed of lactose. Fibers of various aspect ratios were prepared using PC-templates of various pore diameters (1 to 5 μm), with constant membrane thickness of 10 μm . Aspect ratios ranging from 2 to 10 were produced. Further increase of the aspect ratio can easily be achieved by using smaller pore sizes. A 20% aqueous lactose solution was infiltrated. Drying was performed at 80°C for 3 h. After template dissolution in DCM and freeze drying overnight, microscopic pictures on a CLSM (Leica DM IRBE with a 30 W UV lamp ($\lambda = 350 \text{ nm}$) as light source) were taken.

5.4. Generating Drug Loaded Microfibers and Introducing Porosity

Fenoterol HBr as short acting β -Sympathomimetikum used in asthma therapy was incorporated into Mannitol microfibers. Mannitol was used to achieve higher degree of crystallinity compared to Lactose microfibers. Fenoterol HBr – Mannitol–Water solution (1-20-100) was prepared and infiltrated into the membrane pores. After infiltration into membrane pores and subsequent drying monodisperse fibers containing drug and carrier material are obtained after template decomposition. Drug incorporation was confirmed by UV spectra after dissolution of the freeze dried powder in water.

To further modify the deposition behaviour of microfibers, porosity was introduced into the fiber morphology. Polystyrene nanoparticles (PS NPs) are physically

entrapped into membrane pores prior to material infiltration. A membrane with pore size smaller than the infiltrated PS NPs is placed into a commercially available membrane holder (Sartorius Stedim Biotech GmbH, Goettingen, Germany) underneath the template membrane to avoid particle penetration through the pores. Three times PS NPs infiltration with Ultrasound treatment of 5 min between each infiltration step resulted in close packed PS NPs. After drying overnight material deposition is performed as described above. During PC template decomposition, PS NPs are dissolved in DCM, resulting in porous fiber structure.

5.5. *Aerosolization of Microfibers*

The aerosolization properties were tested in an Andersen Cascade Impactor (ACI). A four stage Anderson Cascade Impactor was used to determine the fine particle fraction (FPF) of prepared microfibers and reference powder. A capsule containing 5 mg of Mannitol-Fenoterol-Microfibers, pure micronized Fenoterol or material blended with Mannitol (1/5) was placed in a HandiHaler®. The capsule was punctured and a pump simulated inspiration of 20 l/min for 12.3 sec. The powder was deposited on Brij 35 coated stainless steel plates or glass fiber filters depending on their aerodynamic diameter. Plates were washed after three capsule actuations with water, and fine particle fraction of particles with aerodynamic diameters below 5 µm determined by UV spectra quantification of Fenoterol HBr. Pure and 1/5 Mannitol blended microfibers of 1, 2 and 5 µm diameter as well as 1 µm microfibers containing 836 nm pores were tested in comparison to micronized Fenoterol HBr and a 1/5 powder blend of micronized Fenoterol / Mannitol. Due to limited powder amounts, each experiment was repeated twofold.

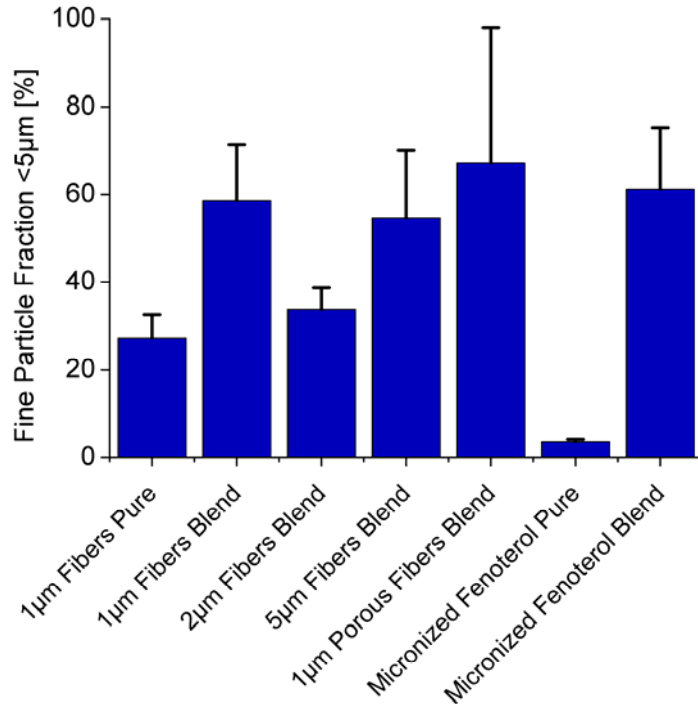


Figure 44: Fine particle fraction of Mannitol-Fenoterol-Microfibers (7.5% Fenoterol content) and pure micronized Fenoterol (100%) or material blended with Mannitol (1/5) tested in an Andresen Cascade Impactor at a flow rate of 20 l/min for 12.3 sec.

5.6. Results and Discussion

This method has proven to allow for generation of fibers consisting of various sugars. SEM imaging of the resulting fibers proved that particles with defined inner structure can be obtained by infiltration of PS NPs

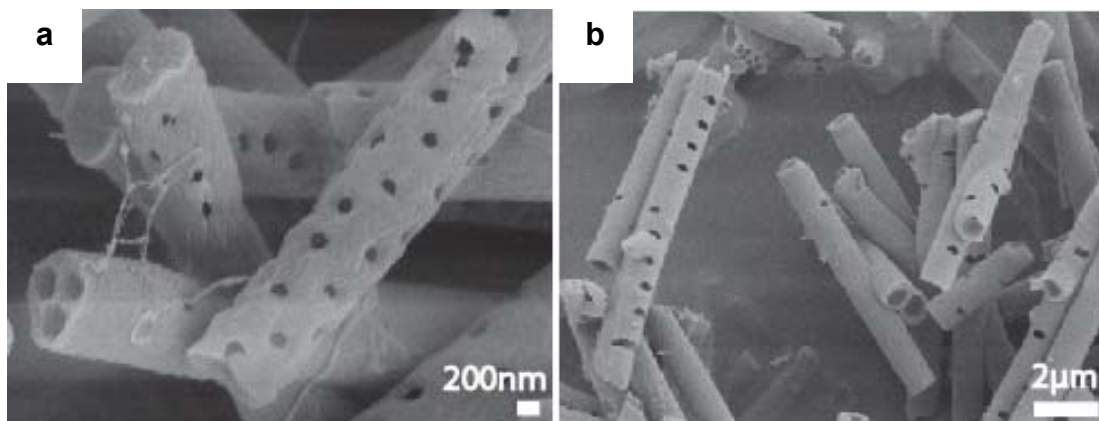


Figure 45: SEM images of lactose microfibers, obtained by using PC membranes with 1 µm cylindrical pores to template infiltration of (a) 428 nm and (b) 836 nm PS NPs. The microfibers are freeze dried after template decomposition and subsequent washing.

The effect of PS NP diameter on the inner porosity of microfibers has been determined, and is shown in Figure 45. The inner porous structure is determined by the ratio of infiltrated PS NP diameter to the pore diameter.

From observations of Figure 46 it can be seen that the particle morphology is independent of the additional incorporation of water-soluble drugs. Well dispersible fibers of various aspect ratios can be obtained by using defined pore diameters. This observation suggests that a broad variety of materials can be blended into sugars as carrier material without changing microfiber dimensions.

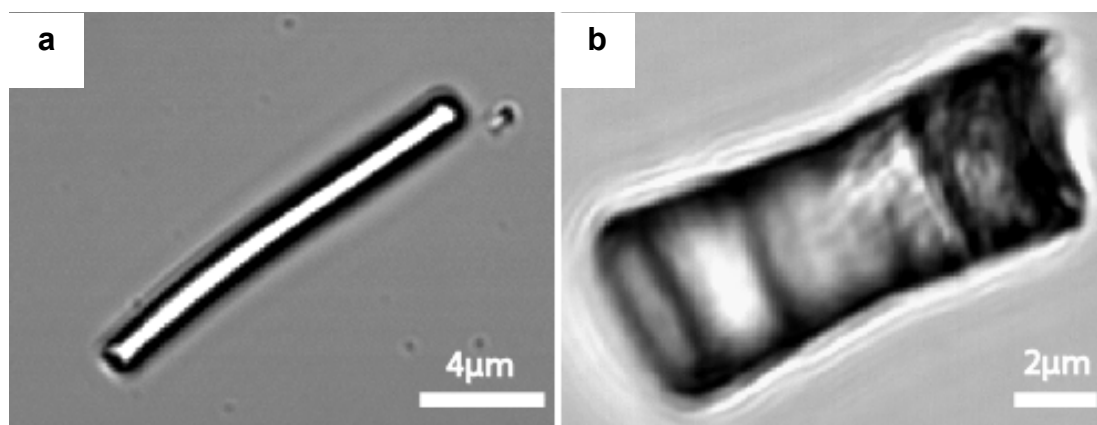


Figure 46: Microscopic images in transmission mode of Fenoterol loaded Mannitol microfibers, obtained by using PC membranes with (a) 1 μm and (b) 5 μm cylindrical pores. The microfibers are freeze dried after template decomposition and subsequent washing.

The UV-spectrum of Figure 47 proved the incorporation of Fenoterol HBr into Mannitol fibers. After fiber purification, freeze drying and subsequent dissolution in water, the Fenoterol HBr peak at 276 nm is present.

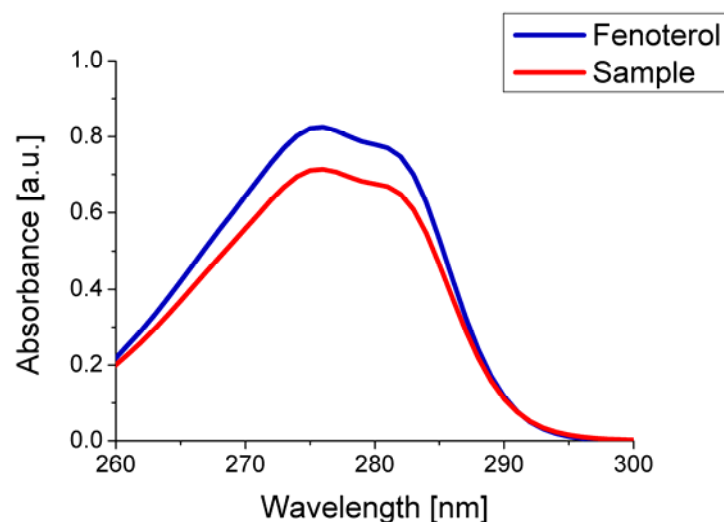


Figure 47: UV-spectrum of Fenoterol loaded lactose fibers (red) after washing and subsequent dissolution in water in comparison to Fenoterol solution (blue).

FPF determination (Figure 44) shows that fibers of various aspect ratios (2 to 10) provide FPF in the range of micronized Fenoterol Mannitol blends (FPF ~ 60%). Compared to pure micronized Fenoterol powder having FPF ~ 3.5%, improved particle deposition for all fibers can be observed. No conclusion can be drawn upon the aspect ratio effect, as insufficient data are available for statistic evidence due to limited availability of powder material. 1 μm porous particles showed FPF of up to 67%, confirming the effect reported by Edwards [11], that large porous particles having small d_{aer} have higher FPF compared to dense particles of the same diameter. Due to impurities of aggregated particles and remnant polymer chains from template decomposition lowering the powder quality, FPF results need to be handled with care and further follow up investigations are needed.

Fiber purification for improved aerosolization properties should allow for better investigation of the aspect ratio effect on the FPF, and improved evidence for the influence of porosity onto the deposition pattern.

5.7. Conclusion

In summary, we have successfully prepared the first drug loaded microfibers from approved excipients for pulmonary drug delivery with tailored porosity. The present protocol is simple and reproducible technique that allows for microfiber preparation with well dimensions. Aerosolization studies with prepared microfibers showed higher

FPF for microfibers compared to micronized Fenoterol, where porosity of microfibers seems to positively impact the FPF.

Our ensuing project is to extend the present protocol to further drugs of pharmaceutical interest. Additional data on aerosolization properties are underway to further investigate parameters modifying microfiber deposition in human airways.

5.8. Experimental Details

PS infiltration: PC membranes (1, 2 and 5 μm pore diameter) were purchased from Whatman. 0.1 wt% aqueous suspensions of PS NPs (428 and 836 nm) purchased from Microparticles were infiltrated into template PC membranes. In order to efficiently block the NPs in the pores of the template membranes, additional PC membranes with the pores much smaller than the NPs were placed underneath the template membranes. The NP infiltration was repeated 2 times with an ultrasound treatment for 5 min after each step. After drying over night at room temperature, NPs deposited on the membrane surfaces were wiped away with Kimtech Science® tissue.

Microfiber synthesis: Capillary infiltration of 20% sugar solution (Mannitol and Lactose provided by Boehringer Ingelheim) into bare or PS NP-loaded membranes was performed. After drying at 80°C for 3 h in the oven, membranes were peeled off from the glass slide. Sugar deposited on the membrane surface was wiped away with Kimtech Science® tissue. Membranes were dissolved by DCM to liberate the microfibers, and to decompose PS NPs resulting in porous microfibers. Threefold washing by DCM, followed by freeze drying yielded well dispersible powder. Microfiber-Mannitol-(1/5) blending was performed for selected samples prior to aerosolization studies by 30 min mixing in a Turbula Mixer.

Aerosolization properties: A 5 mg capsule of Mannitol-Fenoterol-Microfibers, pure micronized Fenoterol or material blended with Mannitol (1/5) was placed in a HandiHaler®. After HandiHaler® attachment onto a four stage ACI, a pump simulated inspiration of 20 l/min for 12.3 sec. was performed. Brij 35 coated stainless steel plates of the ACI were washed after three capsule actuations with water, and $\text{FPF}_{5\mu\text{m}}$ determined by UV spectra Fenoterol HBr quantification at 276 nm.

6. Overall Conclusion and Outlook

The European Lung Foundation assumes that in 2020 11.9 million death will be caused by lung diseases around the world, where COPD (4.7 million) and tuberculosis (2.5 million) account for half of the death rate [181]. 102 billion euro expenses caused by COPD, asthma, pneumonia and tuberculosis need to be covered by the European health system in 2010. Improved drug therapy can help to lower the costs and improve patient compliance. Specific targeting and prolonged drug release are two major objects of drug carrier design, in order to reduce systemic side effects and to reduce dosing intervals. Asymmetric particles showing optimized deposition behaviour seem to be promising candidates for next generation drug delivery devices for lung application.

In this context the template technique represents a valuable tool to synthesise promising microfibers, which will allow for deeper understanding of asymmetric particle–cell interaction, microfiber fate in vivo, as well as improving pulmonary drug delivery. A most important result from the work presented is that well dispersible, biocompatible microfibers of tuneable porosity and aspect ratio can be prepared. The finding, that macrophage uptake depends on the fiber diameter and that the microfiber orientation mainly impacts on the success of phagocytosis, will help in developing optimized carrier shape with respect to the application. Future experiments to test the mucoadhesive behaviour of microfibers in order to allow for prolonged drug release after inhalation are needed. Intense aerosolization studies in the future require scale up of the invented method in order to produce sufficient microfiber material. Microfiber release from the template pores, avoiding template decomposition, will therefore be one of the major challenges that need to be solved to allow for commercial large scale production.

The new synthesis approach allows producing high quality microfibers of various materials with tailored properties, such as modified porosity, versatile drug loading approaches as well as aspect ratio dependent macrophage uptake. It allows for optimizing pulmonary drug delivery, and thereby fighting costs and death caused by lung diseases.

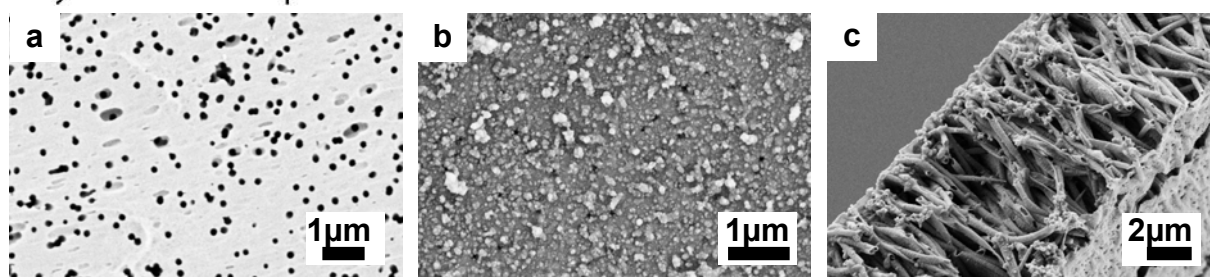
7. Annex

7.1. Particle Aggregation

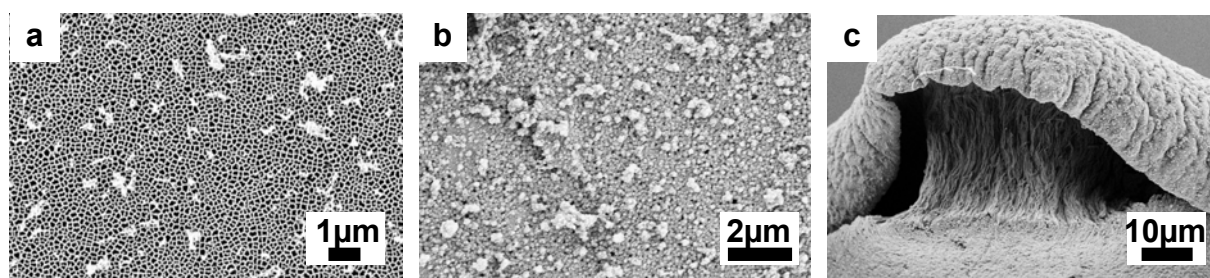
7.1.1. General Consideration

Microfiber aggregation is a major drawback of the template technique. Due to untargeted material deposition outside template pores, microfibers are severely interconnected after template decomposition (Figure 48). Therefore many approaches to arrive at a successful preparation failed. This section therefore describes and discusses these approaches to help future generations of scientists.

Polycarbonate template



Bare template → Polymer coated template → Liberated aggregates



AAO template

Figure 48: Formation of particle aggregates during polymer deposition on PC templates. Bare membranes (a) are coated with 8 bilayers PAH/PSS (b). Big particle aggregates are obtained after template decomposition (c) caused by untargeted material deposition outside template pores.

Resulting microfiber aggregates will show different biological response compared to well separate microfibers in vivo. Various strategies to overcome untargeted material deposition and/or to remove the interconnecting film were tested. Plasma-Cleaning

was applied to etch untargeted material, while gold layer and sacrificial layer attempts were used to mechanically remove undesired material. All strategies aimed for the post-deposition removal of interconnecting material in order to obtain well dispersible microfibers after template decomposition. The deposition of a gold layer and their subsequent hydrophobization on the template surface on the other side aimed to avoid undesired material deposition outside template pores during microfiber preparation. All strategies are discussed below.

7.1.2. Plasma Cleaning

Plasma is a highly reactive ionized gas phase, created by using high frequency electric fields. The ionic, high energetic species can react with surface located species on the material to be cleaned by collision. Produced gaseous products can be removed by applied vacuum. Ions of the plasma vibrate due to the absorbed electrical energy followed by temperature increase used to generate the plasma, thereby scrubbing the surface [182].

Oxygen plasma cleaner (Plasma Cleaner / Sterilizer PDC-32G, Harrick, Ithaca, USA) was used to clean membrane surfaces after LbL deposition in order to avoid microfiber aggregation after template decomposition. Plasma power (100, 200 and 500 Watt) and etching time (1 to 60 min) were varied. The influence of plasma etching on particle morphology and membrane were studied.

200 and 500 Watt resulted in complete destruction of the PC-membrane. 100 Watt for 5min removed the polyelectrolyte coating on the PC template surface, yielding well separated microfibers. The obtained results were not reproducible. Plasma appeared to not selectively remove surface material, but to affect template and pore structure, thereby modifying microfiber morphology (Figure 49).

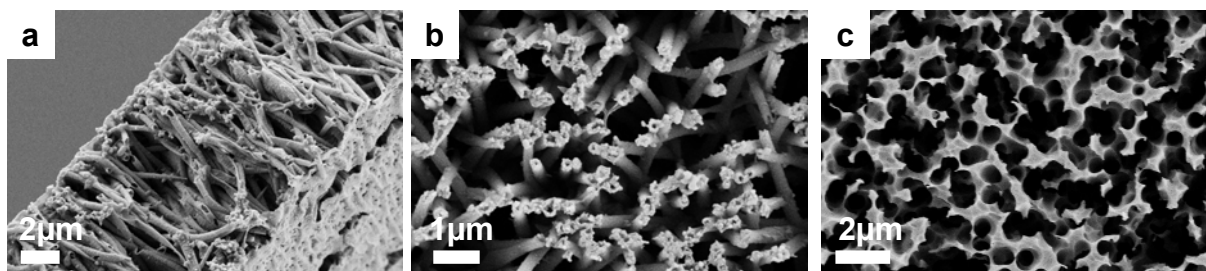


Figure 49: SEM images of (PAH/PSS)₈ microfibers obtained using PC membranes with 0.2 μm cylindrical pores. Intact aggregated (PAH/PSS)₈ microfibers (a) obtained without Plasma treatment, (b) separated microfibers after Plasma treatment (100 Watt, 5 min) and subsequent template dissolution in DCM (b) and bare PC membrane with affected pore structure after Plasma treatment (100 Watt, 5 min).

AAO templates treated at 100 Watt for 5 min showed smaller aggregates. Microfibers inside the AAO template pores were affected by the plasma, producing instable porous microfibers (Figure 50).

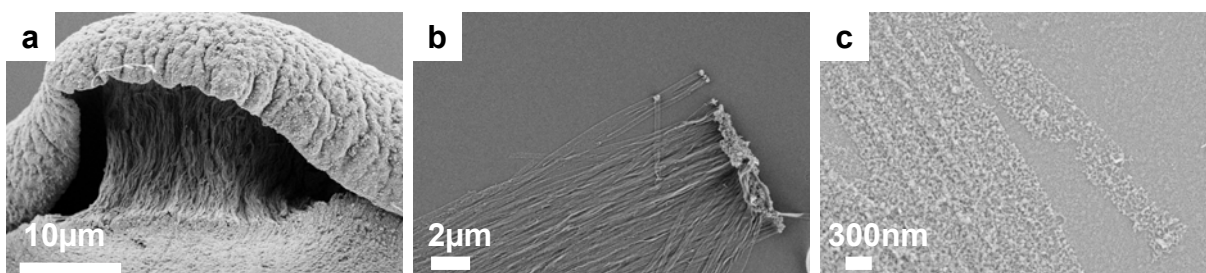


Figure 50: SEM images of (PAH/PSS)₈ microfibers obtained using AAO membranes with 0.2 μm cylindrical pores. Intact aggregated (PAH/PSS)₈ microfibers (a) obtained without Plasma treatment, (b) separated microfibers after Plasma treatment (100 Watt, 5 min) and subsequent template dissolution in DCM (b) and magnification (c).

Plasma Cleaning allows for the production of smaller aggregates, but is unsuccessful to yield reproducible well dispersible microfibers with intact morphology.

7.1.3. Gold Layer

Material adsorption outside template pores was shown to be avoided by gold sputtering of the membrane faces [183]. Furthermore gold layers were peeled off after partial template dissolution, thereby removing adsorbed material from the membrane surface.

25 nm gold was sputtered onto the membrane faces and 8 bilayers PAH/PSS deposited via the LbL technique as described previously. PC and AAO templates were processed differently.

AAO templates were partially dissolved by 1min immersion in 1 M NaOH, forming a gap between the gold layer and the template, followed by peeling off the gold layer by tweezers, and AAO template decomposition in 1 M NaOH for 24 h. Liberated microfibers were filtered through 0.2 μm PTFE membrane, washed three times with water to remove free salt, and visualized by SEM (Gemini LEO 1550, operated at 3 kV).

PC templates were placed in a solution (0.4 mg/ml $\text{K}_4\text{Fe}(\text{CN})_6$, 3.3 mg/ml $\text{K}_3\text{Fe}(\text{CN})_6$, 19 mg/ml $\text{K}_2\text{S}_2\text{O}_3 \times \text{H}_2\text{O}$, 56 mg/ml KOH) to decompose the gold layer, and thereby remove the adjacent polyelectrolyte multilayers. PC templates were dissolved in DCM for 2 h. Liberated microfibers were filtered through 0.2 μm PTFE membrane, washed three times by DCM to remove free polymer chains and visualized by SEM.

No gap between template and gold was found for the partially etched AAO templates. Therefore the gold layer could not be removed, resulting in strongly aggregated microfibers comparable to aggregates formed without prior gold sputtering of the AAO template. The etching strategy to remove the gold could not be applied to the AAO template, as it takes place at high pH values, decomposing the AAO template.

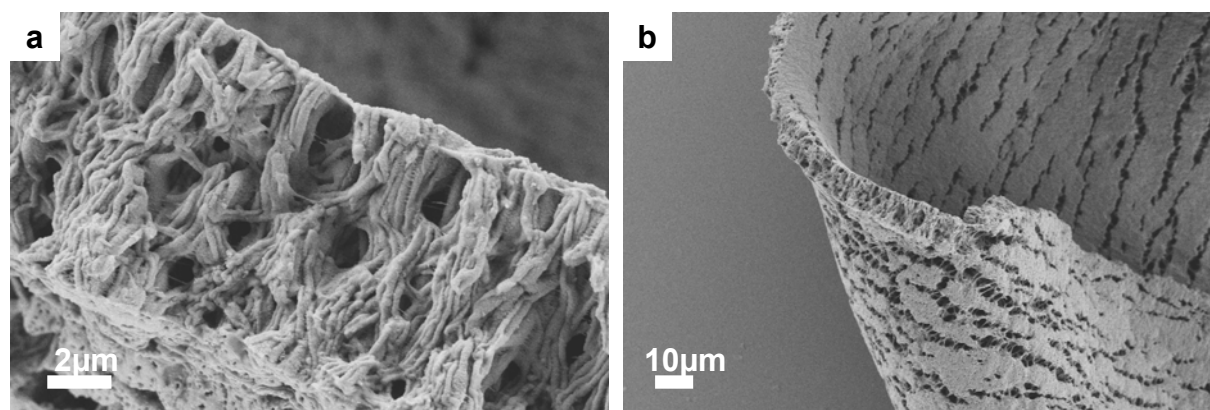


Figure 51: SEM images of (a) close up and (b) overview of aggregated (PAH/PSS)₈ microfibers obtained by using 25 nm gold sputtered 1 μm pore size PC membranes after gold layer decomposition.

Big aggregates were found after dissolution of the gold layer and subsequent decomposition of the PC template (Figure 51). Unmodified gold sputtering onto PC template faces is insufficient to prevent polyelectrolyte adsorption, and etching of gold is furthermore unsuccessful to remove deposited material from the surface.

7.1.4. Gold Layer and Hydrophobisation

Hydrophobisation of gold sputtered membranes is promising to avoid untargeted material deposition outside on template faces. Preventing the formation of interconnecting films will allow for preparation of well dispersible microfibers.

25 nm gold was sputtered onto one membrane surface, followed by 2 h incubation in 1 mg/ml hexadecanethiol ($C_{16}SH$) solution in Toluol, and five times washing in EtOH, while the other template face remained untreated. Contact angle measurements were performed to confirm successful hydrophobisation. Only one membrane side was sputtered to compare bare and hydrophobised membrane sides after template decomposition.

8 bilayers PAH/PSS were deposited via the LbL technique as described above. PC templates were dissolved in DCM for 2h, while AAO templates were decomposed by immersion in 5% H_3PO_4 for 24h. Liberated microfibers were filtered through 0.2 μm PTFE membrane, washed by DCM three times to remove free polymer and visualized by SEM (Gemini LEO 1550, operated at 3 kV).

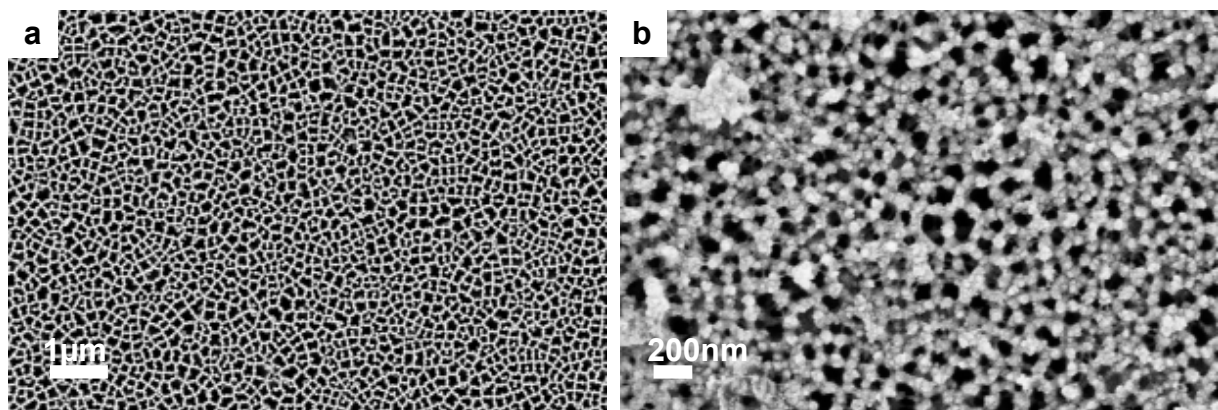


Figure 52: SEM images of 0.2 μm pore diameter AAO membranes sputtered with 25 nm gold after hydrophobisation with $C_{16}SH$, before (a) and after (b) 8bilayer deposition of PAH/PSS.

Successful hydrophobisation of AAO and PC templates was confirmed by contact angle measurements showing angles $>90^\circ$.

AAO membranes show open pore structure after gold sputtering and subsequent hydrophobisation. Polyelectrolyte deposition was confirmed by membrane surface observations by SEM following multilayer deposition (Figure 52). The rough structures present on template faces prove the deposition of polyelectrolyte multilayers.

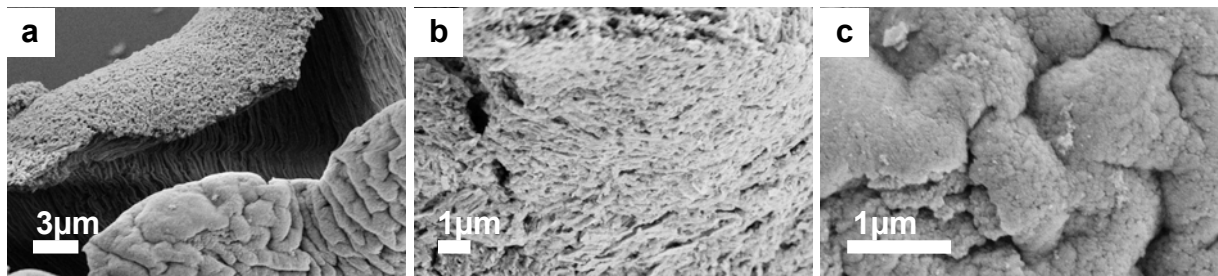


Figure 53: SEM images of 0.2 μm pore diameter AAO membranes sputtered with 25 nm gold after hydrophobisation with C_{16}SH , before (a) and after (b) 8bilayer deposition of PAH/PSS.

Different multilayer structures can be observed after AAO template decomposition, as one template side was sputtered followed by hydrophobisation, while the other side remained untreated. Rough multilayer composition was observed for microfiber aggregates after template decomposition, comparable to multilayer roughness of interconnecting films on untreated template without gold sputtering. The other microfiber aggregation side was smoother (Figure 53). Therefore it can be concluded, that gold sputtering with subsequent hydrophobisation allows limiting multilayer formation on template substrates, but does not avoid adsorption completely. Therefore aggregation can be decreased by hydrophobisation, but not prevented.

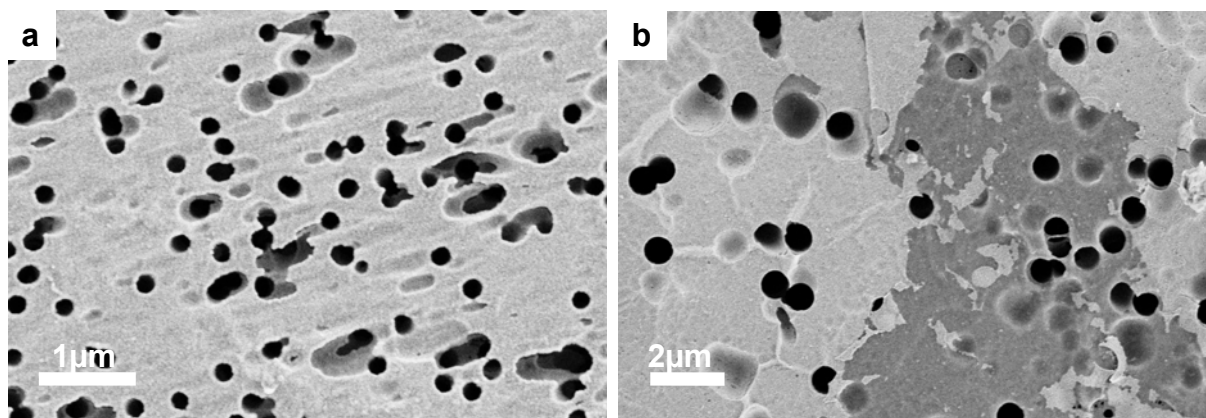


Figure 54: SEM images of 0.2 μm pore diameter PC membranes sputtered with 25 nm gold after hydrophobisation with C_{16}SH , before (a) and after (b) 8bilayer deposition of PAH/PSS.

PC templates hydrophobised showed no polyelectrolyte adsorption after multilayer assembly (Figure 54). No microfibers could be observed in SEM after template decomposition. Gold sputtering selectively coats the template surface, therefore membrane pores should remain hydrophilic during surface hydrophobisation by C_{16}SH . As no microfibers are formed, investigations of the pore walls need to be carried out, to investigate the pore environment.

7.1.5. Sacrificial Layer

Ono et al. [184] reported the successful application of sacrificial layers to form free-standing polyelectrolyte films. By pH responsive decomposition of LbL assembled polyelectrolyte multilayers, free standing pH insensitive multilayer films were prepared. Therefore this strategy was tested for its ability to dismantle the surface polymer coatings on porous membranes.

Sacrificial layer deposition was prepared as described above. Subsequently uncoated membranes were immersed in aqueous solutions of PAH (3 mg/ml, containing 0.5 M NaCl, pH = 2) for 30min, followed by 3 times washing with water. The membranes were consecutively immersed in aqueous solutions of polyacrylic acid (PAA) (3 mg/ml, containing 0.5M NaCl, pH = 2) for 30 min, followed by 3 times washing with water. Membranes are denoted as $(\text{PAH/PAA})_n$. After desired repetitions of this cycle, deposition of pH insensitive multilayers is performed.

pH insensitive multilayer deposition was prepared similar to sacrificial layer deposition. Subsequently, sacrificial layer coated membranes were immersed in aqueous solutions of PAH (3 mg/ml, containing 0.5 M NaCl, pH = 2) for 30 min, followed by 3 times washing with water. The membranes were consecutively immersed in aqueous solutions of PSS (3 mg/ml, containing 0.5 M NaCl, pH = 2) for 30 min, followed by 3 times washing with water. After desired repetition of this cycle, deposition of pH insensitive multilayers is performed. $(\text{PAH/PAA})_n/(\text{PAH/PSS})_m$ coated membranes are obtained.

To easily distinguish sacrificial and pH insensitive multilayers by CLSM, one PAH layer of each was labelled with different fluorescent dyes; the former was labelled by FITC the latter by Rhodamine, or vice versa. All experiments were prepared using PC templates, as AAO templates would be degraded in acidic pH during multilayer assembly.

Sacrificial layer decomposition was performed by immersion of $(\text{PAH/PAA})_n/(\text{PAH/PSS})_m$ coated membranes into 0.5 M HCl for 24 h, followed by washing and subsequent immersion into 0.5 M NaOH for 15 min and additional washing. PC templates were dissolved in DCM for 2h. Liberated microfibers were filtered through 0.2 μm PTFE membrane, washed three times by DCM to remove free polymer and visualized by SEM (Gemini LEO 1550, operated at 3kV) and CLSM (Leica DM IRBE with a 30 W UV lamp ($\lambda = 350 \text{ nm}$) as the light source).

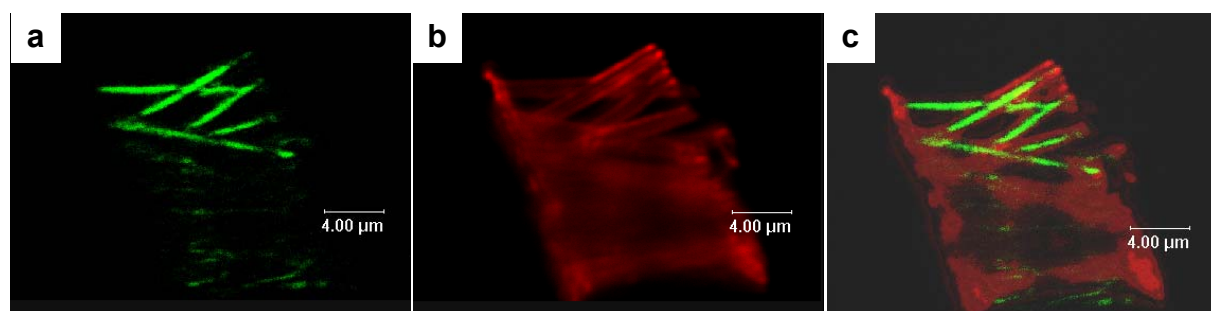


Figure 55: Fluorescence (a and b) and overlay (c) CLSM images of $(\text{PAH/PAA})_7/(\text{PAH/PSS})_{12}$ microfibers, obtained by using PC membranes with 1 μm cylindrical pores. Rhodamin labelled PAH was infiltrated for once thus the sacrificial layer is red fluorescent, and fluorescein-labeled PAH was infiltrated for once during pH insensitive multilayer formation for green fluorescence. Sacrificial layer is decomposed by 12 h immersion in 3M NaOH.

Sacrificial layer was only partially decomposed at low pH, determined by CLSM investigations (Figure 55). Strong interpenetration during multilayer formation prevents complete sacrificial layer decomposition. To avoid aggregation after sacrificial layer decomposition, thicker sacrificial layers need to be deposited. Thereby gap formation during sacrificial layer decomposition accompanied by removal of microfiber interconnecting pH insensitive material outside of template pores might be achieved. Increased sacrificial layer thickness can be achieved by increasing multilayer numbers, or by using salt solution during washing steps.

Further optimization to control sacrificial layer interpenetration and the removal of undesired deposited multilayer material should be carried out in future.

7.2. Cytotoxicity Test

7.2.1. MTT Assay

Cytotoxicity of materials can be determined by a standard colorimetric assay. Viable cells have the ability to reduce the tetrazolium salt MTT by a mitochondrial dehydrogenase enzyme (Figure 56). The enzyme cleaves the tetrazolium rings of MTT, resulting in a color change from pale yellow MTT to dark purple formazan. The dark purple formazan crystals accumulate in healthy cells due to their impermeability to cross the cell membranes. Liberation of the crystals is achieved by solubilisation of the cells, allowing for determination of the metabolic cell activity, as it is proportional to the concentration of formed crystals. The color of the formazan product can be quantified by colorimetric assays [179].

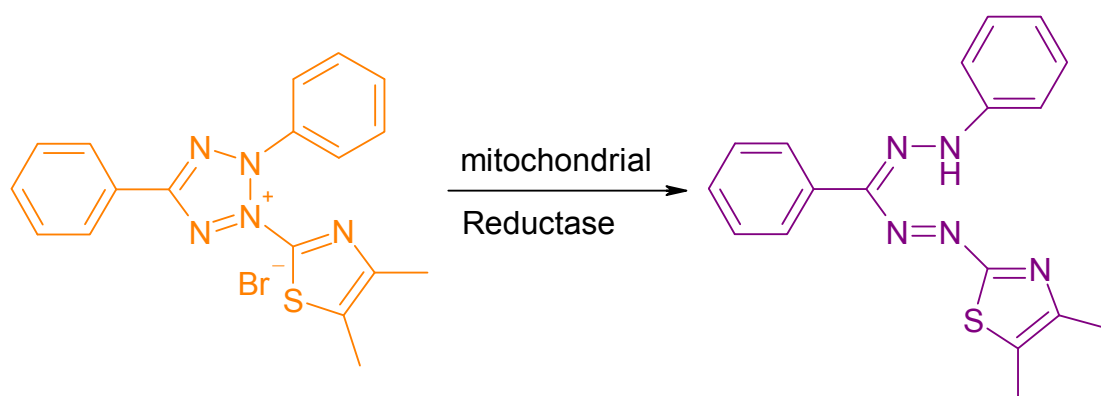


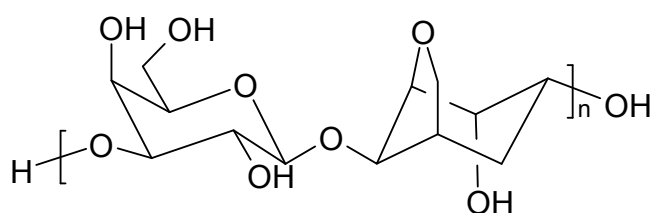
Figure 56: Principle of MTT-test: Reduction of water soluble, yellow colored 3-(4,5-Dimethylthiazol-2-yl)-2,5-diphenyltetrazoliumbromide (MTT) to form water insoluble, violet Formazan.

7.2.2. LDH Assay

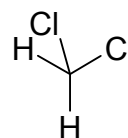
Cell membrane damage can be used to quantify cytotoxicity of applied materials. Cell death is accompanied by cell membrane damage and irreparable loss of its integrity. Therefore cytoplasmic enzymes are released into cell culture supernatant. Due to this leakage lactate dehydrogenase (LDH) activity can be used to determine cytotoxic effects of administered material.

LDH oxidises lactate to form pyruvate, and in parallel reduces NAD^+ to NADH/H^+ . In a second step a catalyst transfers hydrogen from NADH/H^+ onto the slightly yellow colored tetrazolium salt INT (2-[4-Iodophenyl]-3-[4-nitrophenyl]-5-phenyltetrazoliumchloride), by thus reducing it to red colored formazan salt. The color of the formazan product can be quantified by colorimetric assays. The cytotoxicity is proportional to LDH released into the supernatant. The amount of released LDH correlates with the amount of formazan formed, and can therefore be used to quantify cytotoxicity of a defined cell number [179].

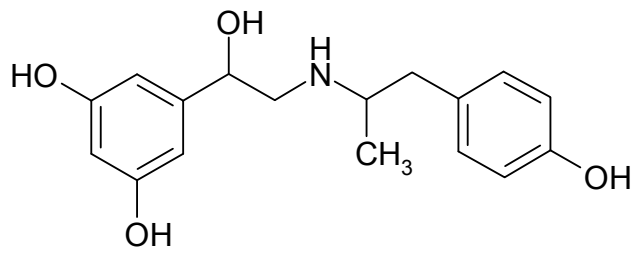
7.3. Chemical Structures



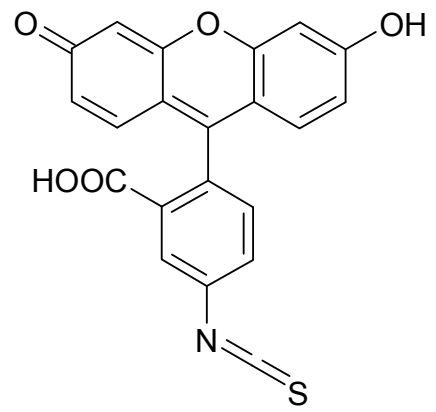
Agarose



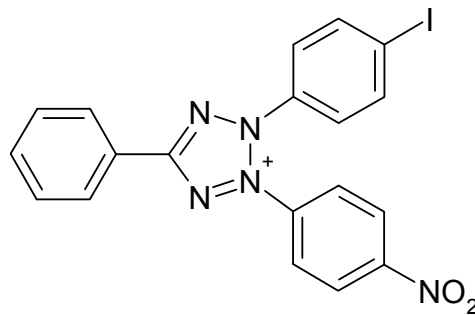
Dichloromethane (DCM)



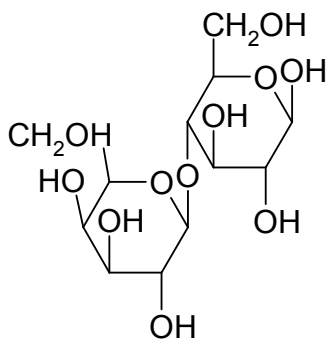
Fenoterol



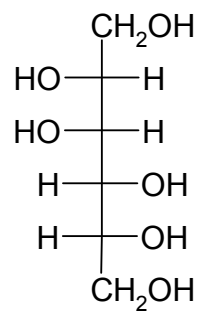
Fluorescein isothiocyanate (FITC)



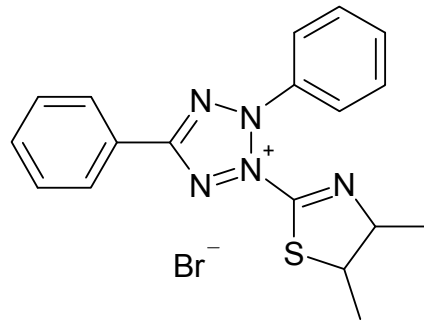
(2-[4-Iodophenyl]-3-[4-nitrophenyl]-5-phenyltetrazoliumchlorid) (INT)



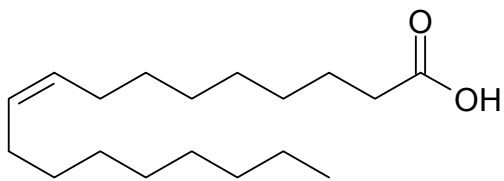
Lactose



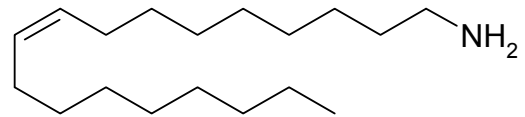
D – Mannitol



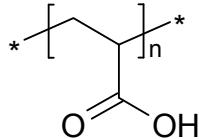
(3-(4,5-Dimethylthiazol)-2,5-diphenyltetrazolium bromide (MTT))



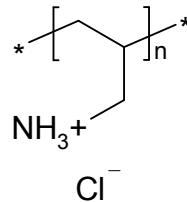
Oleic acid



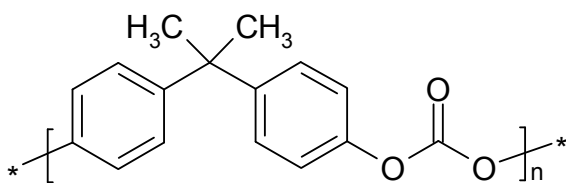
Oleylamine



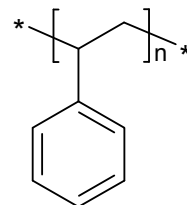
Polyacrylic acid (PAA)



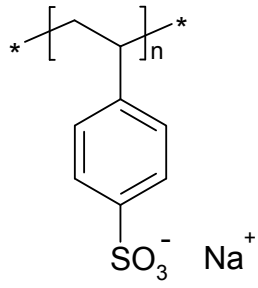
Polyallylamine hydrochloride (PAH)



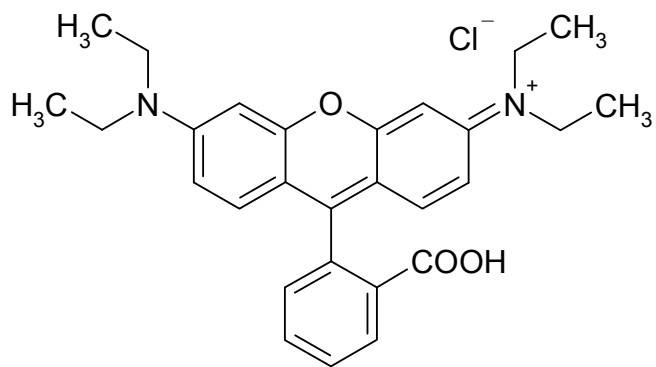
Polycarbonate (PC)



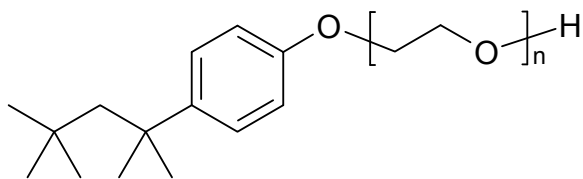
Polystyrene (PS)



Poly (sodium 4-styrenesulfonate) (PSS)



Rhodamine B



Triton X

8. List of Abbreviations

AAO:	Anodic Aluminium Oxide
ACI:	Andresen Cascade Impactor
API:	Active Pharmaceutical Ingredient
AM:	Alveolar Macrophage
CNT:	Carbon Nanotubes
COPD:	Chronical Obstructive Pulmonary Disease
d_{aer} :	Aerodynamic Diameter
DCM:	Dichloromethane
d_{geo} :	Geometric Diameter
DD:	Delivered Dose
DPI:	Dry Powder Inhalers
ED:	Emitted Dose
EMA:	European Medicines Agency
FDA:	Food and Drug Administration
FITC:	Fluorescein isothiocyanate
FPF:	Fine Particle Fraction
GI:	Gastro Intestinal Tract
INT:	(2-[4-Iodophenyl]-3-[4-nitrophenyl]-5-phenyltetrazoliumchloride)
LbL:	Layer-by-Layer
LDH:	Lactate Dehydrogenase
MRI:	Magnetic Resonance Imaging
MTT:	3-(4,5-Dimethylthiazol-2-yl)-2,5-diphenyltetrazoliumbromide
MWCNT:	Multi-walled Carbon Nanotubes
NPs:	Nanoparticles
PAA:	Polyacrylic Acid
PAH:	Polyallylamine Hydrochloride
PC:	Polycarbonate
PEs:	Polyelectrolyte
PS:	Polystyrene
PSD:	Particle Size Distribution
PSS:	Poly (sodium 4-styrenesulfonate)
QD:	Quantum Dots

SEM: Scanning Electron Micrograph
SWCNT: Single-walled Carbon Nanotubes

9. References

1. Patton, J.S., C.S. Fishburn, and J.G. Weers, *The lungs as a portal of entry for systemic drug delivery*. Proc Am Thorac Soc, 2004. **1**(4): p. 338-344.
2. Klinke, R., H.C. Pape, and S. Silbernagel, *Physiologie*. Georg Thieme Verlag, Stuttgart, 2005. **5**.
3. Patton, J.S. and P.R. Byron, *Inhaling medicines: Delivering drugs to the body through the lungs*. Nature Reviews Drug Discovery, 2007. **6**(1): p. 67-74.
4. Lippmann, M., D.B. Yeates, and R.E. Albert, *DEPOSITION, RETENTION, AND CLEARANCE OF INHALED PARTICLES*. British Journal of Industrial Medicine, 1980. **37**(4): p. 337-362.
5. Weibel, E.R., *MORPHOLOGICAL BASIS OF ALVEOLAR-CAPILLARY GAS-EXCHANGE*. Physiological Reviews, 1973. **53**(2): p. 419-495.
6. Gehr, P. and J. Heyder, *Particle-Lung-Interactions*. Marcel Dekker, NY, 2000.
7. Gill, S., et al., *Nanoparticles: Characteristics, mechanisms of action, and toxicity in pulmonary drug delivery - A review*. Journal of Biomedical Nanotechnology, 2007. **3**(2): p. 107-119.
8. Sung, J.C., B.L. Pulliam, and D.A. Edwards, *Nanoparticles for drug delivery to the lungs*. Trends in Biotechnology, 2007. **25**(12): p. 563-570.
9. Chow, A.H.L., et al., *Particle engineering for pulmonary drug delivery*. Pharmaceutical Research, 2007. **24**(3): p. 411-437.
10. Edwards, D.A., A. Ben-Jebria, and R. Langer, *Recent advances in pulmonary drug delivery using large, porous inhaled particles*. 1998. p. 379-385.
11. Edwards, D.A., et al., *Large porous particles for pulmonary drug delivery*. Science, 1997. **276**(5320): p. 1868-1871.
12. Pharmacotherapy, *Pharmacotherapy publications*. 2004.
13. *Europäisches Arzneibuch 6. Ausgabe*. Deutscher Apotheker Verlag, 2008.
14. *United States Pharmacopeia 34*. 2010.
15. Marple, V.A. and B.Y.H. Liu, *CHARACTERISTICS OF LAMINAR JET IMPACTORS*. Environmental Science & Technology, 1974. **8**(7): p. 648-654.
16. Mitchell, J., S. Newman, and H.K. Chan, *In Vitro and In Vivo Aspects of Cascade Impactor Tests and Inhaler Performance: A Review*. Aaps Pharmscitech, 2007. **8**(4): p. 12.
17. Dolovich, M.A., et al., *Consensus statement: aerosols and delivery devices*. American Association for Respiratory Care. Respir Care, 2000. **45**(6): p. 589-96.

18. Vallet-Regi, M., F. Balas, and D. Arcos, *Mesoporous materials for drug delivery*. *Angewandte Chemie-International Edition*, 2007. **46**(40): p. 7548-7558.
19. Duddu, S.P., et al., *Improved lung delivery from a passive dry powder inhaler using an engineered PulmoSphere (R) powder*. *Pharmaceutical Research*, 2002. **19**(5): p. 689-695.
20. Mitragotri, S., *In Drug Delivery, Shape Does Matter*. *Pharmaceutical Research*, 2009. **26**(1): p. 232-234.
21. Sturm, R. and W. Hofmann, *A theoretical approach to the deposition and clearance of fibers with variable size in the human respiratory tract*. *Journal of Hazardous Materials*, 2009. **170**(1): p. 210-218.
22. Gelperina, S., et al., *The Potential Advantages of Nanoparticle Drug Delivery Systems in Chemotherapy of Tuberculosis*. *Am. J. Respir. Crit. Care Med.*, 2005. **172**(12): p. 1487-1490.
23. Muttill, P., C.C. Wang, and A.J. Hickey, *Inhaled Drug Delivery for Tuberculosis Therapy*. *Pharmaceutical Research*, 2009. **26**(11): p. 2401-2416.
24. Pandey, R. and G.K. Khuller, *Antitubercular inhaled therapy: opportunities, progress and challenges*. *Journal of Antimicrobial Chemotherapy*, 2005. **55**(4): p. 430-435.
25. Champion, J. and S. Mitragotri, *Shape Induced Inhibition of Phagocytosis of Polymer Particles*. *Pharmaceutical Research*, 2009. **26**(1): p. 244-249.
26. Morgan, A., *Effect of length on the clearance of fibres from the lung and on body formation*. *IARC Sci Publ*, 1980(30): p. 329-35.
27. Bhaskar, S., et al., *Towards Designer Microparticles: Simultaneous Control of Anisotropy, Shape, and Size*. *Small*, 2010. **6**(3): p. 404-411.
28. Simone, E.A., T.D. Dziubla, and V.R. Muzykantov, *Polymeric carriers: role of geometry in drug delivery*. *Expert Opinion on Drug Delivery*, 2008. **5**(12): p. 1283-1300.
29. Shekunov, B.Y., et al., *Particle size analysis in pharmaceuticals: Principles, methods and applications*. *Pharmaceutical Research*, 2007. **24**(2): p. 203-227.
30. Shekunov, B.Y., et al., *Aerosolisation behaviour of micronised and supercritically-processed powders*. *Journal of Aerosol Science*, 2003. **34**(5): p. 553-568.
31. Pilcer, G. and K. Amighi, *Formulation strategy and use of excipients in pulmonary drug delivery*. *International Journal of Pharmaceutics*, 2010. **392**(1-2): p. 1-19.
32. Byron, P.R., *PREDICTION OF DRUG RESIDENCE TIMES IN REGIONS OF THE HUMAN RESPIRATORY-TRACT FOLLOWING AEROSOL INHALATION*. *Journal of Pharmaceutical Sciences*, 1986. **75**(5): p. 433-438.

33. Henning, A.M., *Nanoparticle Clearance from the Airways*. Saarbrücken, 2008.
34. Oberdoerster, G., E. Oberdoerster, and J. Oberdoerster, *Nanotoxicology: An emerging discipline evolving from studies of ultrafine particles*. Environmental Health Perspectives, 2005. **113**(7): p. 823-839.
35. WHO, *Referenz Method for Measuring Airborne Man-Made Mineral Fibres (MMMMF)*. Environmental Health Report 4. Environmental Health Report 4, 1985: p. 16-35.
36. Su, W.C. and Y.S. Cheng, *Deposition of fiber in a human airway replica*. Journal of Aerosol Science, 2006. **37**(11): p. 1429-1441.
37. Bechthold-Peters, K. and H. Luessen, *Pulmonary Drug Delivery*. Editio Cantor Verlag, 2005.
38. Tabata, Y. and Y. Ikada, *Effect of the size and surface charge of polymer microspheres on their phagocytosis by macrophage*. Biomaterials, 1988. **9**(4): p. 356-362.
39. Torchilin, V.P., *Multifunctional nanocarriers*. Advanced Drug Delivery Reviews, 2006. **58**(14): p. 1532-1555.
40. Zhou, H.J., et al., *Water-Dispersible, Multifunctional, Magnetic, Luminescent Silica-Encapsulated Composite Nanotubes*. Small, 2010. **6**(3): p. 412-420.
41. Chen, D., et al., *Thin Film Instabilities in Blends under Cylindrical Confinement*. Macromolecular Rapid Communications, 2009. **30**(4-5): p. 377-383.
42. Dames, P., et al., *Targeted delivery of magnetic aerosol droplets to the lung*. Nature Nanotechnology, 2007. **2**(8): p. 495-499.
43. Nunes, J., et al., *Multifunctional Shape and Size Specific Magneto-Polymer Composite Particles*. Nano Letters, 2010. **10**(4): p. 1113-1119.
44. Park, J.H., et al., *Magnetic iron oxide nanoworms for tumor targeting and imaging*. Advanced Materials, 2008. **20**(9): p. 1630-1635.
45. Veiseh, O., J.W. Gunn, and M.Q. Zhang, *Design and fabrication of magnetic nanoparticles for targeted drug delivery and imaging*. Advanced Drug Delivery Reviews, 2010. **62**(3): p. 284-304.
46. Delcea, M., et al., *Multicompartmental Micro- and Nanocapsules: Hierarchy and Applications in Biosciences*. Macromolecular Bioscience, 2010. **10**(5): p. 465-474.
47. Geng, Y., et al., *Shape effects of filaments versus spherical particles in flow and drug delivery*. Nat Nano, 2007. **2**(4): p. 249-255.
48. Nishiyama, N., *Nanomedicine: Nanocarriers shape up for long life*. Nat Nano, 2007. **2**(4): p. 203-204.

49. Veblen, D.R. and A.G. Wylie, *MINERALOGY OF AMPHIBOLES AND 1/1 LAYER SILICATES*, in *Health Effects of Mineral Dusts*, G.D. Guthrie and B.T. Mossman, Editors. 1993, Mineralogical Soc America: Washington. p. 61-137.
50. Dodson, R.F., M.A.L. Atkinson, and J.L. Levin, *Asbestos fiber length as related to potential pathogenicity: A critical review*. American Journal of Industrial Medicine, 2003. **44**(3): p. 291-297.
51. Currie, G.P., S.J. Watt, and N.A. Maskell, *An overview of how asbestos exposure affects the lung*. British Medical Journal, 2009. **339**: p. 9.
52. Donaldson, K. and C.A. Poland, *NANOTOXICOLOGY New insights into nanotubes*. Nature Nanotechnology, 2009. **4**(11): p. 708-710.
53. Lam, C.W., et al. *Pulmonary toxicity of single-wall carbon nanotubes in mice 7 and 90 days after intratracheal instillation*. in *42nd Annual Meeting of the Society-of-Toxicology*. 2003. Salt Lake City, Utah: Oxford Univ Press.
54. Donaldson, K., et al., *Carbon nanotubes: A review of their properties in relation to pulmonary toxicology and workplace safety*. Toxicological Sciences, 2006. **92**(1): p. 5-22.
55. Thess, A., et al., *Crystalline ropes of metallic carbon nanotubes*. Science, 1996. **273**(5274): p. 483-487.
56. Eastes, W. and J.G. Hadley, *A mathematical model of fiber carcinogenicity and fibrosis in inhalation and intraperitoneal experiments in rats*. Inhalation Toxicology, 1996. **8**(4): p. 323-343.
57. Tran, C.L., et al., *Inhalation of poorly soluble particles. II. Influence of particle surface area on inflammation and clearance*. Inhalation Toxicology, 2000. **12**(12): p. 1113-1126.
58. Lippmann, M., *Effects of fiber characteristics on lung deposition, retention, and disease*. Environmental Health Perspectives, 1990. **88**: p. 311-317.
59. *CRITERIA FOR THE DIAGNOSIS OF ASBESTOSIS AND CONSIDERATIONS IN THE ATTRIBUTION OF LUNG-CANCER AND MESOTHELIOMA TO ASBESTOS EXPOSURE*. International Archives of Occupational and Environmental Health, 1982. **49**(3-4): p. 357-361.
60. Mossman, B.T. and A. Churg, *Mechanisms in the pathogenesis of asbestosis and silicosis*. American Journal of Respiratory and Critical Care Medicine, 1998. **157**(5): p. 1666-1680.
61. Mauderly, J.L., Y.S. Cheng, and M.B. Snipes, *PARTICLE OVERLOAD IN TOXICOLOGICAL STUDIES - FRIEND OR FOE*. Journal of Aerosol Medicine-Deposition Clearance and Effects in the Lung, 1990. **3**: p. S169-S187.
62. Davis, J.M.G. and A.D. Jones, *COMPARISONS OF THE PATHOGENICITY OF LONG AND SHORT FIBERS OF CHRYSOTILE ASBESTOS IN RATS*. British Journal of Experimental Pathology, 1988. **69**(5): p. 717-737.

63. Coin, P.G., V.L. Roggli, and A.R. Brody, *PERSISTENCE OF LONG, THIN CHRYSOTILE ASBESTOS FIBERS IN THE LUNGS OF RATS*. Environmental Health Perspectives, 1994. **102**: p. 197-199.
64. Miller, F.J., *Dosimetry of particles in laboratory animals and humans in relationship to issues surrounding lung overload and human health risk assessment: A critical review*. Inhalation Toxicology, 2000. **12**(1-2): p. 19-57.
65. Fischer, K.E., et al., *Biomimetic Nanowire Coatings for Next Generation Adhesive Drug Delivery Systems*. Nano Letters, 2009. **9**(2): p. 716-720.
66. Autumn, K., et al., *Adhesive force of a single gecko foot-hair*. Nature, 2000. **405**(6787): p. 681-685.
67. Doshi, N. and S. Mitragotri, *Macrophages Recognize Size and Shape of Their Targets*. Plos One, 2010. **5**(3): p. 6.
68. Beningo, K.A. and Y.L. Wang, *Fc-receptor-mediated phagocytosis is regulated by mechanical properties of the target*. Journal of Cell Science, 2002. **115**(4): p. 849-856.
69. Champion, J.A., Y.K. Katare, and S. Mitragotri. *Particle shape: A new design parameter for micro- and nanoscale drug delivery carriers*. in *4th International Nanomedicine and Drug Delivery Symposium*. 2006. Omaha, NE: Elsevier Science Bv.
70. Cannon, G.J. and J.A. Swanson, *THE MACROPHAGE CAPACITY FOR PHAGOCYTOSIS*. Journal of Cell Science, 1992. **101**: p. 907-913.
71. Gratton, S.E.A., et al., *The effect of particle design on cellular internalization pathways*. Proceedings of the National Academy of Sciences of the United States of America, 2008. **105**(33): p. 11613-11618.
72. Champion, J.A. and S. Mitragotri, *Role of target geometry in phagocytosis*. Proceedings of the National Academy of Sciences of the United States of America, 2006. **103**(13): p. 4930-4934.
73. Huang, Z.M., et al., *A review on polymer nanofibers by electrospinning and their applications in nanocomposites*. Composites Science and Technology, 2003. **63**(15): p. 2223-2253.
74. Greiner, A., et al., *Biohybrid nanosystems with polymer nanofibers and nanotubes*. Applied Microbiology and Biotechnology, 2006. **71**(4): p. 387-393.
75. Doshi, J. and D.H. Reneker, *ELECTROSPINNING PROCESS AND APPLICATIONS OF ELECTROSPUN FIBERS*. Journal of Electrostatics, 1995. **35**(2-3): p. 151-160.
76. Kenawy, E.R., et al., *Release of tetracycline hydrochloride from electrospun poly(ethylene-co-vinylacetate), poly(lactic acid), and a blend*. Journal of Controlled Release, 2002. **81**(1-2): p. 57-64.

77. Yoo, H.S., T.G. Kim, and T.G. Park, *Surface-functionalized electrospun nanofibers for tissue engineering and drug delivery*. *Advanced Drug Delivery Reviews*, 2009. **61**(12): p. 1033-1042.
78. Bognitzki, M., et al., *Polymer, metal, and hybrid nano- and mesotubes by coating degradable polymer template fibers (TUFT process)*. *Advanced Materials*, 2000. **12**(9): p. 637-640.
79. Martin, C.R., *TEMPLATE SYNTHESIS OF POLYMERIC AND METAL MICROTUBULES*. *Advanced Materials*, 1991. **3**(9): p. 457-459.
80. Martin, C.R., *NANOMATERIALS - A MEMBRANE-BASED SYNTHETIC APPROACH*. *Science*, 1994. **266**(5193): p. 1961-1966.
81. Martin, C.R., R. Parthasarathy, and V. Menon, *Template synthesis of electronically conductive polymers - A new route for achieving higher electronic conductivities*. *Synthetic Metals*, 1993. **55**(2-3): p. 1165-1170.
82. Martin, C.R., et al., *TEMPLATE SYNTHESIS OF ORGANIC MICROTUBULES*. *Journal of the American Chemical Society*, 1990. **112**(24): p. 8976-8977.
83. Steinhart, M., et al., *Nanotubes by template wetting: A modular assembly system*. *Angewandte Chemie-International Edition*, 2004. **43**(11): p. 1334-1344.
84. Steinhart, M., et al., *Polymer nanotubes by wetting of ordered porous templates*. *Science*, 2002. **296**(5575): p. 1997-1997.
85. Steinhart, M., J.H. Wendorff, and R.B. Wehrspohne, *Nanotubes a la carte: Wetting of porous templates*. *Chemphyschem*, 2003. **4**(11): p. 1171-1176.
86. Schlitt, S., A. Greiner, and J.H. Wendorff, *Cylindrical polymer nanostructures by solution template wetting*. *Macromolecules*, 2008. **41**(9): p. 3228-3234.
87. Kyotani, T., L.F. Tsai, and A. Tomita, *Preparation of ultrafine carbon tubes in nanochannels of an anodic aluminum oxide film*. *Chemistry of Materials*, 1996. **8**(8): p. 2109-2113.
88. Ai, S.F., et al., *Highly flexible polyelectrolyte nanotubes*. *Journal of the American Chemical Society*, 2003. **125**(37): p. 11140-11141.
89. Dougherty, S. and J. Liang, *Fabrication of segmented nanofibers by template wetting of multilayered alternating polymer thin films*. *Journal of Nanoparticle Research*, 2009. **11**(3): p. 743-747.
90. Dougherty, S.A., D.W. Zhang, and J.Y. Liang, *Fabrication of Protein Nanotubes Using Template-Assisted Electrostatic Layer-by-Layer Methods*. *Langmuir*, 2009. **25**(22): p. 13232-13237.
91. Hou, S.F., et al., *Layer-by-layer nanotube template synthesis*. *Journal of the American Chemical Society*, 2004. **126**(18): p. 5674-5675.

92. Tian, Y., et al., *Fabrication of protein nanotubes based on layer-by-layer assembly*. *Biomacromolecules*, 2006. **7**(9): p. 2539-2542.
93. Tian, Y., et al., *Assembly of nanotubes of poly(4-vinylpyridine) and poly(acrylic acid) through hydrogen bonding*. *Chemistry-a European Journal*, 2006. **12**(18): p. 4808-4812.
94. Tian, Y., et al., *Fabrication of fluorescent nanotubes based on layer-by-layer assembly via covalent bond*. *Langmuir*, 2006. **22**(1): p. 360-362.
95. Hillebrenner, H., et al., *Template synthesized nanotubes for biomedical delivery applications*. *Nanomedicine*, 2006. **1**(1): p. 39-50.
96. Son, S.J., et al., *Template synthesis of multifunctional nanotubes for controlled release*. *Journal of Controlled Release*, 2006. **114**(2): p. 143-152.
97. Yang, Y., et al., *Assembled alginate/chitosan nanotubes for biological application*. *Biomaterials*, 2007. **28**(20): p. 3083-3090.
98. Mitchell, D.T., et al., *Smart nanotubes for bioseparations and biocatalysis*. *Journal of the American Chemical Society*, 2002. **124**(40): p. 11864-11865.
99. He, Q., et al., *Layer-by-layer assembly of magnetic polypeptide nanotubes as a DNA carrier*. *Journal of Materials Chemistry*, 2008. **18**(7): p. 748-754.
100. Hou, S.F., J.H. Wang, and C.R. Martin, *Template-synthesized DNA nanotubes*. *Journal of the American Chemical Society*, 2005. **127**(24): p. 8586-8587.
101. Li, S.F.Y., S.S. Mark, and L.J. Kricka, *Polymeric Nanotubes and Nanorods for Biomedical Applications*. *Current Nanoscience*, 2009. **5**(2): p. 182-188.
102. Son, S.J., et al. *Template synthesis of multifunctional nanotubes for controlled release*. in *3rd International Nanomedicine and Drug Delivery Symposium*. 2005. Baltimore, MD: Elsevier Science Bv.
103. Grimm, S., et al., *Nondestructive replication of self-ordered nanoporous alumina membranes via cross-linked polyacrylate nanofiber arrays*. *Nano Letters*, 2008. **8**(7): p. 1954-1959.
104. Grimm, S., et al., *Nondestructive mechanical release of ordered polymer microfiber arrays from porous templates*. *Small*, 2007. **3**(6): p. 993-1000.
105. Steinhart, M., *Supramolecular Organization of Polymeric Materials in Nanoporous Hard Templates*, in *Self-Assembled Nanomaterials II: Nanotubes*. 2008, Springer-Verlag Berlin: Berlin. p. 123-187.
106. Masuda, H. and K. Fukuda, *ORDERED METAL NANO HOLE ARRAYS MADE BY A 2-STEP REPLICATION OF HONEYCOMB STRUCTURES OF ANODIC ALUMINA*. *Science*, 1995. **268**(5216): p. 1466-1468.
107. Baker, L.A. and S.P. Bird, *Nanopores - A makeover for membranes*. *Nature Nanotechnology*, 2008. **3**(2): p. 73-74.

108. Baker, L.A., P. Jin, and C.R. Martin, *Biomaterials and biotechnologies based on nanotube membranes*. Critical Reviews in Solid State and Materials Sciences, 2005. **30**(4): p. 183-205.
109. Osullivan.Jp and G.C. Wood, *MORPHOLOGY AND MECHANISM OF FORMATION OF POROUS ANODIC FILMS ON ALUMINIUM*. Proceedings of the Royal Society of London Series a-Mathematical and Physical Sciences, 1970. **317**(1531): p. 511-&.
110. Thompson, G.E., et al., *NUCLEATION AND GROWTH OF POROUS ANODIC FILMS ON ALUMINUM*. Nature, 1978. **272**(5652): p. 433-435.
111. Schlitt, S., *NANOSTRUKTUREN DURCH LÖSUNGSBENETZUNG VON PORÖSEN TEMPLATEN*. Dissertation, 2007.
112. Xiao, Z.L., et al., *Fabrication of alumina nanotubes and nanowires by etching porous alumina membranes*. Nano Letters, 2002. **2**(11): p. 1293-1297.
113. Fleisher, R.L., P.B. Price, and R.M. Walker, *Nuclear tracks in solids*. University of California Press, Berkley, CA, 1975.
114. Hulteen, J.C. and C.R. Martin, *A general template-based method for the preparation of nanomaterials*. Journal of Materials Chemistry, 1997. **7**(7): p. 1075-1087.
115. Ai, S.F., et al., *Conductive polypyrrole and poly(allylamine hydrochloride) nanotubes fabricated with layer-by-layer assembly*. Macromolecular Rapid Communications, 2005. **26**(24): p. 1965-1969.
116. He, Q., H. Mohwald, and J.B. Li, *Layer-by-Layer Assembled Nanotubes as Biomimetic Nanoreactors for Calcium Carbonate Deposition*. Macromolecular Rapid Communications, 2009. **30**(18): p. 1538-1542.
117. Roy, C.J., et al., *Growth Mechanism of Confined Polyelectrolyte Multilayers in Nanoporous Templates*. Langmuir, 2010. **26**(5): p. 3350-3355.
118. Gong, X.Z., et al., *Preparation and characterization of La-Co alloy nanowire arrays by electrodeposition in AAO template under nonaqueous system*. Transactions of Nonferrous Metals Society of China, 2008. **18**(3): p. 642-647.
119. Huang, J. and T. Kunitake, *Nanotubings of titania/polymer composite: template synthesis and nanoparticle inclusion*. Journal of Materials Chemistry, 2006. **16**(43): p. 4257-4264.
120. Dougherty, S. and J. Liang, *Core-shell polymer nanorods by a two-step template wetting process*. Nanotechnology, 2009. **20**(29): p. 7.
121. Parthasarathy, R.V. and C.R. Martin, *TEMPLATE-SYNTHESIZED POLYANILINE MICROTUBULES*. Chemistry of Materials, 1994. **6**(10): p. 1627-1632.

122. Yang, S.M., K.H. Chen, and Y.F. Yang, *Synthesis of polyaniline nanotubes in the channels of anodic alumina membrane*. Synthetic Metals, 2005. **152**(1-3): p. 65-68.
123. Parthasarathy, R.V. and C.R. Martin, *SYNTHESIS OF POLYMERIC MICROCAPSULE ARRAYS AND THEIR USE FOR ENZYME IMMOBILIZATION*. Nature, 1994. **369**(6478): p. 298-301.
124. Zhang, M.F., et al., *Wetting transition in cylindrical alumina nanopores with polymer melts*. Nano Letters, 2006. **6**(5): p. 1075-1079.
125. DeGennes, P.G., *WETTING - STATICS AND DYNAMICS*. Reviews of Modern Physics, 1985. **57**(3): p. 827-863.
126. Moon, S.I. and T.J. McCarthy, *Template synthesis and self-assembly of nanoscopic polymer "pencils"*. Macromolecules, 2003. **36**(12): p. 4253-4255.
127. Martin, J. and C. Mijangos, *Tailored Polymer-Based Nanofibers and Nanotubes by Means of Different Infiltration Methods into Alumina Nanopores*. Langmuir, 2009. **25**(2): p. 1181-1187.
128. Steinhart, M., et al., *Morphology of polymer/liquid-crystal nanotubes: Influence of confinement*. Advanced Functional Materials, 2005. **15**(10): p. 1656-1664.
129. Zheng, R.K., et al., *A simple and convenient route to prepare poly(vinylidene fluoride trifluoroethylene) copolymer nanowires and nanotubes*. Chemical Communications, 2005(11): p. 1447-1449.
130. Decher, G., *Fuzzy nanoassemblies: Toward layered polymeric multicomposites*. Science, 1997. **277**(5330): p. 1232-1237.
131. Decher, G. and J.B. Schlenoff, *Multilayer Thin Films*. Wiley-VCH Verlag GmbH & Co. KGaA, 2002.
132. Iler, R.K., *MULTILAYERS OF COLLOIDAL PARTICLES*. Journal of Colloid and Interface Science, 1966. **21**(6): p. 569-&.
133. Ariga, K., J.P. Hill, and Q.M. Ji, *Layer-by-layer assembly as a versatile bottom-up nanofabrication technique for exploratory research and realistic application*. Physical Chemistry Chemical Physics, 2007. **9**(19): p. 2319-2340.
134. Bertrand, P., et al., *Ultrathin polymer coatings by complexation of polyelectrolytes at interfaces: suitable materials, structure and properties*. Macromolecular Rapid Communications, 2000. **21**(7): p. 319-348.
135. Volodkin, D. and M. Mohwald, *Drug Delivery: Polyelectrolyte Multilayers*. Encyclopedia of Surface and Colloidal Science, 2009. **Second Edition**.
136. Caruso, F., *Hollow capsule processing through colloidal templating and self-assembly*. Chemistry-a European Journal, 2000. **6**(3): p. 413-419.
137. Caruso, F., *Hollow inorganic capsules via colloid-templated layer-by-layer electrostatic assembly*. Colloid Chemistry li, 2003. **227**: p. 145-168.

138. Caruso, F., R.A. Caruso, and H. Moehwald, *Nanoengineering of inorganic and hybrid hollow spheres by colloidal templating*. *Science*, 1998. **282**(5391): p. 1111-1114.
139. Lynn, D.M., *Layers of opportunity: nanostructured polymer assemblies for the delivery of macromolecular therapeutics*. *Soft Matter*, 2006. **2**(4): p. 269-273.
140. Cooper, T.M., A.L. Campbell, and R.L. Crane, *FORMATION OF POLYPEPTIDE-DYE MULTILAYERS BY AN ELECTROSTATIC SELF-ASSEMBLY TECHNIQUE*. *Langmuir*, 1995. **11**(7): p. 2713-2718.
141. Fendler, J.H., *Self-assembled nanostructured materials*. *Chemistry of Materials*, 1996. **8**(8): p. 1616-1624.
142. De Geest, B.G., et al., *Release mechanisms for polyelectrolyte capsules*. *Chem Soc Rev*, 2007. **36**(4): p. 636-49.
143. Manna, U. and S. Patil, *Dual Drug Delivery Microcapsules via Layer-by-Layer Self-Assembly*. *Langmuir*, 2009. **25**(18): p. 10515-10522.
144. Schlenoff, J.B., S.T. Dubas, and T. Farhat, *Sprayed polyelectrolyte multilayers*. *Langmuir*, 2000. **16**(26): p. 9968-9969.
145. Köhler, K., *Temperature-Induced Rearrangements of Polyelectrolyte Multilayer Capsules: Mechanisms and Applications*. Dissertation, 2006: p. 142.
146. Elsner, N., *Nanomechanik und Adhäsion von Polyelektrolytemultischicht-Hohlkapseln*. Dissertation, 2005.
147. Ladam, G., et al., *In situ determination of the structural properties of initially deposited polyelectrolyte multilayers*. *Langmuir*, 2000. **16**(3): p. 1249-1255.
148. Dubas, S.T. and J.B. Schlenoff, *Factors controlling the growth of polyelectrolyte multilayers*. *Macromolecules*, 1999. **32**(24): p. 8153-8160.
149. Losche, M., et al., *Detailed structure of molecularly thin polyelectrolyte multilayer films on solid substrates as revealed by neutron reflectometry*. *Macromolecules*, 1998. **31**(25): p. 8893-8906.
150. Dubas, S.T. and J.B. Schlenoff, *Swelling and smoothing of polyelectrolyte multilayers by salt*. *Langmuir*, 2001. **17**(25): p. 7725-7727.
151. Jomaa, H.W. and J.B. Schlenoff, *Salt-induced polyelectrolyte interdiffusion in multilayered films: A neutron reflectivity study*. *Macromolecules*, 2005. **38**(20): p. 8473-8480.
152. Dubas, S.T., T.R. Farhat, and J.B. Schlenoff, *Multiple membranes from "true" polyelectrolyte multilayers*. *Journal of the American Chemical Society*, 2001. **123**(22): p. 5368-5369.
153. Dubas, S.T. and J.B. Schlenoff, *Polyelectrolyte multilayers containing a weak polyacid: Construction and deconstruction*. *Macromolecules*, 2001. **34**(11): p. 3736-3740.

154. Cho, J. and F. Caruso, *Polymeric multilayer films comprising deconstructible hydrogen-bonded stacks confined between electrostatically assembled layers*. *Macromolecules*, 2003. **36**(8): p. 2845-2851.
155. Sukhishvili, S.A. and S. Granick, *Layered, erasable, ultrathin polymer films*. *Journal of the American Chemical Society*, 2000. **122**(39): p. 9550-9551.
156. Sukhishvili, S.A. and S. Granick, *Layered, erasable polymer multilayers formed by hydrogen-bonded sequential self-assembly*. *Macromolecules*, 2002. **35**(1): p. 301-310.
157. Köhler, K. and G.B. Sukhorukov, *Heat treatment of polyelectrolyte multilayer capsules: A versatile method for encapsulation*. *Advanced Functional Materials*, 2007. **17**(13): p. 2053-2061.
158. Mansouri, S., F.M. Winnik, and M. Tabrizian, *Modulating the release kinetics through the control of the permeability of the layer-by-layer assembly: a review*. *Expert Opinion on Drug Delivery*, 2009. **6**(6): p. 585-597.
159. Lee, D., et al., *pH-induced hysteretic gating of track-etched polycarbonate membranes: Swelling/deswelling behavior of polyelectrolyte multilayers in confined geometry*. *Journal of the American Chemical Society*, 2006. **128**(26): p. 8521-8529.
160. Dai, J.H., G.L. Baker, and M.L. Bruening, *Use of porous membranes modified with polyelectrolyte multilayers as substrates for protein arrays with low nonspecific adsorption*. *Analytical Chemistry*, 2006. **78**(1): p. 135-140.
161. Lee, D., R.E. Cohen, and M.F. Rubner, *Heterostructured magnetic nanotubes*. *Langmuir*, 2007. **23**(1): p. 123-129.
162. Alem, H., et al., *Layer-by-layer assembly of polyelectrolytes in nanopores*. *Macromolecules*, 2007. **40**(9): p. 3366-3372.
163. Champion, J.A., Y.K. Katare, and S. Mitragotri, *Making polymeric micro- and nanoparticles of complex shapes*. *Proceedings of the National Academy of Sciences of the United States of America*, 2007. **104**(29): p. 11901-11904.
164. Dendukuri, D., et al., *Continuous-flow lithography for high-throughput microparticle synthesis*. *Nature Materials*, 2006. **5**(5): p. 365-369.
165. Martin, C.R., R. Parthasarathy, and V. Menon, *Template synthesis of electronically conductive polymers--preparation of thin films*. *Electrochimica Acta*, 1994. **39**(8-9): p. 1309-1313.
166. Hurst, S.J., et al., *Multisegmented one-dimensional nanorods prepared by hard-template synthetic methods*. *Angewandte Chemie-International Edition*, 2006. **45**(17): p. 2672-2692.
167. Erickson, R.O., *Tubular Packing of Spheres in Biological Fine Structure*. *Science*, 1973. **181**(4101): p. 705-716.

168. Li, F., et al., *Fabrication of colloidal crystals with tubular-like packings*. Journal of the American Chemical Society, 2005. **127**(10): p. 3268-3269.
169. Li, F., et al., *Synthesis of porous wires from directed assemblies of nanospheres*. Journal of the American Chemical Society, 2003. **125**(52): p. 16166-16167.
170. Tymczenko, M., et al., *Colloidal crystal wires*. Advanced Materials, 2008. **20**(12): p. 2315-2318.
171. Quinn, J.F., et al., *Next generation, sequentially assembled ultrathin films: beyond electrostatics*. Chemical Society Reviews, 2007. **36**(5): p. 707-718.
172. Botterhuis, N.E., et al., *Hollow silica spheres with an ordered pore structure and their application in controlled release studies*. Chemistry-a European Journal, 2006. **12**(5): p. 1448-1456.
173. Duan, H.W., et al., *Colloidally stable amphibious nanocrystals derived from poly {[2-(dimethylamino)ethyl] methacrylate} capping*. Angewandte Chemie-International Edition, 2005. **44**(11): p. 1717-1720.
174. Mao, Z.W., et al., *Hydrogen-Bond-Selective Phase Transfer of Nanoparticles across Liquid/Gel Interfaces*. Angewandte Chemie-International Edition, 2009. **48**(27): p. 4953-4956.
175. Peyratout, C.S. and L. Dähne, *Tailor-made polyelectrolyte microcapsules: From multilayers to smart containers*. Angewandte Chemie - International Edition, 2004. **43**(29): p. 3762-3783.
176. Bai, S., et al., *Using Hydrogels to Accommodate Hydrophobic Nanoparticles in Aqueous Media via Solvent Exchange*. Advanced Materials, 2010. **22**(30): p. 3247-3250.
177. Kreyling, W. and G. Scheuch, *Clearance of Particles Deposited in the Lungs*. Particle-Lung-Interaction, 2000: p. 323-376.
178. Sukhorukov, G., A. Fery, and H. Mohwald, *Intelligent micro- and nanocapsules*. Progress in Polymer Science (Oxford), 2005. **30**(8-9): p. 885-897.
179. Daum, N., et al., *In Vitro Systems for Studying Epithelial Transport of Macromolecules*. 2010. p. 1-14.
180. Chanana, M., et al., *Interaction of Polyelectrolytes and Their Composites with Living Cells*. Nano Letters, 2005. **5**(12): p. 2605-2612.
181. <http://www.de.european-lung-foundation.org/index.php?id=181>, 28.10.2010.
182. Atkins, P.W., *Physical Chemistry*. Oxford University Press, 1994 (5th Edition).
183. Hou, S.F., J.H. Wang, and C.R. Martin, *Template-synthesized protein nanotubes*. Nano Letters, 2005. **5**(2): p. 231-234.

184. Ono, S.S. and G. Decher, *Preparation of ultrathin self-standing polyelectrolyte multilayer membranes at physiological conditions using pH-responsive film segments as sacrificial layers*. Nano Letters, 2006. **6**(4): p. 592-598.

Curriculum Vitae

Personal Data:

Date of Birth: 18.08.1983
Place of Birth: Hamburg, Germany
Nationality: German

Education:

- Since 2008: **PhD**
"Preparation of asymmetric particles"
Supervision: Prof. C.M. Lehr, Jun. Prof. M. Schneider, Prof. H. Möhwald, Prof. D. Wang, Dr. M. Wolkenhauer
Collaboration: Pharmaceutical Technology at Saarland University
Department of Pharmaceutics and Pharmaceutical Technology, Max Planck Institute of Colloids and Interfaces, Boehringer Ingelheim
- 2002 – 2007 : **University**
Degree in Pharmacy at University of Bonn (Germany)
- 2007 : **Clinical traineeship**
Alte Apotheke, Bonn (Germany)
- 2007 : **Clinical traineeship**
Boehringer Ingelheim, Ingelheim (Germany), Pharmaceutical Company
Pulmonary drug delivery, clinical traineeship
- 2005 : **Erasmus (8month)**
Erasmus project at University of Tromso (Norway) at the pharmaceutical technology department under supervision of Prof. A. Bauer Brandl
- 1993 – 2002 : **A-levels**
Gutenberg Schule, Wiesbaden (Germany)
- 1999 - 2000 : **Boarding School**
King's Hospital (Dublin/Ireland)

Internship:

- 2006 : **Internship (3weeks)**
Institute of clinical pharmacy, Bonn (Germany), pharmaceutical advisory research under supervision of Prof. U. Jaehde and Dr. S. Simons
- 2004 : **Internship (2weeks)**
Boehringer Ingelheim, Ingelheim (Germany), Pharmaceutical Company
Introduction in the development of new products
- 2003 : **Internship (4weeks)**
Falkenapotheke, Naurod (Germany), clinical traineeship (4weeks)
Introductions in workflow in the official pharmacy
- 2003 : **Internship (4weeks)**
Institute of pharmaceutical chemistry, Bonn (Germany), clinical traineeship under supervision of Prof. C. Müller, Dr. M. Andrä,

Language Competences:

- English (speak, read and write fluently)
- German (native speaker)

Fields of research:

- Nanoparticles
- Synthesis of asymmetric particles
- Layer by Layer method
- Pulmonary drug delivery

Conference Contributions:

1. Biological barriers 2010, Saarbrücken, Germany. Talk: *"Elongated asymmetric polyelectrolyte particles from particles"* (2010).
2. Controlled Release society 2010, Portland, USA. Talk: *"Preparation of elongated polyelectrolyte particles from particles"* (2010).
3. NanoBio 2010, Zürich, Swiss, Poster: *"Elongated asymmetric polyelectrolyte particles from particles"* (2010).

Awards:

Travel grant, Controlled release society, German chapter (2010)
1st price: Photo competition, NanoBioNet (2010) "Gefrorene Welle"

Publication List

Contribution to Scientific Conferences

Podium:

Kohler D., Schneider M., Lehr C.-M., Krüger M., Möhwald H., Wang, D.: Preparation of elongated polyelectrolyte particles from particles. *8th international conference and workshop on biological barriers*, Saarbrücken, Germany, March 2010

Kohler D., Schneider M., Lehr C.-M., Krüger M., Möhwald H., Wang, D.: Preparation of elongated polyelectrolyte particles from particles. *37th Annual Meeting and Exposition of the Controlled Release Society*, Portland, USA, July 2010

Posters:

Schoenbrodt T., Egen M., Heyder K., Kohler D., Kranz Y., Mueller C., Schiewe J.: Method Development for Deposition Studies in a Nasal Cast. *Respiratory Drug Delivery*, Orlando, USA, April 2010-10-13

Kohler D., Schneider M., Lehr C.-M., Krüger M., Möhwald H., Wang, D.: Preparation of elongated polyelectrolyte particles from particles. *3rd International NanoBio Conference*, Zurich, Switzerland, August 2010

Acknowledgements

First, I would like to thank Prof. Dr. Claus-Michael Lehr for giving me the opportunity to join his working group and write my Ph.D. thesis there.

I owe my deepest gratitude to Prof. Dr. Helmuth Möhwald, in whose institute was allowed to carry out most of my experiments. In this department there was always an open, international atmosphere as well as outstanding equipment placed at my disposal. Thank you for the invaluable scientific input and for all your personal advice over the past three years.

This thesis would not have been possible without the numerous discussions with Prof. Dayang Wang, who helped to successfully move my thesis forward with all his ideas and suggestions for optimizing the techniques used.

Furthermore I would like to thank Jun. Prof. Marc Schneider, my supervisor in Saarbrücken, for his scientific input and assistance with administrative questions.

Without the co-operation of Boehringer Ingelheim, in particular Dr. Michael Krüger, Dr. Regis Cartier and Dr. Markus Wolkenhauer, this thesis would not have been possible. Thanks for all the brainstorming sessions and for providing me access to Boehringer Ingelheim facilities to carry out experiments.

Without “the coffee corner” and all the members of my working group the past three years would not have been as stimulating and lively. I am indebted to my many colleagues for their support. I am especially grateful to my constant summerschool roommate Stephanie Riedel for always being there when I needed her. My thanks also go to Dmitri Fix for his company in the basement during endless CLSM measurements and for all his help with various computer programs. I am grateful to all my office colleagues for the great working atmosphere, all their help with SEM measurements (Dr. Zhengwei Mao and Dr. Wei Li), and for the new laughter lines on my face (Dr. Marta Kolasińska, Prof. Dr. Ali Abou Hassan und Dr. Antonio Stocco).

Furthermore I would like to thank my hockey team for helping me maintain a healthy balance between work and leisure; I have had an unforgettable time in Berlin.

Finally and most importantly, I would like to thank my family, who have suffered with me in bad times and shared the joy in good times. Thanks for your endless love and support for everything I do.